REPORT DOCUMENTATION PAGE

Dist: A

Form Approved
OMB No. 0704-0188

Public reporting burden for this collection of information is estimated to average 1 hour per response, including the time for reviewing instructions, searching existing data sources, gathering and maintaining the data needed, and completing and reviewing the collection of information. Send comments regarding this burden estimate or any other aspect of this collection of information, including suggestions for reducing this burden, to Washington Headquarters Services, Directorate for Information Operations and Reports, 1215 Jefferson Davis Highway, Suite 1204, Arlington, VA 22202-4302, and to the Office of Management and Budget, Paperwork Reduction Project (0704-0188), Washington, DC 20503.

1. AGENCY USE ONLY (Leave blank)	2. REPORT DATE 10/25/94	3. REPORT TYPE AND DATES COVERED Final Technical Report 1/1/92-6/30/94

4. TITLE AND SUBTITLE

Interaction of Turbulence with Complex Shock Waves

5. FUNDING NUMBERS

F49620-92-J-0128

2307/AS

6. AUTHOR(S)

Parviz Moin & Sanjiva Lele

7. PERFORMING ORGANIZATION NAME(S) AND ADDRESS(ES)

Stanford University
Mechanical Engineering, Thermosciences Division
Stanford, CA 94305-3030

8. PERFORMING ORGANIZATION REPORT NUMBER

2-DJA-422

AFOSR-TR- 95 0054

9. SPONSORING/MONITORING AGENCY NAME(S) AND ADDRESS(ES)

AIR FORCE OFFICE OF SCIENTIFIC RESEARCH
DIRECTORATE OF AEROSPACE SCIENCES
BOLLING AFB, DC 20332-6448

10. SPONSORING/MONITORING AGENCY REPORT NUMBER

F49620-92-J-0128

11. SUPPLEMENTARY NOTES

DTIC SELECTED FEB.01 1995 B

12a. DISTRIBUTION/AVAILABILITY STATEMENT

APPROVED FOR PUBLIC RELEASE
DISTRIBUTION IS UNLIMITED

12b. DISTRIBUTION CODE

A

13. ABSTRACT (Maximum 200 words) Linear analysis and direct numerical simulation (DNS) are used to study the interaction of a shock wave with a turbulent flow. Effects central to shock wave/boundary layer interaction are identified and explained. The quantitative importance of the turbulence anisotropy and the shock oblique angle is demonstrated. Drop in Reynolds shear stress across a normal shock is shown. The implication for Reynolds stress models is discussed. The role of dilatational turbulent fluctuations on turbulence amplification is studied in detail. An explanation is suggested for lower amplification reported in wind-tunnel studies. Linear analysis & DNS are used to demonstrate the considerable influence of entropic fluctuations on turbulence evolution across a shock. Positive correlation between u' and T' suppress amplification while negative correlation enhances it. Invalidity of Morkovin's hypothesis is demonstrated. A high order scheme is developed to allow strong shock/turbulence interaction. Results are presented for isotropic turbulence/normal shock interaction.

DTIC QUALITY INSPECTED 3

14. SUBJECT TERMS

numerical simulation, linear analysis, shock wave, turbulence, shear flow, isotropic shear stress, kinetic energy, acoustic waves, entropy fluctuations, shock capturing.

15. NUMBER OF PAGES

16. PRICE CODE

17. SECURITY CLASSIFICATION OF REPORT	18. SECURITY CLASSIFICATION OF THIS PAGE	19. SECURITY CLASSIFICATION OF ABSTRACT	20. LIMITATION OF ABSTRACT
UNCLASSIFIED	UNCLASSIFIED	UNCLASSIFIED	
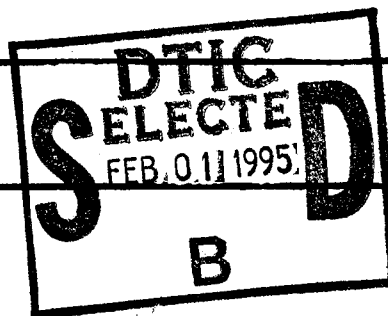
OVERVIEW

This report summarizes our study of the interaction of a shock wave with turbulent flows over the period 1992-1994. Two doctoral students were supported by this program; Dr. Sangsan Lee obtained his degree in 1992 (his thesis was published as Report TF-52; a copy was sent to Dr. Sakell) and Mr. Krishnan Mahesh is expected to complete his work in 1994. The salient achievements of this program are presented below. Details are provided in the attached enclosures of relevant reports and journal publications.

A combination of linear analysis and direct numerical simulation was used by Lee, Lele and Moin[1-3] to study the interaction of isotropic turbulence with a normal shock wave. Subsequent to graduation, Dr. Lee continued work on this problem as a post-doctoral fellow at the Center for Turbulence Research. His principal accomplishments are as follows:

1. A numerical scheme that made possible the first direct numerical simulation of shock / turbulence interaction was developed. The significant achievements include the development of a method to specify 'turbulence' at the inflow boundaries of computational domains and the adaptation of a high order shock-capturing scheme to allow accurate computation of strong shocks.

2. Linear analysis was conducted in parallel to the simulations. The analysis was seen to reproduce most features of the interaction, an aspect that suggests its incorporation into turbulence models. The analysis also offers strong support for the decrease in turbulence length scale across the shock wave - a fact that points to inadequacies in some of the current experimental work on this problem.

3. The database generated was used to examine a model for the evolution of the shock front in a turbulent flow by Kevlahan,Mahesh and Lee[4]. Further use to evaluate turbulence models is anticipated.

The project was extended by Mahesh, Lele and Moin[5-8] to study the interaction of a turbulent shear flow with a shock wave. Both analysis and direct numerical simulation were used. Mr. Mahesh is currently in the final stages of his dissertation. His principal achievements are summarized below:

1. The method to specify inflow turbulence was considerably improved upon. The modified method made possible the shear flow computation which we believe is the first of

its kind. Other direct numerical and large eddy simulations at Stanford and elsewhere have now adopted this method.

2. Linear analysis was used to identify and explain the considerable importance of the anisotropy of the incident turbulence in shock/turbulence interaction. The inability of current models to reproduce these effects was documented.

3. Analysis and computation were used to demonstrate the considerable influence of entropy fluctuations and the nature of their correlation with the velocity field in shock/turbulence interaction. The results were explained and a scaling developed to allow modeling of these effects whose importance in shock wave /boundary layer interaction seems to have gone unnoticed.

4. The effect of compressibility on the evolution of compressible turbulence across a shock wave was studied in detail. The results suggest a possible explanation for wind tunnel experiments on shock/turbulence interaction reporting different results from shock tube experiments.

5. The shear flow computation is currently in progress and reveals effects that were hitherto unreported in the literature. The preceding analyses explain the observed behavior. A database is currently being generated to allow evaluation of turbulence models.

This report is organized as follows. An introduction to Mr. Mahesh's Ph.D thesis is provided in Part 1. Parts 2 and 3 deal with the influence of the anisotropy of the turbulence and turbulent entropy fluctuations respectively on shock/turbulence interaction. The influence of compressibility on shock/turbulence interaction is described in Part 4. Part 5 concludes the report with the interaction of isotropic turbulence with a strong shock wave.

REFERENCES

1. LEE, S., LELE, S.K. & MOIN, P. 1992 Interaction of isotropic turbulence with a shock wave , Report No. TF-52, Dept. of Mechanical Engineering, Stanford University, Stanford, California.

2. LEE, S., LELE, S.K. & MOIN, P. 1993 Direct numerical simulation of isotropic turbulence interacting with a weak shock wave. *J. Fluid Mech.* **251**, 533-562.

3. LEE, S. LELE, S.K. & MOIN, P. 1994 Interaction of isotropic turbulence with a strong shock wave. Paper in preparation.

4. KEVLAHAN, N., MAHESH, K. & LEE, S. 1992 Evolution of the shock front and turbulence structures in the shock/turbulence interaction. *Proc. 1992 Summer Program*,Center for Turbulence Research, Stanford, CA.

5. MAHESH, K., LELE, S.K. & MOIN, P. 1994a The response of anisotropic turbulence to rapid homogeneous one-dimensional compression. *Phys. Fluids.* **6,** 1052-1062.

6. MAHESH, K., LEE, S., LELE, S.K. & MOIN, P. 1994b The interaction of an isotropic field of acoustic waves with a shock wave. Submitted to *J. Fluid Mech.*

7. MAHESH, K., LELE, S.K. & MOIN, P. 1994c The combined interaction of vorticity and entropy fluctuations with a shock wave. Paper in preparation.

8. MAHESH, K., LELE, S.K. & MOIN, P. 1994d The interaction of a shock wave with a turbulent shear flow. PhD Thesis in preparation, Stanford University, Stanford, California.

PART ONE

INTRODUCTION

1.1 Motivation and background

Recent interest in high speed civil transport aircraft and hypersonic propulsion systems has resulted in a resurgence of research into compressible turbulent flows. At high speeds, compressible effects become very important to the design of both external and internal surfaces such as wings, fins, control surfaces and nozzle intakes. The compressibility of the medium results in large gradients in the mean thermodynamic properties, large fluctuations in the thermodynamic variables and high levels of mean dilatation. Simple extensions of incompressible turbulence models appear unable to predict these phenomena, particularly those associated with mean and fluctuating dilatation. Incorporating these effects of compressibility into turbulence models has motivated fundamental research into the physics of these flows.

The presence of shock waves is an important feature that distinguishes high speed flows from low speed ones. Interaction with shock waves is known to significantly alter the hydrodynamics and acoustics of high speed shear layers. Shock wave/boundary layer interaction, a common flow configuration, can induce flow separation and strong fluctuating pressure loads on external surfaces. The presence of shock waves in high speed unadapted jets is known to significantly increase the emitted noise. On the constructive side, shock waves offer the potential to increase the mixing in high speed flows. Current understanding of the physics of the interaction is limited.

This work is a fundamental study of the interaction of a shock wave with a turbulent shear flow. We use linear analysis and direct numerical simulation to study the interaction of a normal shock wave with a shear flow having transversely uniform mean velocity gradient and Mach number.

1.2 Review of past work

This review deals with the hydrodynamics of the interaction of shock waves with non-reacting turbulent flows in the non-hypersonic regime. Phenomena such as detonation waves, Richtmeyer-Meshkov instability, regimes of shock-reflection and shock-related noise (eg. 'screech') are not discussed. Experimental work, linear analysis and numerical computation are reviewed here. Experimental work and analysis of shock turbulence/interaction span about five decades. Computational work on the other hand is very recent.

1.2.1 Experiments

A large body of experimental work exists on the interaction of shock waves with a turbulent boundary layer. Most experiments have examined the flow in a compression corner with some experiments studying normal shock/boundary layer interaction and supersonic shear layers at reattachment.

Green (1970), Korkegi (1971) and Hankey and Holden (1975) provide reviews of earlier experimental work on shock wave/boundary layer interaction. The AGARDograph by Fernholz and Finley (1981) provides a comprehensive summary of experiments prior to 1981. More recent reviews are written by Delery (1985) and Marvin and Delery (1987). A lot of experimental data has been gathered in the last decade. Current experiments provide data on mean velocity and wall pressure, streamwise Reynolds stress, shear stress and wall pressure fluctuations. Some information on two point correlations, spectra and PDFs is also available (*eg* Smits and Muck, 1989).

The flow regime covered by experiments on compression-corner flows extends from attached to separated. Amplification of the streamwise Reynolds stress ($\overline{u^2}$), structure parameter ($\overline{uv}/\overline{u^2}$) and temperature fluctuations across the shock wave was observed by Debieve, Gouin and Gaviglio (1982a, 1982b), Dussauge, Muck and Andreopoulous (1986), Smits and Muck (1989), and Selig, Andreopoulous, Muck, Dussauge and Smits (1989). Kuntz, Amaducci and Addy (1987) observed that the boundary layer after the interaction showed an acceleration of the mean flow near the wall as it recovered to equilibrium and that the mean streamwise velocity profile downstream of the corner was wavy.

The unsteadiness of the shock wave in the separated regime was studied by Andreopoulous and Muck (1987) who analyzed wall pressure signals and concluded that the frequency of the shock wave motion was controlled by the bursting frequency of the incident boundary layer. Subsequent experiments by Erengil and Dolling (1991) also show a direct correlation between the motion of the shock wave and pressure fluctuations in the upstream boundary layer. Further work aimed at correlating the motion of the shock wave to pressure fluctuations in the boundary layer is conducted by Erengil and Dolling (1990), McClure (1992) and Gramann and Dolling (1992).

One of the results of shock-induced separation is fluctuating pressure loads on the wall. Dolling and coworkers have conducted several investigations into the wall pressure fluctuations produced by shock/wave boundary layer interaction. Both two-dimensional and three dimensional flows are considered. An extensive review of experimental data is provided by Dolling (1993).

An experiment by Hayakawa *et al* (1984) examined a reattaching supersonic flow. Strong longitudinal compression was found at reattachment resulting in a three-fold rise in the peak level of mass flux ($\overline{\rho u}$). A comparable subsonic reattachment experiment by Bradshaw and Wong (1972) showed a two-fold drop in the level of u.

In recognition of the complex nature of shock wave/boundary layer interaction, recent experiments have studied the interaction of a shock wave with 'free' turbulence. Debieve and Lacharme (1986) examined the interaction of a shock wave with the separated shear layer over a compression ramp. They concluded that turbulence levels were amplified and Taylor microscales increase through the interaction. An intermittency effect in turbulent statistics at the shock front location was also described.

The interaction of grid generated turbulence with a shock wave was studied by Keller and Merzkirch (1990). Amplification of kinetic energy was observed along with an apparent increase in the Taylor microscale of density across the shock wave. Honkan and Andreopoulous (1990) examined the response of grid generated turbulence to a normal shock. Considerable amplification of turbulence levels was noted. The amplification was seen to depend on the length scale and intensity of the incident flow. Another experimental investigation of the interaction of a shock wave with grid generated turbulence was conducted by Jacquin, Blin and Geffroy (1991) who noticed negligible amplification of kinetic energy across the shock wave.

Detailed experiments on the interaction of a weak shock wave with random fluctuations in density were conducted by Hesselink and Sturtevant (1988). Considerable distortion of the shock front was observed by them which they explained in terms of focusing and defocusing of the shock front in response of density gradients in the medium.

As noted by Jacquin, Cambon and Blin (1993), experiments on grid turbulence/shock wave interaction are not easy to conduct and certain points of contention exist. The increase in length scale that experiments report is both counter-intuitive and in contradiction to computation and linear analysis. Lele (1993) observes that the inconsistency is currently unresolved. Another feature is the lower amplification of kinetic energy reported by wind tunnel experiments as compared to shock tube experiments. Mahesh *et al* (1993) suggest that the presence of acoustic waves in the wind-tunnel experiments is responsible; however further data is needed to resolve this issue.

1.2.2 Linear analysis

The analysis of shock/turbulence interaction is based upon the decomposition of a compressible flow field into vorticity, acoustic and entropy modes as suggested by Kovasz-

nay(1953). The independence of these modes for inviscid, uniform mean flow is used to study the interaction of each of these modes with a shock wave. Both free shock waves and wedge-attached shocks have been considered in the literature. The analyses by different workers differ in detail but are conceptually similar. The linearized Euler equations are used to describe the flow upstream and downstream of the shock wave which is modelled as a discontinuity. The linearized Rankine-Hugoniot equations yield boundary conditions at the shock front. The resulting boundary value problem for the flow downstream of the shock wave is then solved to yield the displacement of the shock front and the flow behind the shock wave.

The earliest studies seem to be those by Blokhintzev (Landau and Lifshitz, 1982), Burgers (1946) and Kantrowitz (1947), who examined the one-dimensional interaction of an acoustic wave with a normal shock wave. Carrier (1949) used linear analysis to study the stability of supersonic flow past a wedge. Interest in the configuration of shock waves in supersonic channel flow prompted Adams (1949) to study the steady interaction between a shock wave and an acoustic wave incident from upstream. Linear analysis was used by Chu (1952) to examine the interaction between a wedge-generated shock wave and an acoustic wave incident from downstream. The interaction between sound and a shock wave was also studied by Lighthill (1949).

Prompted by the problem of 'shock-noise', Ribner (1953) studied in detail the interaction between a vorticity wave and a shock wave. He (1954) subsequently extended his analysis to consider a spectrum of incident vorticity waves (in three dimensions) and computed, for an isotropic incident spectrum, detailed statistics of the downstream flow field with emphasis on the generated noise. Ribner appears to have been the first to predict the interaction of isotropic turbulence with a shock wave. He noted (1953,1969) that weak levels of incident turbulence produce high levels of noise downstream of the shock and later (1987) extended his analysis to predict one-dimensional power spectra of the fluctuations behind the shock wave.

Around the same time as Ribner's pioneering study, Moore (1954) performed detailed analysis of the unsteady interaction of an obliquely incident acoustic wave with a shock wave of infinite extent. He studied acoustic waves that were incident from downstream as well as upstream and also outlined extension of his analysis to study the interaction of a vorticity wave with a shock wave. Other workers that have studied the interaction of unsteady disturbances with a shock wave include Kerrebrock (1956), Johnson and Laporte (1958), Lowson (1968) and McKenzie and Westphal (1968).

Most of these workers considered the interaction of vorticity and acoustic waves with a

shock wave. Chang (1957) used linear analysis to examine the interaction of a plane entropy wave with an oblique shock. In addition to considering the general case of an infinite oblique shock, Chang also considered the case where the oblique shock was produced by a wedge and accounted for reflections from the wedge. Chang's theoretical results were subsequently used by Cuadra (1968) to perform a numerical parametric study of the infinite oblique shock problem.

These earlier studies were largely motivated by issues of shock-stability and the 'shock-noise' phenomenon. Recent interest in the interaction of shock waves with turbulent flows has led to renewed interest in linear analysis. Lee, Lele and Moin (1992, 1993, 1994) repeated Ribner's (1953,1954) analysis and extended it to examine some turbulent statistics that Ribner had not considered. Mahesh, Lee, Lele and Moin (1994a) extended Moore's analysis to examine the interaction of an isotropic field of acoustic waves with a shock wave. They also outlined description of the simultaneous interaction of a field of acoustic and vortical disturbances with a shock wave. Mahesh, Lele and Moin (1994c) have examined the simultaneous interaction of vorticity and entropy fluctuations with a shock wave of infinite extent. The interaction of both single modes and an isotropic field of fluctuations with the shock wave was studied. Interest in receptivity led Duck, Lasseigne and Hussaini (1994) to study the processing of free stream disturbances by a wedge-generated shock wave. The different regimes of the pressure field behind the shock wave were discussed.

Recently, Lee, Lele and Moin (1992) have suggested that idealization of a shock wave as a homogeneous one-dimensional compression and examination of the temporal response of turbulence to this compression might approximate the spatial evolution of turbulence through a shock wave. Linear, inviscid equations or Rapid Distortion Theory (RDT) were used to study this problem. The results showed reasonable agreement with Ribner's analysis for shock waves whose mean Mach number was less than 2. Significant disagreement was seen for stronger shock waves. This conclusion is reiterated by Jacquin, Cambon and Blin (1993) who in addition compare the homogeneous compression of *compressible* turbulence to Ribner's results and note that the difference is larger than observed by Lee *et al.*

It is difficult to systematically outline the differences between the two analyses; however certain general comments can be made. Idealization of a shock wave as a one-dimensional compression prevents it from distorting in response to the incident fluctuations; as a result RDT cannot represent the effect that shock front distortion has on the evolution of the turbulence. Also RDT has no knowledge of the Rankine Hugoniot equations; as a result solenoidal fluctuations do not produce all three kinds of modes upon

compression. Another important difference between the two analyses is the behavior of acoustic fluctuations. The acoustic fluctuations in the spatial problem can either propagate unattenuated or decay exponentially behind the shock wave depending upon the angle of incidence of the disturbance. RDT cannot reproduce this behavior. Mahesh *et al* (1994b) compare their analysis of a shock wave interacting with acoustic fluctuations to Jacquin *et al*'s (1993) compression of compressible turbulence and note that the results are different over the entire range of Mach numbers. It appears that the homogeneous problem can approximate the evolution of solenoidal fluctuations across shock waves of moderate strength; however it is quite inappropriate as the incident turbulence becomes increasingly compressible.

There has been some recent work on the evolution of shock waves in an unsteady field of disturbances. Lele (1992) has used Rapid Distortion Theory to calculate changes in the shock-speed caused by the interaction of isotropic turbulence with a shock wave. Kevlahan, Mahesh and Lee (1992) modelled the shock front as a propagating surface and compared the resulting evolution to numerical simulation. Good agreement was obtained for the cases considered. A recent paper by Giddings, Rusak and Cole (1993) has developed a transonic small disturbance model to analyze the interaction of a weak shock wave with random perturbations. The model allows effects such as nonlinear steepening, focusing and the formation of caustics to be represented.

1.2.3 Numerical computation

Numerical computation of shock/turbulence interaction is a fairly recent undertaking. The first such computation appears to be a detailed study of isotropic turbulence interacting with a weak normal shock ($M_1 \leq 1.2$) by Lee, Lele and Moin (1992, 1993). Lee *et al* solved the three dimensional compressible Navier Stokes equations, using a non-uniform mesh to resolve the thickness of the shock wave. Subsequently, they (1994) used a high order shock capturing scheme to study stronger shock waves ($M_1 = 2, 3$). Their results corroborated Ribner's (1954) linear analysis. Amplification of vorticity, kinetic energy and thermodynamic fluctuations was observed along with decrease in Taylor microscale.

Subsequently, Hannappel and Friedrich (1994b) have used shock capturing to compute compressible isotropic turbulence interacting with a shock wave with $M_1 = 2$. The interaction of compressible fluctuations (kinetic energy equally distributed between solenoidal and dilatational modes) was contrasted with that of solenoidal fluctuations. The amplification of kinetic energy was seen to be lower when the incident fluctuations were compressible. Hannappel and Friedrich's computation might suffer from insufficient resolution of the

shock front (Lee *et al*, ...); their results however are in qualitative agreement with the linear analysis of Mahesh *et al* (1994b).

Prior to Lee *et al*'s (1992) study, computations were largely restricted to the interaction of a shock wave with single waves of vorticity, sound and entropy or deterministic flow inhomogeneities such as hot spots and vortices. There appear to be only two detailed studies (in two dimensions) of the interaction of a shock wave with a random field of disturbances.

Zang *et al* (1984) evaluated the linear analysis of McKenzie and Westphal (1968) by comparison to their numerical solution of the two-dimensional Euler equations. They examined the effect of incident angle, shock-strength and the amplitude of the incident disturbance in the interaction of acoustic and vorticity waves with a shock wave. Results were presented only in the freely propagating regime. The dependence on incident angle was examined in the interaction of disturbances of amplitude 0.1% and 10% with a shock wave of Mach number 8. Good agreement was seen away from the critical angle; divergence from the linear analysis prediction was seen within about 20° of the critical angle. The linear analysis predictions were quite robust in terms of dependence on shock strength and disturbance amplitude. For an incident angle of 30°, the linear predictions were valid for disturbance amplitudes as high as 25% for acoustic waves and 100% for vorticity waves and shock waves whose Mach number was close to unity.

More recently, Mahesh, Lee, Lele and Moin (1994) have computed the interaction of a Mach 1.5 shock wave with an acoustic wave incident from upstream. The dependence upon the incident angle was examined and the results were compared to the linear analysis of Moore (1954). Good agreement was seen except within 25° of the critical angles. This disagreement was explained by noting that the region around the critical angle corresponded to transonic flow in transformed coordinates and hence linear approximation would be inconsistent in that regime.

Hannappel and Friedrich (1994a) have computed the interaction of a Mach 8 shock wave with vorticity and acoustic waves incident at 45° from upstream. They contrasted the evolution of these two waves. The terms in the averaged equations for the kinetic energy were also examined in their study.

Numerical calculations of the interaction of coherent flow disturbances with a shock wave have also been performed. Hussaini *et al* (1986) studied the effect of upstream eddy motion and temperature inhomogeneity on the enhancement and production of turbulence. Meadows *et al* (1991) examined the effect of vortex strength in a study of two-dimensional

shock/vortex interaction. Several workers have computed the interaction of a shock wave with a density inhomogeneity to examine the nature of the vorticity field that is produced. A list of references may be found in a recent paper by Yang, Kubota and Zukoski (1994).

Rotman (1991) performed numerical solution of the two-dimensional Euler equations to study the response of an isotropic random field of disturbances to a moving shock wave. Amplification of kinetic energy and decrease of length scale were observed in his study. Comparison of Rotman's results to linear analysis by Lee (Private communication) showed good agreement.

Prior to their three dimensional computation, Lee, Lele and Moin (1991) solved the two-dimensional compressible Navier Stokes equations to study the interaction of two-dimensional isotropic turbulence with a shock wave. A non-uniform mesh was used to resolve the thickness of the shock wave. Amplification of vorticity and kinetic energy was observed accompanied by a drop in Taylor microscale.

1.3 Overview

Our primary objective is to study the interaction of a shock wave with a turbulent shear flow. Both linear analysis and direct numerical simulation are used for this purpose. To our knowledge, DNS of this problem has not been conducted before. The DNS provides a database that can be used to elucidate the flow physics as well as to test turbulence models. The linear analyses were conducted to supplement the simulations in predicting the interaction.

The principal contributions and findings of this work are listed below.

- Rapid Distortion Theory was used to study the response of turbulent shear flows to rapid one-dimensional compression. Both normal and oblique compressions were considered.

- The anisotropy of shear flows (as determined by $E_{11}(\kappa_1)$ and $\overline{u^2}/q^2$) and the obliquity of compression were shown to strongly affect the evolution of the Reynolds stresses upon compression.

- Reynolds stress modelling of the normal compression problem was considered in the RDT limit. The inability of popular pressure strain models to predict the evolution of kinetic energy and the decrease in the magnitude of shear stress was demonstrated.

- Linear analysis of the combined interaction of vorticity and entropy fluctuations with a shock wave was carried out. The interaction of a single wave as well as an isotropic field of fluctuations was studied.

11

- Significant dependence of the downstream solution on the amplitude ratio and phase difference between the vorticity and entropy waves was demonstrated.

- The presence of negatively correlated velocity and temperature fluctuations was shown to increase the amplification of kinetic energy and pressure fluctuations across the shock wave. Likewise, positively correlated temperature and velocity fluctuations resulted in suppression of amplification.

- The inapplicability of the Strong Reynolds Analogy (SRA) across a shock wave was demonstrated and explained.

- The interaction of a Mach 1.5 shock wave with a single acoustic wave was numerically computed and the dependence upon the incident angle examined. The results were compared to linear analysis and limits placed on the range of validity of linear analysis. The requirement of transonic small disturbance equations to model the interaction around the critical angle was demonstrated.

- Linear analysis was used to study the interaction of an isotropic field of acoustic waves with a shock wave. The evolution of kinetic energy, sound level and thermodynamic fluctuations were examined in detail.

- The spatial evolution of kinetic energy behind the shock wave was examined and the rapid non-monotonic variation immediately downstream of the shock wave explained.

- The kinetic energy of acoustic fluctuations was shown to *decrease* across the shock for Mach numbers varying from 1.25 to 1.8. For Mach numbers exceeding 3, the kinetic energy was seen to amplify by levels that far exceeded those found in the interaction of vortical fluctuations with a shock wave. These trends were explained.

- The linear analysis was used to suggest acoustic fluctuations in the upstream turbulence as a possible explanation for wind-tunnel experiments on grid turbulence/shock wave interaction reporting lower levels of kinetic energy amplification.

- Comparison of the linear analysis to Jacquin *et al*'s analysis of the homogeneous compression of compressible turbulence revealed that the homogeneous problem was quite inappropriate as the the incident turbulence became increasingly compressible.

- Direct numerical simulation of the interaction of a shock wave with a turbulent shear flow was performed. The method of specifying inflow turbulence developed by Lee, Lele and Moin (1992) was modified to reduce the evolution length of the inflow disturbances by a factor of 4-5.

This report is organized as follows. Rapid Distortion Theory is used to study the response of a homogeneous turbulent shear flow to rapid compression in Chapter 2. Chapter 3 discusses linear analysis of the combined interaction of vorticity and entropy fluctuations with a shock wave. Details of the direct numerical simulation are presented in Chapter 4. The significant results and suggestions for future work are outlined in Chapter 5. Of the three appendices, Appendix A describes the linear analysis of the interaction of a shock wave with an isotropic field of acoustic waves. Details of the analysis of interaction of vorticity and entropy waves with a shock wave are presented in Appendix B. Finally, Appendix C outlines the modified method for specification of inflow turbulence in numerical simulations.

REFERENCES

ADAMS, M. C. 1949 On shock waves in inhomogeneous flow. *J. Aero. Sci.* **16**, 685-690.

ANDREOPOULOUS, J. & MUCK, K.C. 1987 Some new aspects of the shock-wave boundary layer interaction in a compression ramp corner. *J. Fluid Mech.* **180**, 405-428.

BURGERS, J.M. 1946 On the transmissions of sound waves through a shock wave. *Koninklijke Nederlandsche Akademie Van Wetenschappen, Proc.* **XLIX**, 273-281.

CARRIER, G.F. 1949 On the stability of the supersonic flows past a wedge. *Quarterly of Applied Mathematics.* **6**, 367-378.

CHANG, C.T. 1957 Interaction of a plane shock and oblique plane disturbances with special reference to entropy waves. *J. Aero. Sci.* **24**, 675-682.

CHU, B.T. 1952 On weak interaction of strong shock and Mach waves generated downstream of a shock. *J. Aero. Sci.* **19**, 433-446.

CUADRA, E. 1968 Flow perturbations generated by a shock wave interacting with an entropy wave. *AFOSR-UTIAS Symposium on Aerodynamic Noise,*Toronto, pp. 251-271.

DEBIEVE, F.R., GOUIN, H. & GAVIGLIO, J. 1982a Evolution of the reynolds stress tensor in a shock wave-turbulence interaction. *Indian Journal of Technology.* **20**, 90-97.

DEBIEVE, F.R., GOUIN, H. & GAVIGLIO, J. 1982b Momentum and temperature fluxes in a shock wave-turbulence interaction. In *Structure of Turbulence in Heat and Mass Transfer* edited by Z.P. Zaric, Hemisphere, New York.

DEBIEVE, J.F. & LACHARME, J.P. 1986 A shock wave/free-turbulence interaction. In *Turbulent Shear Layer/Shock Wave Interactions* (ed. J.Délery). Springer.

DOLLING, D.S. 1993 Fluctuating loads in shock wave/turbulent boundary layer interaction: tutorial and update. *AIAA Paper 93-0284.*

DUCK, P.W., LASSEIGNE, D.G. & HUSSAINI, M.Y. 1994 On the interaction between the shock wave attached to a wedge and freestream disturbances.

DUSSAUGE, J.P., MUCK, K.C. & ANDREOPOULOUS, J. 1986 Properties of wall pressure fluctuations in a separated flow over a compression ramp. In *Turbulent Shear Layer/Shock Wave Interactions* edited by J. Delery, Springer, Berlin.

ERENGIL, M.E. & DOLLING, D.S. 1990 Correlation of separation shock motion in a comressible ramp interaction with pressure fluctuations in the incoming boundary layer. *AIAA Paper 90-1646.*

ERENGIL, M.E. & DOLLING, D.S. 1991 Correlation of separation shock motion with pressure fluctuations in the incoming boundary layer. *AIAA Journal.* **29**, 1868-1877.

FERNHOLZ, F.F. & FINLEY, P.J. 1981 A further compilation of compressible boundary layer data with a survey of turbulence data. *AGARDograph 263.*

GRAMANN, R.A & DOLLING, D.S. 1992 Examination of turbulent structures associated with unsteady shock motion in a Mach 5 interaction. *AIAA Paper 92-0744.*

GREEN, J.E. 1970 Interaction between shock waves and turbulent boundary layers. *Prog. Aerosp. Sci.* **11**, 235-340.

HANKEY, W.L. & HOLDEN, M.S. 1975 Two-dimensional shock wave-boundary layer interactions in high speed flows. *AGARDograph 203.*

HANNAPPEL, R. & FRIEDRICH, R. 1994a On the interaction of wave-like disturbances with shocks - two idealizations of the shock/turbulence interaction problem. *In Acta Mechanica 4 69-77.*

HANNAPPEL, R. & FRIEDRICH, R. 1994 DNS of a M=2 shock interacting with isotropic turbulence. In *Proc. First ERCOFTAC Workshop on DNS and LES*, Guildford, Surrey, U.K.

HESSELINK, L. & STURTEVANT, B. 1988 Propagation of weak shocks through a random medium. *J. Fluid Mech.* **196**, 513-553.

HONKAN, A. & ANDREOPOULOUS, J. 1992 Rapid compression of grid-generated turbulence by a moving shock wave. *Phys. Fluids A.* 4, 2562-2572.

HUSSAINI, M.Y., COLLIER, F. & BUSHNELL, D.M. 1986 Turbulence alteration due to shock motion. In *Turbulent Shear Layer/Shock Wave Interactions* edited by J. Delery, Springer, Berlin.

JACQUIN, L., BLIN, E. & GEFFROY, P. 1991 Experiments on free turbulence/shock wave interaction. *Proc. Eighth Symp. on Turbulent Shear Flows, Munich* (ed. F.Durst, R.Friedrich, B.E.Launder, F.W.Schmidt, U.Schumann & J.H.Whitelaw). Springer.

JACQUIN, L., CAMBON, C. & BLIN, E. 1993 Turbulence amplification by a shock wave and rapid distortion theory. *Phys. Fluids A.* **5**, 2539-2550.

JOHNSON, W.R. & LAPORTE, O. 1958 Interaction of cylindrical sound waves with a stationary shock wave. *Phys. Fluids.* **1**, 82-94.

KANTROWITZ, A. 1947 The formation and stability of normal shock waves in channel flow. *NACA TN 1225.*

KELLER,J. & MERZKIRCH, W. 1990 Interaction of a normal shock wave with a compressible turbulent flow. *Exp. Fluids.* **8**, 241-248.

KERREBROCK, J.L. 1956 The interaction of flow discontinuities with small disturbances in a compressible fluid. *PhD Thesis, California Institute of Technology.*

KEVLAHAN, N., MAHESH, K. & LEE, S. 1992 Evolution of the shock front and turbulence structures in the shock/turbulence interaction. *Proc. 1992 Summer Program*, Center for Turbulence Research, Stanford, CA.

KORKEGI, R. 1971 Survey of viscous interactions associated with high Mach number flight. *AIAA J.* **9**, 771-784.

KOVASZNAY, L.S.G. 1953 Turbulence in supersonic flow. *J. Aero. Sci.* **20**, 657-682.

KUNTZ, D.W., AMADUCCI, V.A. & ADDY, A.L. 1987 Turbulent boundary layer properties downstream of the shock wave/boundary layer interaction. *AIAA J.* **25**, 668-675.

LANDAU, L.D. & LIFSHITZ, E.M. 1982 Fluid Mechanics. *Course of Theoretical Physics,* Vol. 6, Pergamon Press, 332-333.

LEE, S., LELE, S.K. & MOIN, P. 1991 Direct numerical simulation and analysis of shock turbulence interaction. *AIAA Paper 91-0523.*

LEE, S., MOIN, P. & LELE, S.K. 1992 Interaction of isotropic turbulence with a shock wave. *Rep.* TF-52. Department of Mechanical Engineering, Stanford University, Stanford, CA.

LEE, S., LELE, S.K. & MOIN, P. 1993 Direct numerical simulation of isotropic turbulence interacting with a weak shock wave. *J. Fluid Mech.* **251**, 533-562.

LEE, S. LELE, S.K. & MOIN, P. 1994b Interaction of isotropic turbulence with a strong shock wave. *AIAA Paper,* 94-0311.

LELE, S.K. 1992 Shock jump conditions in a turbulent flow. *Phys. Fluids A.* **4**, 2900-2905.

LELE, S.K. 1994 Compressibility Effects on Turbulence. *Annu. Rev. Fluid Mech.* **26**, 211-254.

LIGHTHILL, M.J. 1949 The flow behind a stationary shock. *Phil. Mag. 40, Ser.7,* No. 301, 214-220.

LOWSON, M.V. 1968 Pressure fluctuations resulting from shock interactions. *J. Sound Vib.* **7**, 380-392.

MAHESH, K., LEE, S., LELE, S.K. & MOIN, P. 1994b The interaction of an isotropic field of acoustic waves with a shock wave. *Submitted to J. Fluid Mech.*

MAHESH, K., LEE, S., LELE, S.K. & MOIN, P. 1994c The combined interaction of vorticity and entropy fluctuations with a shock wave. *Submitted to J. Fluid Mech.*

MCCLURE, W.B. 1992 An experimental study of the driving mechanism and control of the unsteady shock-induced turbulent separation in a Mach 5 compression corner flow. Ph.D Dissertation, Dept. of Aerospace Engineering and Engineering Mechanics, The Univ. of Texas at Austin.

MCKENZIE, J.F. & WESTPHAL, K.O. 1968 Interaction of linear waves with oblique shock waves. *Phys. Fluids.* **11**, 2350-2362.

MEADOWS, K.R., KUMAR, A. & HUSSAINI, M.Y. 1991 Computational study of the interaction between a vortex and a shock wave. *AIAA J.* **29**, 174-179.

MOORE, F.K. 1954 Unsteady Oblique Interaction of a Shock Wave with a Plane Disturbance. *NACA TN 2879.*

RIBNER, H.S. 1953 Convection of a Pattern of Vorticity through a Shock Wave. *NACA TN 2864.*

RIBNER, H.S. 1954 Shock-Turbulence Interaction and the Generation of Noise. *NACA TN 3255.*

RIBNER, H.S. 1969 Acoustic energy flux from shock-turbulence interaction. *J. Fluid Mech.* **35** 299-310.

RIBNER, H.S. 1987 Spectra of noise and amplified turbulence emanating from shock-turbulence interaction. *AIAA Journal.* **25,** 436-442.

ROTMAN, D. 1991 Shock wave Effects on a Turbulent Flow. *Phys. Fluids A.* **3,** 1792-1806.

SELIG, M.S., ANDREOPOULOUS, J., MUCK, K.C., DUSSAUGE, J.P. & SMITS, A.J. 1989 Turbulence structure in a shock wave/turbulent boundary layer interaction. *AIAA J.* **27,** 862-869.

SMITS, A.J. & MUCK, K.C. 1987 Experimental study of three shock wave/turbulent boundary layer interactions. *J. Fluid Mech.* **182,** 294-314.

YANG, J., KUBOTA, T. & ZUKOSKI, E.E. 1994 A model for characterization of a vortex pair formed by shock passage over a light-gas inhomogeneity. *J. Fluid Mech.* **258,** 217-244.

ZANG, T.A., HUSSAINI, M.Y. & BUSHNELL, D.M. 1984 Numerical computations of turbulence amplification in shock-wave interactions. *AIAA Journal.* **22,** 13-21.

PART TWO

THE RAPID COMPRESSION OF A TURBULENT SHEAR FLOW

2.1 Background

This chapter uses rapid distortion theory (RDT) to examine the response of turbulent shear flows to rapid one-dimensional compression. Answers are sought to the following questions: How does the response of a turbulent shear flow to compression differ from that of isotropic turbulence ? How does a shear flow respond to oblique compression as compared to normal compression ?

One-dimensional compression is used to model the shock wave in this chapter. The turbulence is constrained to be homogeneous and solenoidal. The time scale of compression is assumed small as compared to the time scale of the turbulence (a reasonable assumption in shock/turbulence interaction). RDT is then used to predict the response of the turbulence to compression. As discussed in Chapter 1, this approach is expected to yield reasonable prediction of the interaction of solenoidal turbulence with shock waves of moderate strength.

The roots of RDT applied to flows under mean compression lie in the work of Prandtl (1933), Taylor (1935), Ribner and Tucker (1953) and Batchelor and Proudman (1954). Motivated by the passage of turbulence through a wind-tunnel contraction, these workers developed RDT for turbulent flows subjected to rapid irrotational distortions. More recently, Lee (1989) has performed a detailed analysis of the response of the turbulence to axisymmetric strain and dilatation. The above studies assumed the turbulence to be incompressible; recent studies by Durbin and Zeman (1992) and Cambon, Coleman and Mansour (1992) have applied RDT to the compression of compressible turbulence. While Durbin and Zeman have examined the pressure fluctuations and the pressure-dilatation correlation in the limit of vanishing turbulent Mach Number (nearly solenoidal turbulence), Cambon *et al.* have considered finite turbulent Mach numbers and shown the negligible effect of pressure fluctuations at high turbulent Mach numbers.

All the above mentioned studies considered the compression of isotropic turbulence. To the best of our knowledge, the response of shear flows to rapid compression has not been studied before. Precedence in the use of RDT to examine the rapid straining of anisotropic turbulence may be found in the work of Townsend (1980), Sreenivasan and Narasimha (1978), Maxey (1982) and Cambon (Private communication).

This chapter is organized as follows. A brief outline of RDT in Section 2.2 is followed in Section 2.3 by the response of turbulent shear flows to normal compression. Section

2.4 deals with the oblique compression of sheared turbulence. Application of the analysis to predict shock/turbulence interaction is described in Section 2.5 and Reynolds stress modeling of the normal compression problem is examined in Section 2.6. Finally, the salient results are summarized in Section 2.7. Most of the work in this chapter is described in Mahesh, Lele and Moin (1993) and Mahesh, Lele and Moin (1994a).

2.2 Theoretical Procedure

Rapid Distortion Theory combines linearization of the governing equations with statistical averaging to describe the statistical evolution of turbulence under rapid mean distortion. The formal development of the RDT approximation is outlined in reviews such as those by Savill (1987) and Hunt and Carruthers (1990). When the time-scale of the mean distortion is much smaller than that of the turbulence, then the turbulence has no time to interact with itself. This allows the neglect of all terms in the governing equations that involve viscosity or the product of fluctuations yielding a set of evolution equations that are linear in the fluctuations. An alternative formulation (Pearson, 1959; Deissler, 1961) corresponding to low Reynolds number or 'weak' turbulence requires retention of the viscous terms. We neglect the viscous terms in our analysis.

Linearization of the continuity and momentum equations yields the following set of equations.

$$\frac{\partial u_i}{\partial x_i} = 0 \tag{2.1a}$$

$$\frac{\partial u_i}{\partial t} + U_j \frac{\partial u_i}{\partial x_j} + u_j \frac{\partial U_i}{\partial x_j} = -\frac{1}{\rho} \frac{\partial p}{\partial x_i} \tag{2.1b}$$

where, U_i and ρ are the mean velocity and density respectively, and u_i and p are the fluctuating velocity field and pressure respectively. For irrotational mean distortions, it is convenient to solve the linearized vorticity equation which reduces to Cauchy's equation.

Note that the fluctuations are assumed to be solenoidal. If the mean distortion is solenoidal, then the above equations correspond to linearization of the incompressible Navier Stokes equations. However, if the mean field is dilatational (as for a one-dimensional compression), then the governing equations are the *compressible* Navier Stokes equations and the above set of equations therefore describe evolution of the solenoidal component of the compressible flow field under the assumption that its evolution is independent of the dilatational component. (Alternatively, equations (2.1a) and (2.1b) describe the evolution of a compressible flow field with spatially uniform but time-dependent density.) The solenoidal and dilatational component are coupled even in the linear limit for rotational

19

mean flows (Blaisdell, Mansour and Reynolds, 1991). However for irrotational mean distortions, the solenoidal component may be assumed to evolve independently in the limit $\Delta m = \Gamma_0 L/a \ll 1$ where, Γ_0 is the mean strain rate, L is a turbulence lengthscale and a is the mean speed of sound ; *i.e.*, the turbulence is nearly incompressible (Cambon, Coleman and Mansour, 1992).

The assumption of homogeneity constrains the mean velocity gradient to be uniform; *i.e.*, the mean velocity is of the form $U_i = A_{ik}(t)x_k$. For incompressible turbulence, this is the only requirement for homogeneity; since as discussed above, we consider evolution of the solenoidal component of of a compressible flow field, we constrain the mean field to satisfy homogeneity for compressible turbulent fluctuations. As a result, in addition to a uniform velocity gradient, the mean field satisfies the compressible Euler equations and has uniform pressure and density (Blaisdell, Mansour and Reynolds, 1991).

The procedure for solution of equations (2.1a) and (2.1b) is fairly well established. One method of solution (Batchelor and Proudman, 1954) involves using a Fourier representation where the wavenumber changes with time as

$$u(\mathbf{x}, t) = \sum_{\mathbf{k}} \hat{u}(\mathbf{k}, t) e^{ik_j(t)x_j}$$

$$p(\mathbf{x}, t) = \sum_{\mathbf{k}} \hat{p}(\mathbf{k}, t) e^{ik_j(t)x_j}$$

where,

$$\frac{\mathrm{d}k_\alpha}{\mathrm{d}t} + k_j A_{j\alpha} = 0 \tag{2.2}$$

An alternative equivalent method of solution (Rogallo, 1981) is to transform coordinates to a system that deforms with the mean field; *i.e.*,

$$\xi_i = B_{ik}(t)x_k \qquad \tau = t$$

where,

$$\frac{\mathrm{d}}{\mathrm{d}t} B_{nk} + A_{jk} B_{nj} = 0 \tag{2.3}$$

The transformed equations are then solved using conventional Fourier representation. Knowledge of the Fourier coefficients enables computation of the energy spectrum tensor which is then integrated over all wavenumbers to determine the Reynolds stresses.

Homogeneous RDT being an initial-value problem, requires specification of the initial energy spectrum. As mentioned previously, earlier studies assume isotropic initial spectrum. Our analysis differs in that the compression of anisotropic turbulence is considered. Details of the analysis are presented in the following sections.

2.3. Normal Compression of Sheared Turbulence

The response of a turbulent shear flow to normal compression is discussed in this section. Description of the problem and the solution procedure is outlined in Section 2.3.1. Results of the analysis are presented and discussed in Sections 2.3.2 and 2.3.3 respectively.

2.3.1 Problem Formulation

Figure 2.1 shows a schematic of the normal compression of a turbulent shear flow. One-dimensional compression is characterized by the following mean field.

$$U_1 = \frac{\Gamma_0}{1 + \Gamma_0 t} x_1, \quad U_2 = U_3 = 0 \tag{2.4a}$$

$$\rho = \frac{\rho_0}{1 + \Gamma_0 t} \tag{2.4b}$$

$$P = \frac{P_0}{[1 + \Gamma_0 t]^\gamma} \tag{2.4c}$$

where U_1, U_2, U_3 are the mean velocity components in the x_1, x_2, x_3 directions respectively; ρ and P are the mean density and pressure respectively, and are uniform in space. Γ_0 is negative for compression and positive for expansion.

Consider isotropic turbulence that is subjected to rapid homogeneous shear *i.e.*,

$$U_1 = S_0 x_2, \quad \rho = \rho_0, \quad P = P_0 \tag{2.5}$$

At a non-dimensional time $\beta_0 = S_0 t_0$ during application of shear, we introduce the one-dimensional compression *i.e.*, for $t > t_0$,

$$U_1 = \frac{\Gamma_0}{1 + \Gamma_0(t - t_0)} x_1 + \frac{S_0}{1 + \Gamma_0(t - t_0)} x_2 \tag{2.6a}$$

$$\rho = \frac{\rho_0}{1 + \Gamma_0(t - t_0)} \tag{2.6b}$$

$$P = \frac{P_0}{[1 + \Gamma_0(t - t_0)]^\gamma} \tag{2.6c}$$

The shear rate changes with time during the application of compression to satisfy the compressible Euler equations. Note that the shear is along x_2 while the compression is along x_1; hence the terminology 'normal compression'.

Under RDT, the Reynolds stresses before compression depend only upon the total shear β_0; their subsequent evolution depends upon β_0, the ratio of shear rate to the rate

21

of compression (S_0/Γ_0) and the total volumetric strain (ρ/ρ_0). Since our interest is in the compression of shear flows, we consider the regime where the shear sets up the initial anisotropic field and is negligible as compared to the subsequently applied compression; *i.e.*, $S_0/\Gamma_0 \ll 1$. In this report S_0/Γ_0 is 0.1 for all cases presented. Lower values of S_0/Γ_0 (for *eg*, $S_0/\Gamma_0 = 0.01$) yielded results identical to those shown here. Thus, we effectively consider the rapid one-dimensional compression of sheared turbulence.

The RDT equations are solved by transforming coordinates to a system that deformed with the mean field. Fourier representation in the transformed coordinates is used to derive ordinary differential equations that describe the evolution of the energy spectrum tensor. The equations are numerically advanced in time and at each time step, the energy spectrum tensor is numerically integrated over all wavenumbers to compute the Reynolds stresses.

As indicated above, the mean field is pure shear for $t < t_0$. The RDT equations for pure shear have been solved analytically (Moffatt, 1965; Townsend, 1970) and hence we do not give the evolution equations for the energy spectrum tensor. We only note that the coordinate transform used is as follows,

$$\xi_1 = x_1 - S_0 t x_2, \quad \xi_2 = x_2, \quad \xi_3 = x_3, \quad \tau = t \qquad (2.7)$$

At time $t_0 = \beta_0/S_0$, the coordinate transformation changes to accommodate the compression. The new transformation is given by

$$\xi_1 = \frac{x_1}{1 + \Gamma_0(t - t_0)} - [\beta_0 + S_0(t - t_0)]x_2, \quad \xi_2 = x_2, \quad \xi_3 = x_3, \quad \tau = t \qquad (2.8)$$

For $t > t_0$, the RDT equations are transformed to the above coordinate system. Using the Fourier representation,

$$u(\xi, \tau) = \sum_{\vec{\kappa}} \hat{u}(\vec{\kappa}, \tau) e^{i \kappa_j \xi_j} \qquad (2.9a)$$

$$p(\xi, \tau) = \sum_{\vec{\kappa}} \hat{p}(\vec{\kappa}, \tau) e^{i \kappa_j \xi_j} \qquad (2.9b)$$

the RDT equations take the following form for $t > t_0$:

$$\frac{d\hat{u}_1}{d\tau} = \frac{1}{1 + \Gamma_0 \tau'} \left[-\Gamma_0 \hat{u}_1 - S_0 \hat{u}_2 + \kappa_1 \frac{i\hat{p}}{\rho} \right] \qquad (2.10a)$$

$$\frac{d\hat{u}_2}{d\tau} = \left[\kappa_2 - \frac{S_0 \tau'}{1 + \Gamma_0 \tau'} \kappa_1 \right] \frac{i\hat{p}}{\rho} \qquad (2.10b)$$

$$\frac{d\hat{u}_3}{d\tau} = \kappa_3 \frac{i\hat{p}}{\rho} \qquad (2.10c)$$

$$\frac{i\hat{p}}{\rho} = \frac{\kappa_1\Gamma_0 \ \hat{u}_1 + [\kappa_1 S_0 + (\kappa_1 S_0 - \kappa_2\Gamma_0)\ (1+\Gamma_0\tau')\ ]\ \hat{u}_2 - \kappa_3\Gamma_0\ (1+\Gamma_0\tau')\ \hat{u}_3}{\kappa_1^2\ [1+(S_0\tau')^2] - 2\ \kappa_1\kappa_2\ S_0\tau'\ (1+\Gamma_0\tau') + (\kappa_2^2 + \kappa_3^2)\ (1+\Gamma_0\tau')^2} \qquad (2.10d)$$

where the variable $\tau' = \tau - \tau_0$. Note that the expression for pressure is obtained through elimination of the continuity equation. Also, $\Gamma_0 = 0$ in the above equations would describe the evolution for $t < t_0$ (Pure shear).

The RDT equations for a pure compression allow analytical solution as do the equations for pure shear. However, as seen above, the combination of shear and compression yields a formidable set of equations which we have not been able to solve analytically. Instead equations (2.10a) through (2.10d) were used to derive evolution equations for the energy spectrum tensor $E_{ij}(\vec{\kappa}, \tau)$, defined as $E_{ij} = \hat{u}_i\hat{u}_j^*$, where the superscript '*' refers to the complex conjugate. For reasons of brevity, the equation for E_{ij} is not reproduced here; it has the following form:

$$\frac{\mathrm{d}E_{ij}}{\mathrm{d}\tau} = C_{il}E_{lj} + C_{jl}E_{li} \qquad (2.11)$$

The above system of equations is integrated numerically to compute $E_{ij}(\vec{\kappa}, \tau)$. E_{ij} is then integrated over all wavenumbers to compute the Reynolds stress tensor $R_{ij}(\tau)$ defined as $R_{ij} = \overline{u_i u_j}$; i.e.,

$$R_{ij}(\tau) = \int E_{ij}(\vec{\kappa}, \tau)\ \mathrm{d}^3\vec{\kappa} \qquad (2.12)$$

The integration is carried out in polar coordinates

$$\kappa_1 = \kappa\cos\phi, \quad \kappa_2 = \kappa\sin\phi\cos\theta, \quad \kappa_3 = \kappa\sin\phi\sin\theta, \quad \mathrm{d}^3\vec{\kappa} = \kappa^2\sin\phi\,\mathrm{d}\phi\,\mathrm{d}\theta\,\mathrm{d}\kappa$$

where, κ varies from 0 to ∞, ϕ, from 0 to π and θ, from 0 to 2π. Note that since at $\tau = 0$, the energy spectrum tensor is assumed to be isotropic; i.e.,

$$E_{ij}(\vec{\kappa}, 0) = \frac{E(\kappa)}{4\pi\kappa^2}\left(\delta_{ij} - \frac{\kappa_i\kappa_j}{\kappa^2}\right)$$

it can be shown that $R_{ij}(\tau)$ is independent of the initial three-dimensional energy spectrum tensor, $E(\kappa)$ and the magnitude of the wavenumber vector.

2.3.2 Results

The analysis described above essentially applies RDT to the compression of a shear flow where the energy spectrum tensor of the shear flow is itself the RDT solution to initially isotropic turbulence subjected to homogeneous shear. The use of RDT to obtain the energy spectrum tensor that characterizes a shear flow is motivated by Townsend (1970) where the

RDT predictions of Reynolds stress correlations, spectra and non-dimensional Reynolds stresses in turbulent shear flows were compared to experiment and good agreement was observed.

This is illustrated in Figure 2.2 where R_{ij}/q^2 as predicted by RDT applied to the rapid shear of initially isotropic turbulence is shown. The quantity plotted on the abscissa is the total shear β defined as $\beta = S_0 t$. Note that after a moderate amount of total shear (β between 2 and 3), the nondimensional Reynolds stresses are quite close to values obtained in shear flows such as homogeneous shear flow, turbulent channel flow (Moin, 1988) and boundary layers (Townsend, 1970). For example, in homogeneous shear flow (Moin, 1988), $R_{11}/q^2, R_{22}/q^2, R_{33}/q^2$ and R_{12}/q^2 are 0.54, 0.16, 0.31 and 0.14 respectively. For a total shear of 2.5, RDT yields values of 0.51, 0.12, 0.36 and 0.16 respectively. Townsend (1970) notes, 'The good agreement of the non-dimensional Reynolds stresses suggests that the large eddies in turbulent shear flows have very nearly the shape suggested by RDT'. This conclusion is further supported by direct numerical simulation (Lee, Kim and Moin, 1990) of turbulence subjected to very high shear rates, where structures similar to near wall 'streaks' were observed.

The evolution of sheared turbulence upon compression is next examined. The abscissa in all plots shown is the total volumetric strain, ρ/ρ_0. q^2 normalized with its value at the start of compression is plotted against the total volumetric strain in Figure 2.3. The different curves correspond to different values of total initial shear (β_0). $\beta_0 = 0$ corresponds to the compression of initially isotropic turbulence. q^2 is seen to amplify upon compression with the amplification ratio increasing as the initial total shear increases. The amplification of turbulent kinetic energy upon normal compression is thus higher for a shear flow than it is for isotropic turbulence.

The evolution of the components of turbulent kinetic energy is plotted in Figure 2.4. β_0 was set to 3 for this case. All three components are seen to amplify with the x_1 (direction of compression) component being amplified the most. The reason for the preferential amplification of the x_1 component is due to the fact that it is directly 'produced' by the compression while the other components amplify through the redistributive nature of the pressure-strain correlation in the Reynolds stress equations. The importance of the initial anisotropy on the amplification of $\overline{u_1^2}$ is gauged by comparing the amplification of $\overline{u_1^2}$ of initially sheared turbulence to that of initially isotropic turbulence (Figure 2.5). Note that the amplification of $\overline{u_1^2}$ in the shear flow is much higher than that of isotropic turbulence. For example, at a density ratio of 3, the amplification ratio is 3.4 for initially isotropic turbulence and 4.85 for initially sheared turbulence - an increase of about 43 %.

As mentioned earlier, shear flows in equilibrium are characterized by typical values of R_{ij}/q^2. It is of interest to see how these values change upon normal compression. Figure 2.6 shows the the diagonal terms of the tensor. Compression increases the contribution of u_1 to the turbulent kinetic energy while decreasing that of u_2 and u_3. Also note (over the range of total volumetric strain shown) that the ordering of kinetic energy components ($u_1 > u_3 > u_2$) is retained upon normal compression.

The evolution of R_{12}/q^2 upon compression is plotted in Figure 2.7. The three curves correspond to different values of total initial shear. Upon normal compression, R_{12}/q^2 decreases in magnitude and for sufficiently large total volumetric strains, it changes sign. This trend was first observed by Cambon (Private communication), and is hastened upon increasing the initial total shear. The terms in the Reynolds shear stress evolution equation provide an explanation for this behavior. The evolution equation for R_{12} is,

$$\frac{\mathrm{d}}{\mathrm{d}t}R_{12} = -\frac{\Gamma_0}{1+\Gamma_0 t}R_{12} - \frac{S_0}{1+\Gamma_0 t}R_{22} + \pi_{12} \qquad (2.13)$$

where π_{ij} is the pressure-strain correlation defined as $\pi_{ij} = \overline{p(u_{i,j} + u_{j,i})}/\rho$. Note that both the strain and shear production terms tend to increase the magnitude of R_{12} (make it more negative). The tendency of $|R_{12}|$ to decrease must therefore be due to the pressure strain correlation. Figure 2.8 illustrates the evolution of terms in the budget of R_{12} for the case with $\beta_0 = 3$. We see that the tendency of R_{12} to decrease upon normal compression is due to amplification of the pressure-strain correlation and the consequent upsetting of the initial balance between 'production' and the pressure-strain correlation in the shear flow.

2.3.3 Interpretation of the results

We have seen that the response of a shear flow to normal compression is quite different from that of isotropic turbulence. A noticeable feature is the higher amplification of $\overline{u_1^2}$ and q^2 in the shear flow. In this section, we attempt to explain this observation by posing the following question, 'What aspect of the initial anisotropic field is important in determining the evolution of kinetic energy during a one-dimensional compression ?'

The evolution equations for $\overline{u_1^2}$ and q^2 during rapid compression are given by

$$\frac{\mathrm{d}\overline{u_1^2}}{\mathrm{d}\tau} = -2\frac{\Gamma_0}{1+\Gamma_0\tau}\overline{u_1^2} + \pi_{11} \qquad (2.14a)$$

$$\frac{\mathrm{d}q^2}{\mathrm{d}\tau} = -2\frac{\Gamma_0}{1+\Gamma_0\tau}\overline{u_1^2} \qquad (2.14b)$$

The pressure-strain correlation 'takes' energy from $\overline{u_1^2}$ and redistributes it among the other components. The amplification of $\overline{u_1^2}$ and hence, q^2 through equation (2.14b), would increase if the pressure-strain correlation were to decrease. Also, since in the RDT limit, the pressure-strain correlation is the only term in the budget apart from the production term, a higher amplification rate automatically implies a lower pressure-strain correlation.

The relative magnitude of the pressure-strain term in the energy budget may be gauged from its short time behavior. It is easily shown that in turbulence subjected to rapid one-dimensional compression π_{11} evolves as,

$$\pi_{11} = -2\Gamma_0 c \int \frac{c^2 \kappa_1^2}{c^2 \kappa_1^2 + \kappa_2^2 + \kappa_3^3} E_{11}(\vec{\kappa}) \mathrm{d}^3 \kappa \qquad (2.15)$$

where, $c = \rho/\rho_0$. π_{11} thus strongly depends upon the spectral distribution of the u_1 component of velocity. Note that as the energy distribution in u_1 moves to smaller κ_1, the magnitude of π_{11} decreases. The small time evolution of π_{11} may be estimated by replacing E_{11} in equation (2.15) with its initial value, E_{11}^0. This small time evolution shows how the spectral distribution of u_1 in the initial field affects the rate of change of $\overline{u_1^2}$ when anisotropic turbulence is compressed.

Since mean shear tends to stretch the turbulence in the streamwise direction, $\hat{u}_1$ in a shear flow has energy at smaller κ_1 as compared to isotropic turbulence and hence according to equation (2.15), a lower initial value of π_{11}. This is shown in Figure 2.9 where the ratio of π_{11} to the production term in the R_{11} equation is plotted. The pressure-strain correlation is indeed seen to be smaller when shear flow is compressed.

As one continues the compression, the energy in u_1 is moved to larger κ_1 and hence, the pressure-strain correlation would progressively become more important. Analysis shows that in the limit of infinite ρ/ρ_0, the ratio of π_{11} to the production term is independent of the initial energy spectrum; it is equal to 1. This is shown as follows. For turbulence subjected to one-dimensional compression, under RDT,

$$E_{11}(\vec{\kappa}) = \frac{c^2 E_{11}^0(\vec{\kappa})}{c^2(\kappa_1/\kappa)^2 + (\kappa_2/\kappa)^2 + (\kappa_3/\kappa)^2} \qquad (2.16)$$

where, $c = \rho/\rho_0$.

Denoting the denominator in the above expression by D, the rate of change of E_{11} is given by,

$$\frac{\mathrm{d}E_{11}}{\mathrm{d}\tau} = \frac{E_{11}^0}{D^2}\left(D\frac{\mathrm{d}c^2}{\mathrm{d}\tau} - c^2\frac{\mathrm{d}D}{\mathrm{d}\tau}\right) \qquad (2.17)$$

Noting that $dc/dt = -\Gamma_0 c^2$ and considering very large compressions, it can be shown that,

$$\lim_{c \to \infty} \frac{dE_{11}}{d\tau} = 0 \qquad (2.18)$$

Since E_{11} when integrated over all wavenumbers yields R_{11}, the above equation implies that in the limit of very large c, $d\overline{u_1^2}/d\tau = 0$. Substitution into equation (2.14a) shows that asymptotically, $\pi_{11} = $ Production. Note that this relation is independent of the initial energy spectrum. The asymptotic behavior shows the diminishing effect of initial anisotropy upon the pressure-strain correlation as time progresses. This is supported by Figure 2.9 where the two curves tend towards each other as c increases. Integration to larger time shows that the two curves do indeed asymptote to 1.

We see that when anisotropic turbulence is compressed (in the x_1 direction), the feature of the initial field that determines kinetic energy evolution is $E_{11}^0(\kappa_1)$. As the energy in u_1^0 moves to smaller κ_1, the relative importance of π_{11} decreases resulting in larger amplification of $\overline{u_1^2}$. The amplification of q^2, in addition to being influenced by E_{11}^0, is also influenced by the initial value of $\overline{u_1^2}/q^2$. This is shown as follows. The kinetic energy equation for a one-dimensional compression (Equation 2.14b) may be rewritten as

$$\frac{1}{2q_0^2} \frac{dq^2}{d\tau} = -\frac{\Gamma_0}{1 + \Gamma_0 \tau} \frac{R_{11}}{R_{11}^0} \frac{R_{11}^0}{q_0^2} \qquad (2.19)$$

Note that as R_{11}^0/q_0^2 increases, the amplification of q^2 increases. This explains the trend seen in Figure 2.3. In addition to having energy at lower κ_1, a shear flow that is subjected to normal compression also has a larger fraction of its energy along the direction of compression, resulting in a higher amplification of q^2 as compared to isotropic turbulence.

2.4. Oblique Compression of Sheared Turbulence

Thus far, we have examined the effect of compression on sheared turbulence normal to the direction of shear. Since shear flows are anisotropic, one would expect the direction of compression relative to the shear to be an important parameter; *i.e.*, the oblique compression of a shear flow would yield results different from normal compression. In the section that follows, we discuss the procedure (Section 2.4.1) and results (Section 2.4.2) of RDT applied to the problem of oblique compression.

2.4.1. Problem Formulation

Under RDT, the obliquity of compression may be characterized by the angle θ between the direction of compression and the direction of the upstream shear flow. Note that $\theta = 0$ corresponds to the normal compression discussed in the previous section. Recall that the normal compression problem was formulated by considering sheared turbulence subjected to simultaneous shear and compression in the regime where the compression rate was much higher than the rate of shear. The sole reason for retention of the shear during compression was to avoid the destruction of vorticity. However, one might adopt the point of view that if the mean shear is not important during the process of compression, then it may be ignored except for its effect on the initial spectrum. This is the approach adopted in this section in applying RDT to the oblique compression of sheared turbulence. We essentially repeat RDT for turbulence subjected to a one-dimensional compression. However the initial energy spectrum instead of being isotropic is the RDT solution to isotropic turbulence subjected to homogeneous shear. Also as mentioned, the initial mean shear is assumed to be at angle θ to the subsequently applied compression. The validity of this approach was verified by comparison of the results for $\theta = 0$ to the more completely formulated normal compression problem.

Figure 2.10 shows a schematic of the the oblique compression problem. Note that the shear is assumed to be in the x_2 direction. For reasons of convenience, the time-dependent wavenumber approach (Batchelor and Proudman, 1954) was used to solve the RDT equations. The RDT solution to the oblique compression problem requires knowledge of the evolution of the energy spectrum tensor when isotropic turbulence is subjected to homogeneous shear and the transfer function of the vorticity spectrum tensor when turbulence (not necessarily isotropic) is subjected to a one-dimensional compression. As indicated earlier, these problems have been solved analytically. Assuming knowledge of these transfer functions, the procedure for RDT applied to the oblique compression problem is as follows:

28

1. Consider isotropic turbulence that is subjected to homogeneous shear in the x_2 direction. Denote the wavenumber vector at $t = 0$ by $\mathbf{k_0}$. For a given total shear (defined in the previous section) compute the energy spectrum tensor at the end of shear.

2. With reference to Figure 2.10, rotate the energy spectrum tensor and the wavenumber vector by the angle θ. This aligns the field with the compression.

3. From the rotated energy spectrum tensor and the wavenumber vector, obtain the vorticity spectrum tensor in the rotated coordinates.

4. Using the transfer functions for the compression problem, obtain the vorticity spectrum tensor and wavenumber vector after compression.

5. Using the inverse of the relation in 3, obtain the energy spectrum tensor after compression in the rotated coordinates. Integrate the energy spectrum tensor over $\mathbf{k_0}$ to obtain the Reynolds stress tensor in rotated coordinates.

6. Rotate the Reynolds stress tensor back by the angle θ. This yields the Reynolds stress tensor after compression in the original coordinate system.

2.4.2. Results

We describe in this section some of the results of RDT applied to the oblique compression of sheared turbulence. The effect of the oblique angle θ, is gauged by comparison to the previously discussed normal compression problem. The amplification of the streamwise component of turbulent kinetic energy upon compression is shown in Figure 2.11 for different angles of obliquity.

The initial condition corresponds to sheared turbulence with $\beta_0 = 3$. Recall that $\theta = 0$ corresponds to normal compression. Note the decrease in amplification ratio with increasing magnitude of oblique angle. The effect of oblique compression on q^2 is shown in Figure 2.12. Once again, the amplification of q^2 decreases as the oblique angle increases. In the previous section, we emphasized the importance of the $E_{11}(\kappa_1)$ and $\overline{u_1^2}/q^2$ on the amplification of kinetic energy. If oblique compression is viewed in a coordinate system aligned with the compression, we see that the effect of oblique compression may be explained by the initial value of $E_{\theta\theta}(\kappa_\theta)$ and $\overline{u_\theta^2}/q^2$, where θ refers to the direction of compression.

In the previous section, we noted how normal compression could significantly change the nondimensional Reynolds stresses of a shear flow. The effect of oblique compression on the diagonal elements of R_{ij}/q^2 is shown in Figures 2.13, 2.14 and 2.15. It is clear that obliquity of compression has a significant effect on the evolution of the Reynolds stresses. The qualitative difference in the curves for different oblique angles is striking to note.

Figure 2.16 shows the evolution of the nondimensional Reynolds shear stress upon oblique compression. Recall the effect of normal compression to decrease R_{12}/q^2 and even change its sign. In comparison, we see that this trend decreases as the compression becomes more oblique and for large oblique angles, R_{12}/q^2 slightly amplifies.

2.5 Application to shock/turbulence interaction

We illustrate application of the analysis to shock/turbulence interaction.

Recall that the Reynolds stress tensor during compression of a shear flow is of the form:

$$R_{ij} = R_{ij} \left(\rho/\rho_0; \beta_0, \theta \right) \tag{2.20}$$

Note that S_0/Γ_0 is assumed negligible in writing the above expression. The parameter θ in the above expression is determined by the oblique angle of the shock wave. Figure 2.17 illustrates a couple of examples that correspond to positive and negative θ. The choice of β_0 depends upon the extent of shear (quantified by Sq^2/ϵ) in the flow upstream of the shock wave. As discussed before $\beta_0 = 2.5$ seems appropriate for shear flows in equilibrium. Higher values of β_0 may be chosen for strongly sheared flows. The variable ρ/ρ_0 in the above expression is the total amount of compression the shear flow experiences. It is equated to the density ratio across the shock wave which the Rankine-Hugoniot equations relate to the shock-normal Mach number, M_n. *i.e.*

$$\frac{\rho}{\rho_0} = \frac{(\gamma + 1)M_n^2}{2 + (\gamma - 1)M_n^2} \tag{2.21}$$

Thus, once the strength and inclination angle of the shock wave is known, its effect on the shear flow can be predicted.

Consider the following two examples: the interaction of a shear flow with a Mach 1.5 normal shock and shock/turbulence interaction in a compression corner with free-stream Mach number 2.9 and wedge angle 8°. The compression corner corresponds to an experiment by Smits and Muck (1989).

The evolution of R_{ij} and R_{ij}/q^2 is predicted for both cases. The incident turbulence is assumed to be in equilibrium and hence β_0 was taken as 2.5. For the normal shock problem, it is clear that M_n and θ are 1.5 and 0° respectively. In the case of the compression corner, these parameters are obtained by assuming that the flow is turned across a single shock wave. Solution of the corresponding oblique shock equations yields $M_n = 1.29$ and $\theta = 63.65°$. Another point to be noted is that the coordinate system in our analysis was

30

aligned with the direction of mean shear. However experimental coordinate systems are aligned with the local wall direction. As a result, the compression corner problem requires that the Reynolds stresses predicted by our analysis be rotated by the wedge angle to be consistent with experiments. The results are tabulated below.

	R_{11}	R_{22}	R_{33}	R_{11}/q^2	R_{22}/q^2	R_{33}/q^2	R_{12}/q^2
Normal	2.60	1.30	1.60	0.64	0.08	0.28	-0.07
Oblique	1.05	2.22	1.40	0.40	0.22	0.38	-0.21

2.6 Application to Reynolds Stress modeling

The analysis described in the preceding sections reveals significant effects of anisotropy on the response of shear flows to compression. The spectral distribution of energy prior to compression is seen to strongly influence the Reynolds stresses through the pressure-strain correlation. In this section, we consider Reynolds stress modeling of the normal compression problem to see if the model equations reproduce the evolution as predicted by RDT. Since the pressure-strain correlation is the only term that needs to be modelled, the RDT limit is a natural choice to evaluate models of the rapid pressure-strain correlation.

We evaluate models of the form: $\pi_{ij} = \pi_{ij}(b_{ij}, S^*_{ij}, \Omega_{ij})$. Linear, quadratic and cubic forms of these models exist. We only consider the linear version of these models. The objective here is to see how these models perform inspite of the absence of explicit spectral information. Consider

$$\pi_{ij} = q^2 \left[\frac{2}{5} S^*_{ij} + C_2 \left(S^*_{il} b_{lj} + S^*_{jl} b_{li} - \frac{2}{3} S^*_{lm} b_{ml} \delta_{ij} \right) + C_3 \left(\Omega_{il} b_{lj} + \Omega_{jl} b_{il} \right) \right] \qquad (2.22)$$

The models of several workers; eg Launder, Reece and Rodi (), Naot, Shavit and Wolfshtein() and Zeman() are of the above form, differing only in the constants C_2 and C_3.

During simultaneous shear and compression (Section 2.3.1) S^*_{ij} and Ω_{ij} are given by,

$$S^*_{ij} = \frac{\Gamma_0}{1 + \Gamma_0 t'} \begin{pmatrix} \frac{2}{3} & \frac{1}{2} \frac{S_0}{\Gamma_0} & 0 \\ \frac{1}{2} \frac{S_0}{\Gamma_0} & -\frac{1}{3} & 0 \\ 0 & 0 & -\frac{1}{3} \end{pmatrix}, \quad \Omega_{ij} = \frac{\Gamma_0}{1 + \Gamma_0 t'} \begin{pmatrix} 0 & \frac{1}{2} \frac{S_0}{\Gamma_0} & 0 \\ -\frac{1}{2} \frac{S_0}{\Gamma_0} & 0 & 0 \\ 0 & 0 & 0 \end{pmatrix} \qquad (2.23)$$

where $t' = t - t_0$. In the limit $S_0/\Gamma_0 \ll 1$,

$$S^*_{ij} = \frac{\Gamma_0}{1 + \Gamma_0 t'} \begin{pmatrix} \frac{2}{3} & 0 & 0 \\ 0 & -\frac{1}{3} & 0 \\ 0 & 0 & -\frac{1}{3} \end{pmatrix}, \quad \Omega_{ij} = 0 \qquad (2.24)$$

31

We consider the evolution of R_{11} and R_{12}. Substitution of S_{ij}^* and Ω_{ij} into equation (2.22) yields

$$\pi_{11} = \frac{2}{3}q^2 \frac{\Gamma_0}{1 + \Gamma_0 t'} \left[\frac{2}{5} + C_2 b_{11} \right] \tag{2.25}$$

Note that the trace-free property of b_{ij} is used to obtain the above expression. Also

$$\pi_{12} = \frac{1}{3}q^2 \frac{\Gamma_0}{1 + \Gamma_0 t'} C_2 b_{12} \tag{2.26}$$

The modeled equations may be solved analytically in the RDT limit to obtain the Reynolds stresses. Consider

$$\frac{dR_{11}}{dt} = -2 \frac{\Gamma_0}{1 + \Gamma_0 t'} R_{11} + \pi_{11} \tag{2.27a}$$

$$\frac{dq^2}{dt} = -2 \frac{\Gamma_0}{1 + \Gamma_0 t'} R_{11} \tag{2.27b}$$

Defining a variable $f = R_{11}/q^2 = b_{11} + 1/3$, the above equations may be manipulated to obtain

$$\frac{df}{dt'} = 2 \frac{\Gamma_0}{1 + \Gamma_0 t'} (f^2 - f) + \frac{\pi_{11}}{q^2} \tag{2.28}$$

Substituting for π_{11}/q^2,

$$\frac{df}{dt'} = 2 \frac{\Gamma_0}{1 + \Gamma_0 t'} \left[f^2 + f\left(\frac{C_2}{3} - 1\right) + \frac{1}{3}\left(\frac{2}{5} - \frac{C_2}{3}\right) \right] \tag{2.29}$$

Denoting f at $t' = 0$ by f_0, the above equation may be integrated to yield

$$f = \frac{r_1 - \kappa r_2}{1 - \kappa} \tag{2.30}$$

where, κ is defined as

$$\kappa = \frac{f_0 - r_1}{f_0 - r_2} (1 + \Gamma_0 t')^{2(r_1 - r_2)} \tag{2.31}$$

r_1 and r_2 are the roots of $f^2 + f\left(\frac{C_2}{3} - 1\right) + \frac{1}{3}\left(\frac{2}{5} - \frac{C_2}{3}\right) = 0$ and are given by

$$r_{1,2} = \frac{1}{2}\left[-\left(\frac{C_2}{3} - 1\right) \pm \sqrt{\left(\frac{C_2}{3} - 1\right)^2 - \frac{4}{3}\left(\frac{2}{5} - \frac{C_2}{3}\right)} \right] \tag{2.32}$$

Once f is known, q^2 may be calculated as follows. We rewrite equation (2.27b) as,

$$\frac{dq^2}{dt'} = -2 \frac{\Gamma_0}{1 + \Gamma_0 t'} f q^2 \tag{2.33}$$

32

Substituting for f and integrating, we get,

$$\frac{q^2}{q_0^2} = \frac{1-\kappa}{1-\kappa_0}\left(\frac{\kappa_0}{\kappa}\right)^{\frac{r_1}{r_1-r_2}} \tag{2.34}$$

where, the subscript '0' corresponds to time $t' = 0$. Note that κ may be expressed in terms of the total volumetric strain ; i.e.,

$$\kappa = \frac{f_0 - r_1}{f_0 - r_2}\left(\frac{\rho}{\rho_0}\right)^{-2(r_1-r_2)} \tag{2.35}$$

We next compare the predicted values of R_{11} and q^2 with the RDT evolution. Our choice of C_2 in the above equations is dictated by the asymptotic behavior of the model solution. Equations (2.32) and (2.35) show that in the limit of infinite volumetric strain, $\kappa \to \infty$ and hence $f \to r_2$. Siince r_2 depends only upon C_2, this suggests that the asymptotic value of R_{11}/q^2 as predicted by the model is independent of the initial anisotropy. This behavior is in agreement with RDT. This independence of R_{11}/q^2 of the initial condition allows the asymptotic values to be determined from the compression of isotropic turbulence. It can be shown (Lee, 1989) that R_{11}/q^2 asymptotes to $1/2$. Equating r_2 to $1/2$ and solving the resulting equation for C_2, we get

$$C_2 = \frac{21}{10} \tag{2.36}$$

Figure 2.18 compares the predicted evolution of R_{11} to the RDT solution. The compression of isotropic turbulence ($\beta_0 = 0$) and sheared turbulence ($\beta_0 = 2.5$) are both plotted. Note that the model predicts R_{11} quite well when the initial state is isotropic. However, the amplification of R_{11} in the shear flow is considerably underpredicted. Similar behavior is observed in Figure 2.19 where the evolution of q^2 is plotted. The evolution of isotropic turbulence is predicted well while the amplification of kinetic energy in the shear flow is underpredicted. This behavior of the model solution is attributed to the lack of spectral information which prevents it from reproducing the suppression of π_{11} in the shear flow.

Similarly the model is unable to reproduce the drop and change in sign of Reynolds shear stress. This is shown as follows. The evolution of R_{12} is given by equation (2.13) as

$$\frac{d}{dt'}R_{12} = \frac{\Gamma_0}{1+\Gamma_0 t'}\left[-R_{12} - \frac{S_0}{\Gamma_0}R_{22}\right] + \pi_{12} \tag{2.37}$$

Using the model expression for π_{12} as given in equation (2.26) we get,

$$\frac{d}{dt'}R_{12} = \frac{\Gamma_0}{1+\Gamma_0 t'}\left[-R_{12} - \frac{S_0}{\Gamma_0}R_{22} + \frac{C_2}{3}R_{12}\right] \qquad (2.38)$$

In the limit $S_0/\Gamma_0 \ll 1$, this becomes

$$\frac{d}{dt'}R_{12} = \frac{\Gamma_0}{1+\Gamma_0 t'}\left(\frac{C_2}{3}-1\right)R_{12} \qquad (2.39)$$

Integration of the above equation yields

$$R_{12} = R_{12}^0\left(1+\Gamma_0 t'\right)^{C_2/3-1} \qquad (2.40)$$

Since Γ_0 is negative, the above equation predicts an *increase* in the Reynolds shear stress upon normal compression. Thus, presence of spectral information seems to be particularly important in predicting the evolution of R_{12}.

2.7. Summary

Homogeneous rapid distortion theory was used to examine the response of incompressible, turbulent shear flows to rapid one-dimensional compression. Both normal and oblique compressions (with respect to the shear) were considered. The response of shear flows to compression is found to be quite different from the previously studied, compression of isotropic turbulence. The differences are interpreted in a more general framework and the relevant parameters influencing kinetic energy amplification are identified.

$E_{11}(\kappa_1)$ of the initial field is found to determine the evolution of the streamwise (the direction of compression) component of kinetic energy. Flows with u_1 at lower κ_1 have a reduced effect of pressure during compression and hence a higher amplification of u_1. The evolution of q^2 upon compression is influenced by the initial fraction of kinetic energy in the direction of compression $(\overline{u_1^2}/q^2)$, in addition to the initial $E_{11}(\kappa_1)$. Flows with a larger value of initial $\overline{u_1^2}/q^2$ and u_1 at lower κ_1 have a larger amplification of q^2.

Upon normal compression, all components of turbulent kinetic energy of sheared turbulence are amplified with the streamwise component being amplified the most. The amplification of $\overline{u_1^2}$ and q^2 is higher than that in isotropic turbulence. Normal compression decreases the turbulent shear stress and for large enough compressions changes its sign. Examination of the terms in the shear stress evolution equation show that amplification of the pressure-strain correlation upon compression is responsible for this behavior.

34

The oblique angle between the directions of shear and compression is seen to significantly affect the response of sheared turbulence to compression. The effect of oblique angle on the evolution of kinetic energy may be explained by the initial distribution of $E_{\theta\theta}(\kappa_\theta)$ and $\overline{u_\theta}^2/q^2$, where θ is the direction of compression. Over a range of oblique angles varying from $-60°$ to $60°$ the amplification of $\overline{u_1^2}$ and q^2 is seen to decrease with increasing magnitude of oblique angle. Also oblique compression reduces the tendency of the shear stress to decrease in magnitude; for large oblique angles the shear stress amplifies.

With respect to shock/turbulence interaction, our results suggest that besides shock strength (defined in terms of the normal Mach number), the anisotropy of the turbulence and the shock inclination angle are important parameters in determining the evolution of turbulence across the shock. It is striking that the evolution of the Reynolds stresses upon oblique compression is qualitatively different for different oblique angles. These important effects of initial anisotropy and the shock inclination angle should be accounted for in the interpretation of experiments on shock/turbulence interaction.
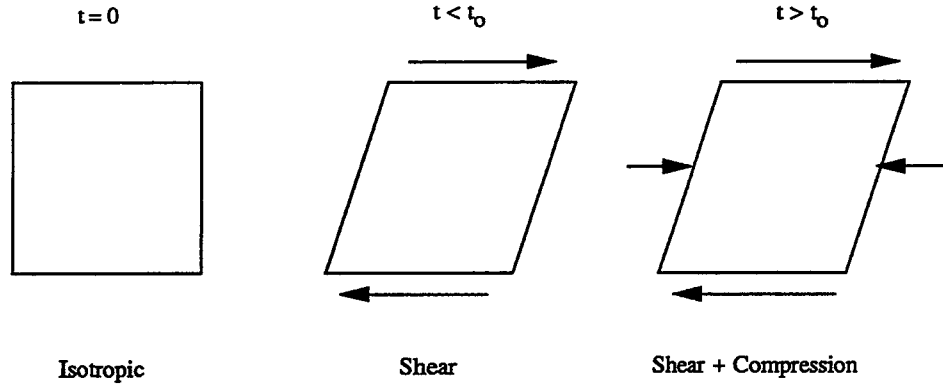
FIG. 2.1. Schematic of the mean velocity field in the normal compression of a turbulent shear flow.
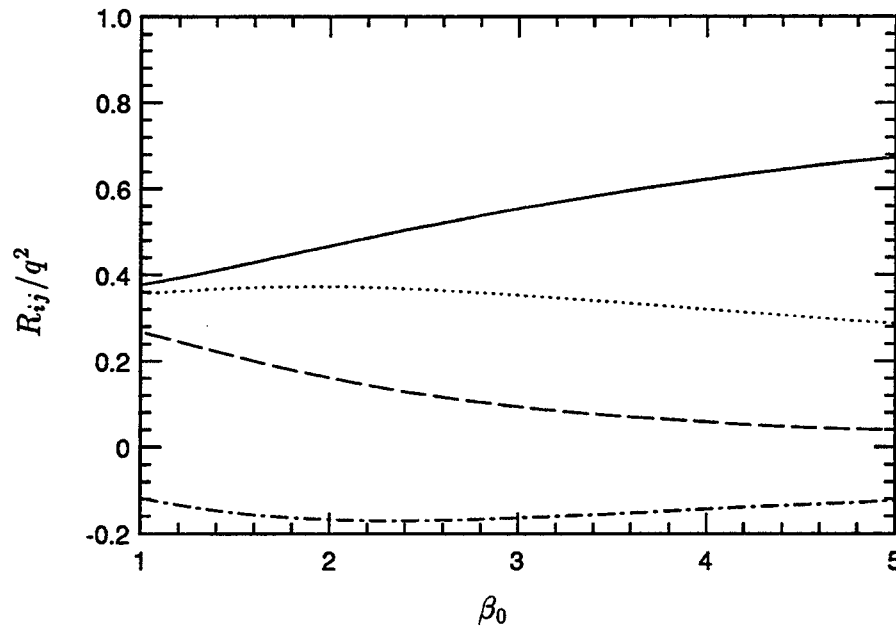
FIG. 2.2. Evolution of R_{ij}/q^2 as predicted by RDT applied to the homogeneous shear of initially isotropic turbulence. ——— (R_{11}/q^2), ---- (R_{22}/q^2), ········ (R_{33}/q^2), —--- (R_{12}/q^2).
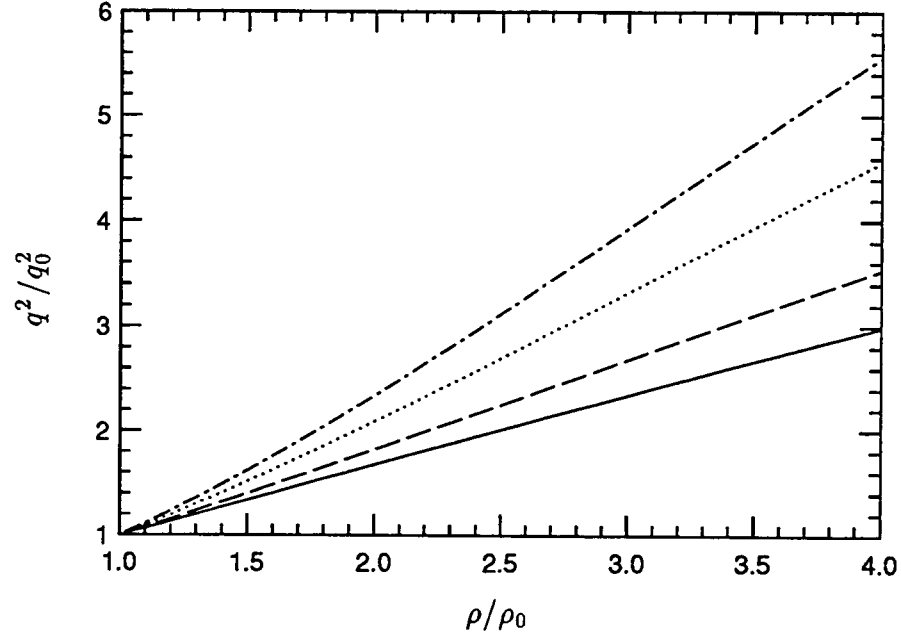
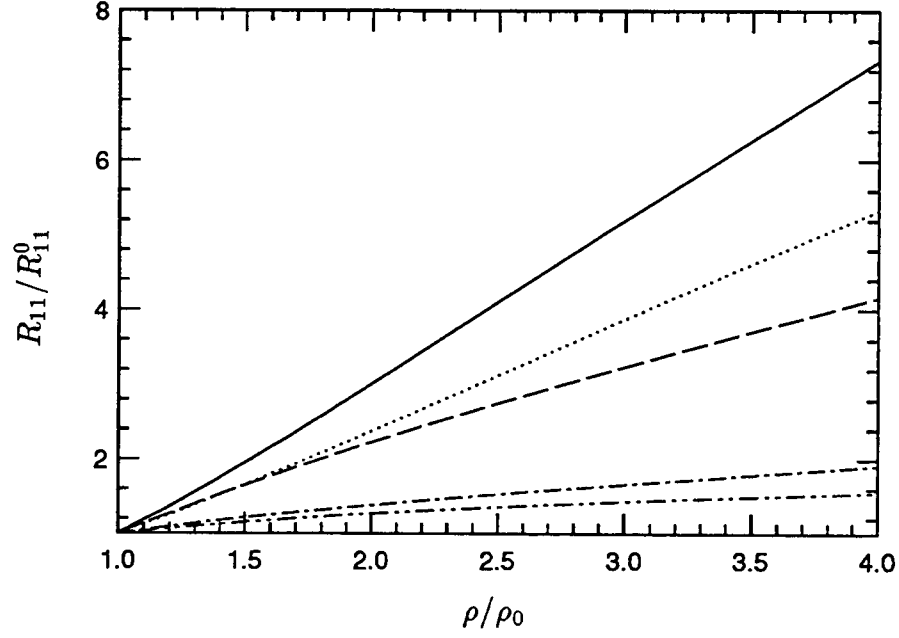FIG. 2.3. Evolution of q^2 upon the normal compression of sheared turbulence. The different curves correspond to different values of initial total shear. ——— ($\beta_0 = 0$), ---- ($\beta_0 = 1$), ········ ($\beta_0 = 2$), ——— ($\beta_0 = 3$).
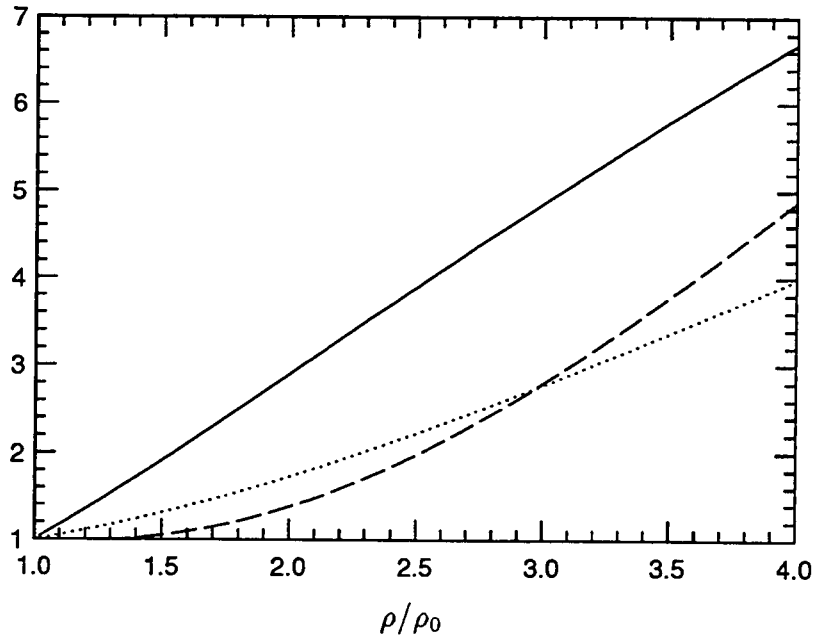
FIG. 2.4. Evolution of the components of turbulent kinetic energy when sheared turbulence ($\beta_0 = 3$), is subjected to normal compression. ——— (R_{11}), ---- (R_{22}), ········ (R_{33}).
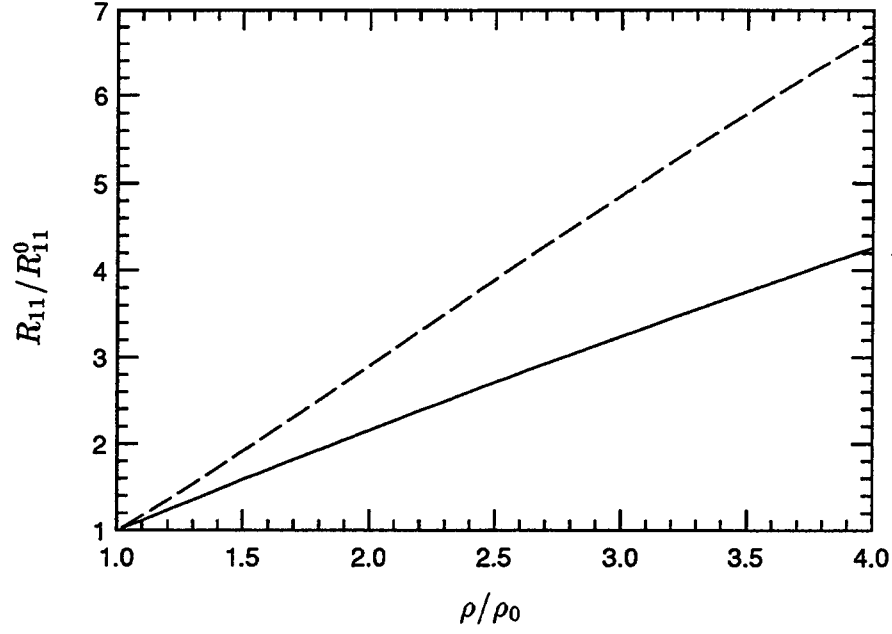
FIG. 2.5. Comparison of the amplification of R_{11} of sheared turbulence ($\beta_0 = 3$) to that of isotropic turbulence. —— (Isotropic), ———— (Sheared).
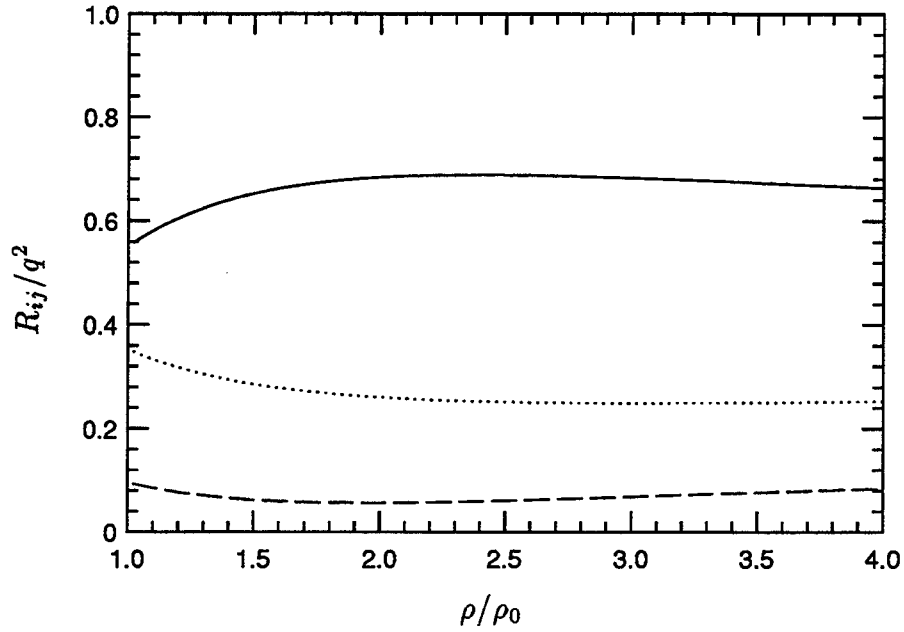
FIG. 2.6. Evolution of R_{ij}/q^2 when sheared turbulence ($\beta_0 = 3$) is subjected to normal compression. —— (R_{11}/q^2), ———— (R_{22}/q^2), ········ (R_{33}/q^2).
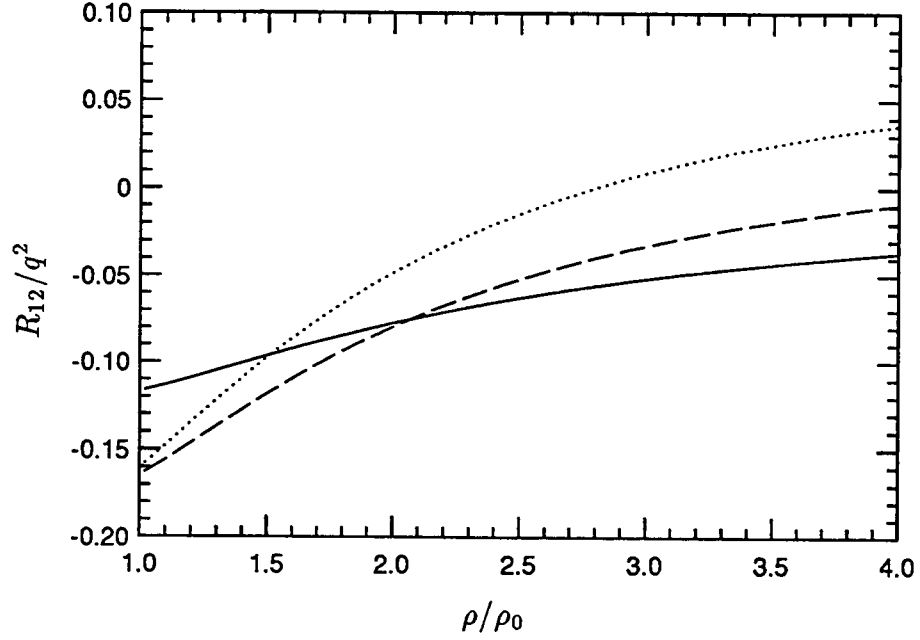
FIG. 2.7. Evolution of R_{12}/q^2 when sheared turbulence is subjected to normal compression. The different curves correspond to different values of initial total shear. ——— ($\beta_0 = 1$), ---- ($\beta_0 = 2$), ········ ($\beta_0 = 3$).
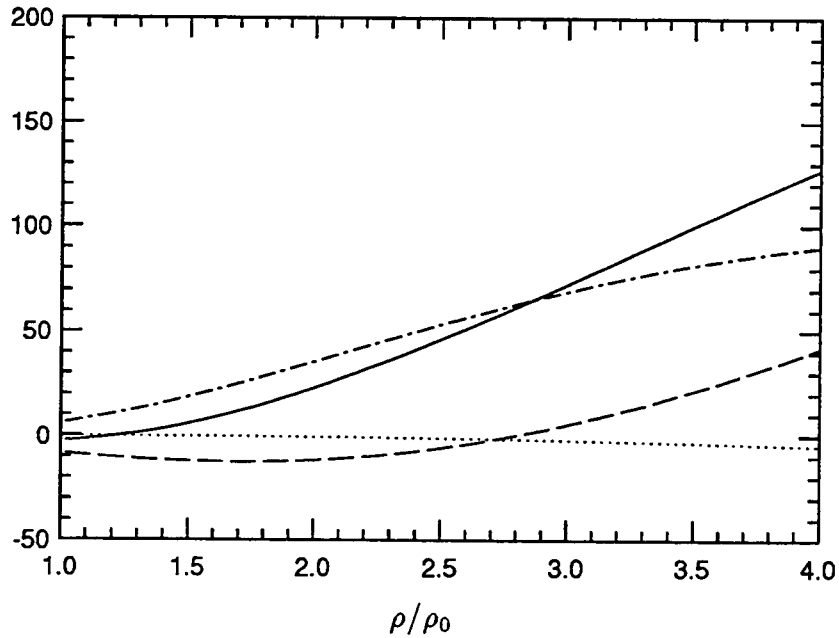
FIG. 2.8. Budget of terms in the R_{12} evolution equation during the normal compression of a shear flow ($\beta_0 = 3$). ——— (LHS), ---- (Compression production), ········ (Shear production), ——— (Pressure-strain correlation).
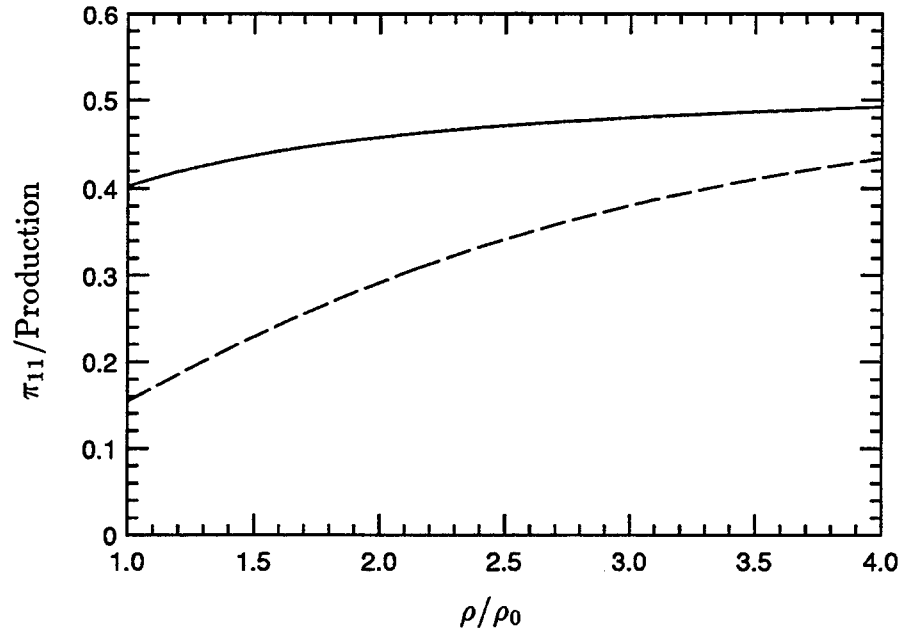
FIG. 2.9. Evolution of the ratio of π_{11} to the production term in the R_{11} equation upon normal compression. The compression of sheared turbulence ($\beta_0 = 3$) is compared to that of isotropic turbulence. ——— (Isotropic), ———— (Sheared).
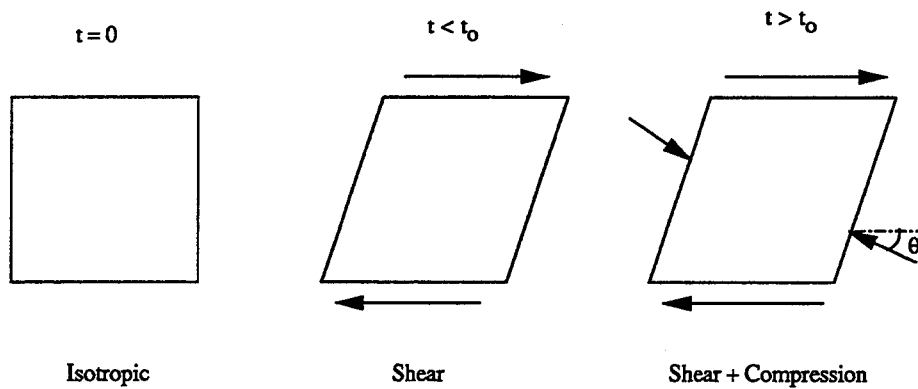
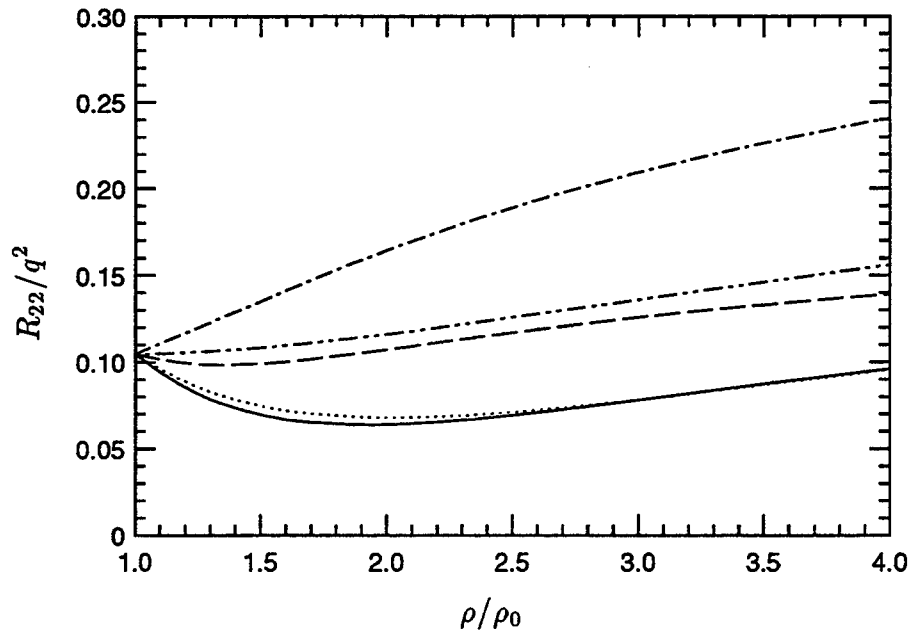FIG. 2.10. Coordinate system used in the analysis of oblique compression of sheared turbulence

40

FIG. 2.11. Evolution of R_{11} upon the oblique compression of sheared turbulence ($\beta_0 = 3$). The different curves correspond to different values of oblique angle. ——— ($\theta = 0°$), ———— ($\theta = 30°$), ········ ($\theta = -30°$), —·— ($\theta = 60°$), —··— ($\theta = -60°$).
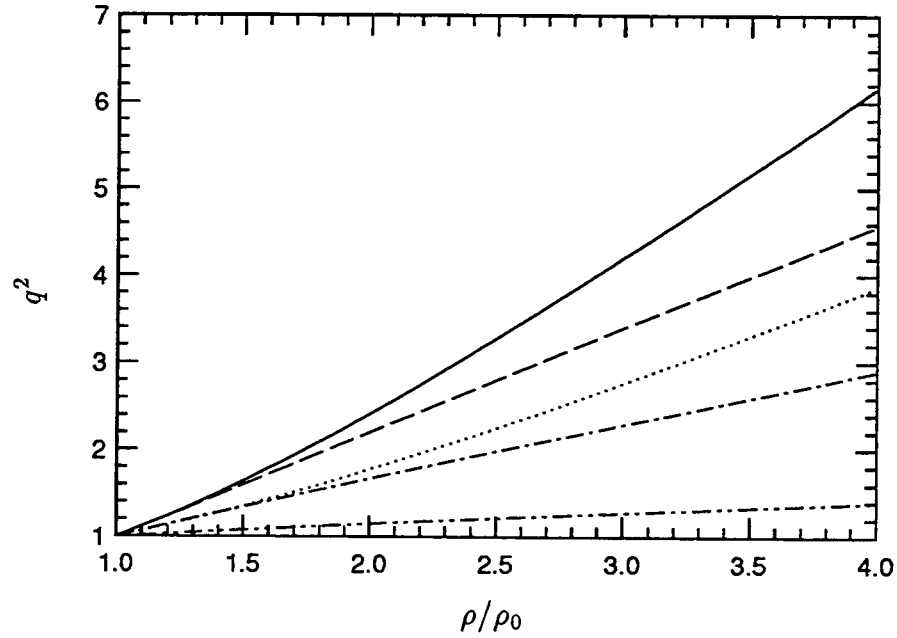
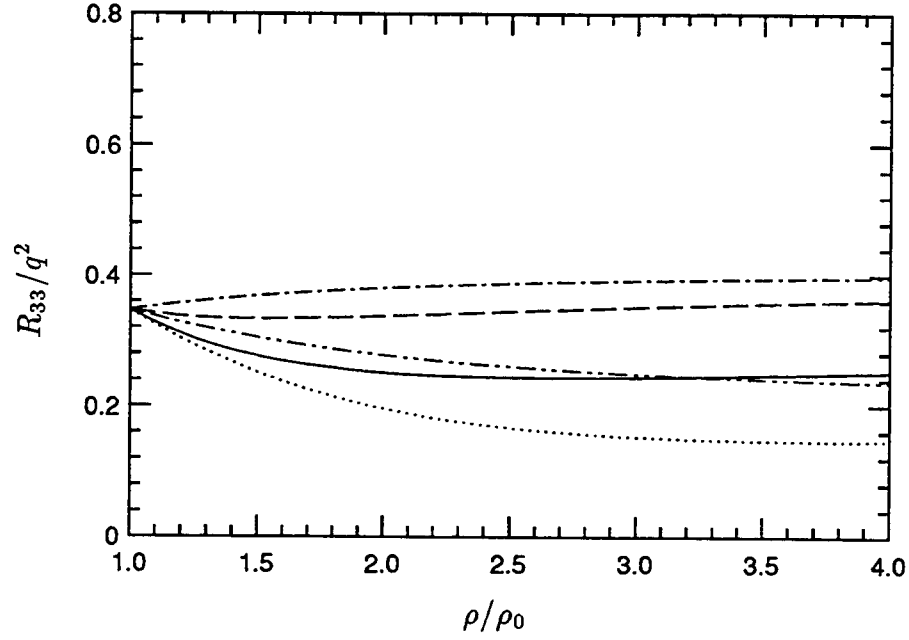
FIG. 2.12. Evolution of q^2 upon the oblique compression of sheared turbulence ($\beta_0 = 3$). The different curves correspond to different values of oblique angle. ——— ($\theta = 0°$), ———— ($\theta = 30°$), ········ ($\theta = -30°$), —·— ($\theta = 60°$), —··— ($\theta = -60°$).
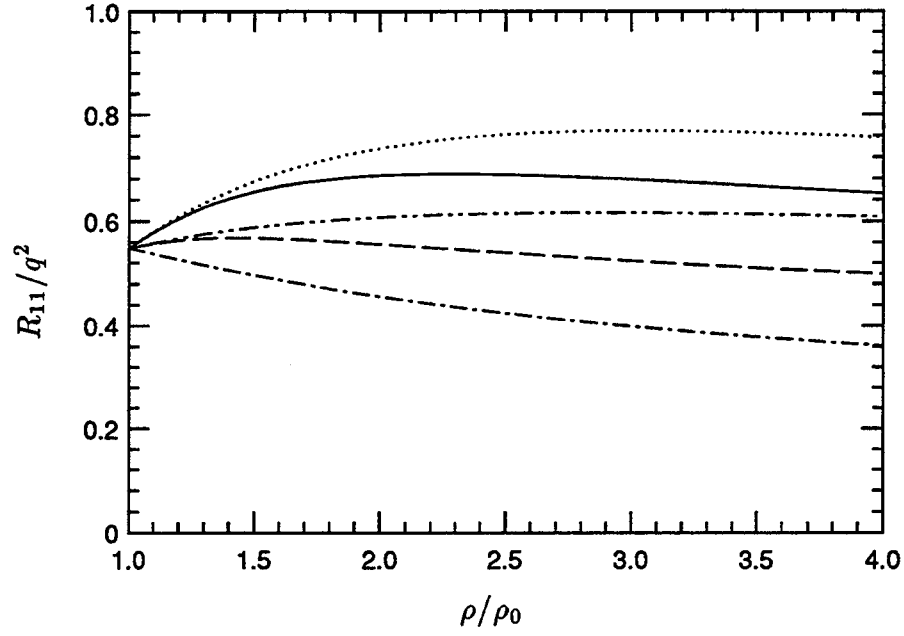
FIG. 2.13. Evolution of R_{11}/q^2 upon the oblique compression of sheared turbulence ($\beta_0 = 3$). The different curves correspond to different values of oblique angle. ——— ($\theta = 0°$), - - - - ($\theta = 30°$), ········ ($\theta = -30°$), — — — ($\theta = 60°$), —·—·— ($\theta = -60°$).
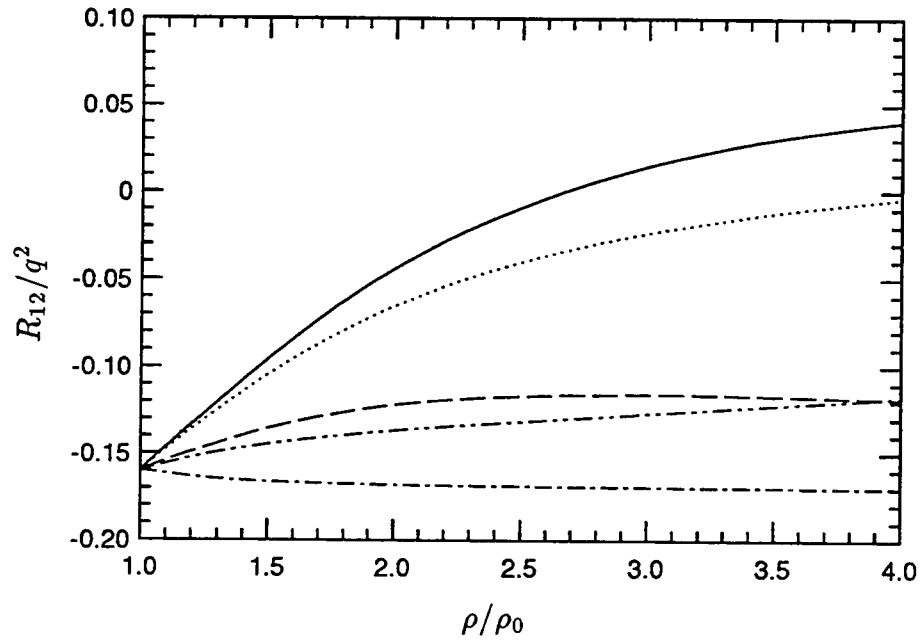

FIG. 2.14. Evolution of R_{22}/q^2 upon the oblique compression of sheared turbulence ($\beta_0 = 3$). The different curves correspond to different values of oblique angle. ——— ($\theta = 0°$), - - - - ($\theta = 30°$), ········ ($\theta = -30°$), — — — ($\theta = 60°$), —·—·— ($\theta = -60°$).

FIG. 2.15. Evolution of R_{33}/q^2 upon the oblique compression of sheared turbulence ($\beta_0 = 3$). The different curves correspond to different values of oblique angle. ———— ($\theta = 0°$), ———— ($\theta = 30°$), ········ ($\theta = -30°$), ———·— ($\theta = 60°$), ——··— ($\theta = -60°$).

FIG. 2.16. Evolution of R_{12}/q^2 upon the oblique compression of sheared turbulence ($\beta_0 = 3$). The different curves correspond to different values of oblique angle. ———— ($\theta = 0°$), ———— ($\theta = 30°$), ········ ($\theta = -30°$), ———·— ($\theta = 60°$), ——··— ($\theta = -60°$).
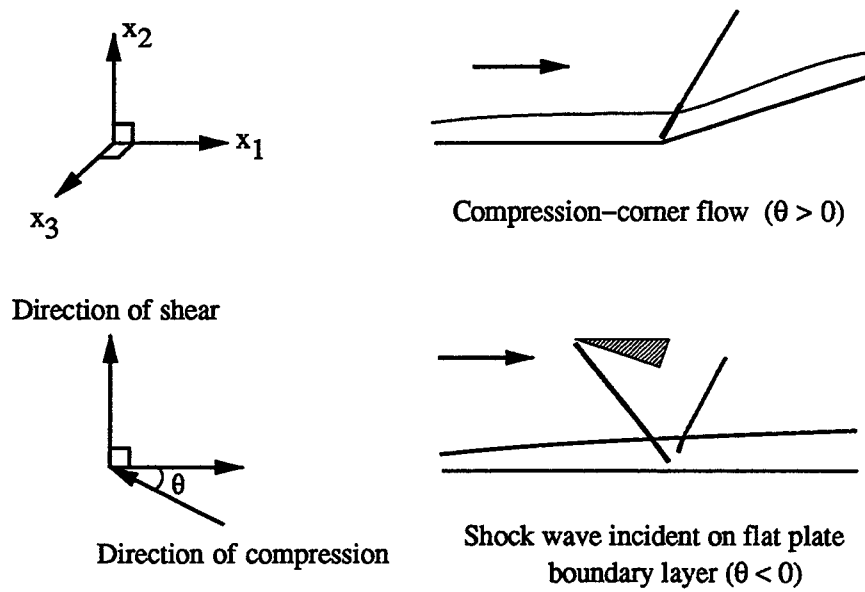
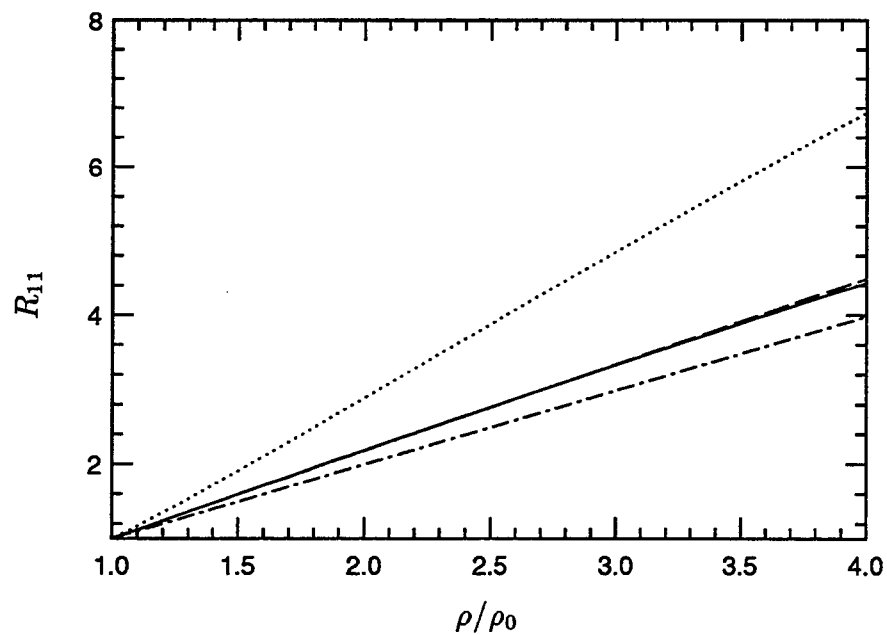FIG. 2.17. Examples of the oblique compression of a shear flow.

FIG. 2.18. Comparison of model solution to RDT prediction of R_{11}. ——— (Isotropic; RDT), ———— (Isotropic; model), ········ (Sheared; RDT), ——·—— (Sheared; model).
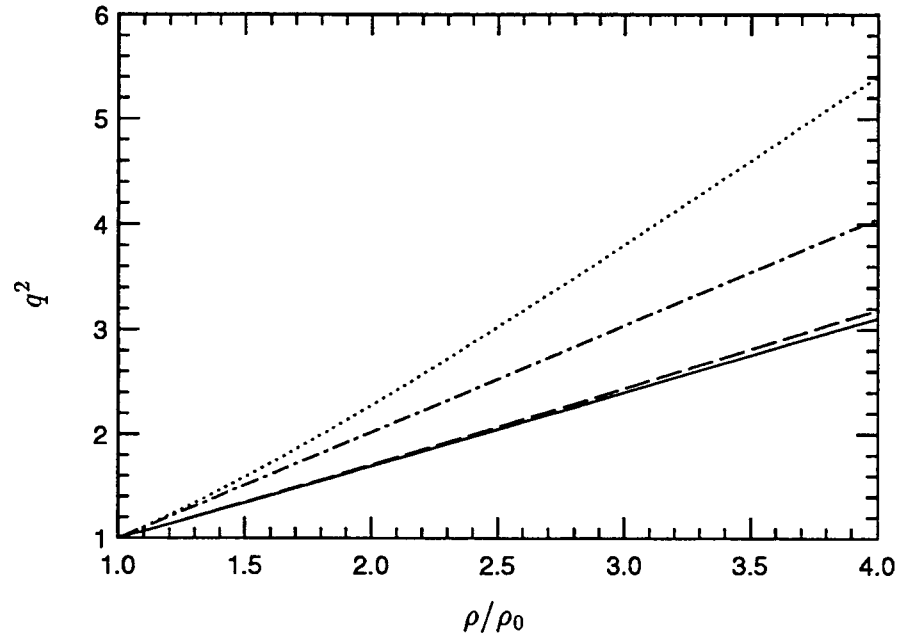
FIG. 2.19. Comparison of model solution to RDT prediction of q^2. —— (Isotropic; RDT), – – – (Isotropic; model), ········ (Sheared; RDT), — – — (Sheared; model).

PART THREE

The combined interaction of vorticity and entropy fluctuations with a shock wave

By KRISHNAN MAHESH, SANJIVA K. LELE[†] AND PARVIZ MOIN[‡]

Department of Mechanical Engineering, Stanford University, Stanford, California 94305, USA

Inviscid linear analysis is used to study the simultaneous interaction of a shock wave with vorticity and entropy fluctuations. The two-dimensional interaction of the shock with a plane vorticity-entropy wave is initially considered. The analysis is compared to numerical computations and then extended to examine the evolution of an isotropic field of vorticity and entropy fluctuations across the shock. Expressions are derived for the flow-field behind the shock and the distortion of the shock front.

The amplitude and nature of correlation between vorticity and entropy fluctuations are shown to significantly affect the level of kinetic energy, sound and thermodynamic fluctuations behind the shock wave. Entropy fluctuations in phase with the vorticity fluctuations (u' and T' negatively correlated) enhance the amplification of kinetic energy, vorticity and thermodynamic fluctuations. Positively correlated fluctuations have the opposite effect. The distortion of the shock front is similarly affected. These trends are explained and a scaling proposed for the evolution of vorticity fluctuations across the shock.

The applicability of Morkovin's hypothesis across a shock wave is examined. Statistics in the far-field indicate that neglect of the acoustic mode is a good approximation in the far-field of shock waves of moderate strength ($M_1 < 2$). The part of the hypothesis relating u' and T' is seen to be invalid behind the shock. The deviation is shown to be a result of oscillation of the shock front.

The results indicate the considerable importance of entropy fluctuations in the evolution of the turbulent fluctuations in a compressible boundary layer upon its interaction with a shock wave.

---

1. Introduction

The interaction of a shock wave with a turbulent boundary layer has received considerable attention over the past five decades. There have been several experimental studies

[†] Also with Department of Aeronautics and Astronautics, Stanford University
[‡] Also with NASA Ames Research Center

of the flow in a compression corner, normal shock/boundary layer interaction and more recently, the interaction of shock waves with three dimensional boundary layers. Green (1970) and Fernholz and Finley (1981) provide comprehensive reviews of earlier data. More recent work is discussed by Settles and Dodson (1994) and Dolling (1993). These experiments testify to the complex flow-field associated with the interaction. Incidence of the shock wave is shown to strongly affect both the mean flow and the turbulent fluctuations. The Reynolds stresses and temperature fluctuations in the boundary layer are seen to amplify across the shock wave. Significant unsteadiness of the shock wave is observed when the boundary layer separates. The motion of the shock wave seems to be correlated with pressure fluctuations in the boundary layer upstream of the shock. Recent experiments by Dolling and coworkers (Dolling; 1993) have examined the fluctuating pressure loads that shock-induced separation produces.

Modeling shock wave/boundary layer interaction remains a challenge. In recognition of the complex nature of the phenomenon, recent studies have examined the simpler and more fundamental problem of the interaction of homogeneous turbulence with a shock. These studies which include experiments, computation and analysis observe the turbulence to be affected in a manner similar to boundary layer turbulence. The experiments of Keller amd Merzkirch (1990) and Honkan and Andreopoulous (1990) report amplification of turbulent kinetic energy of grid-generated turbulence across a shock wave. The simulations of Lee, Lele and Moin (1993,1994) and Hannapel and Friedrich (1994) report similar enhancement in vorticity, kinetic energy and thermodynamic fluctuations. A point of contention exists between experiment and computation; experiments report an increase in turbulence lengthscale across the shock while computations show a drop. As noted by Lele (1993) this issue is currently unresolved.

There has been renewed interest in the linear analysis of shock/turbulence interaction. Issues of 'shock-noise' and shock-stability in the past led several workers to examine the interaction of a shock wave with a weak field of unsteady disturbances. A brief review of linear analysis is given by Mahesh, Lee, Lele and Moin (1994b). Ribner (1953, 1954, 1969, 1987) appears to have been the first to use linear analysis to predict the interaction of isotropic vortical turbulence with a shock wave. Detailed comparison by Lee, Lele and Moin (1994) show good agreement between their computations and Ribner's analysis. Moore (1954) and Chang (1957) have performed detailed analysis of the interaction of a shock wave with an acoustic wave and entropy wave respectively. The influence of the dilatational component on the evolution of a turbulent flow across a shock was examined by Mahesh, Lee, Lele and Moin (1994b) who extended Moore's analysis to consider the

interaction of an isotropic field of acoustic waves with a shock wave. A drop in kinetic energy was observed for Mach numbers between 1.25 and 1.8. For Mach numbers beyond 3, the kinetic energy was found to amplify by levels significantly exceeding those in Ribner's problem. Anisotropy of the turbulence and the obliquity of the shock wave were identified as important parameters in shock wave/boundary layer interaction by the analysis of Mahesh, Lele and Moin (1994a).

The importance of entropy fluctuations in shock wave/boundary layer interaction seems to be underappreciated. Morkovin (1961) hypothesized that the turbulent fluctuations in compressible boundary layers are essentially composed of vorticity and entropy modes; *i.e.* the acoustic mode is negligible. This hypothesis along with the assumption of negligible fluctuations in stagnation temperature leads to the following relation between the thermodynamic and velocity field,

$$\frac{\rho'}{\bar{\rho}} = -\frac{T'}{\bar{T}} = (\gamma - 1)M^2 \frac{u'}{U} \tag{1}$$

A considerable body of experimental evidence supports the above hypothesis. In fact, Bradshaw (1977) states 'There is little point in taking turbulence measurements in constant pressure boundary layers at $M < 5$ to check Morkovin's hypothesis, except possibly for intermittency measurements'. Morkovin's hypothesis suggests that in addition to being correlated, the intensity of vorticity and entropy fluctuations in a turbulent boundary layer are of comparable magnitude. Experimental data (Fernholz and Finley; 1981) shows $\rho'/\bar{\rho}$ in a constant pressure boundary layer to have a maximum value of about $5\% - 10\%$.

This suggests that entropy fluctuations would play an important role in the interaction of a boundary layer with a shock wave. Study of the influence of entropy fluctuations on shock/turbulence interaction seems to have been restricted to the analysis of plane entropy waves interacting with a shock (Morkovin; 1960, Chang; 1957, Cuadra; 1968). Hesselink and Sturtevant (1988) have conducted experiments on the passage of a shock wave through a random field of entropy fluctuations. Their interest however was in the problem of the sonic boom; the strongest shock they considered was Mach 1.1. The evolution of the shock front in this field of entropy fluctuations was examined in their study. A related problem that several workers have examined is the interaction of a shock wave with a density inhomogeneity. A list of references may be found in a recent paper by Yang, Kubota and Zukoski (1994).

In this paper we seek to identify the quantitative influence that entropy fluctuations exert on the evolution of a turbulent flow across a shock wave. We use inviscid linear analysis to study the combined interaction of vorticity and entropy fluctuations with a shock wave.

To the best of our knowledge, the interaction of a field of entropy fluctuations with a shock wave has not been considered before. Nor does effect of the correlation between vorticity and entropy fluctuations appear to be emphasized.

This paper is organized as follows. The simultaneous interaction of a shock wave with a vorticity and entropy wave (henceforth referred to as vorticity-entropy wave) is formulated in Section 2. Results of the linear analysis are presented in Section 3 and compared in Section 4 to numerical computation. Sections 5 and 6 provide an explanation for the influence of entropy fluctuations and suggest a scaling for the evolution of vorticity across the shock. The analysis is extended in Section 7 to consider the evolution of an isotropic field of vorticity-entropy waves across a shock wave. Section 8 discusses the results. The paper is concluded with a summary of the important conclusions in Section 9. A detailed version of the paper is presented in a report by Mahesh, Lele and Moin (1994c).

2. The interaction of a vorticity-entropy wave with a shock wave

2.1 The three modes in a compressible medium

Kovasznay (1953) showed that fluctuations of small amplitude in a compressible medium could be decomposed into vorticity, acoustic and entropy modes. These modes were shown to evolve independently in the inviscid limit for uniform mean flow. The vorticity mode as defined by Kovasznay has no pressure or density fluctuations. It has a solenoidal velocity field that is convected by the mean flow. The acoustic mode travels at the speed of sound relative to the mean flow, has isentropic pressure and density fluctuations and a corresponding irrotational velocity field that satisfies the acoustic wave equation. The entropy mode is convected by the mean flow and has no velocity or pressure fluctuations; it has only density and temperature fluctuations.

The independent evolution of these modes in the inviscid limit implies that the fluctuating velocity field is a linear superposition of acoustic and vortical modes. Similarly, the density and temperature fields are superpositions of acoustic and entropic components. The pressure field is associated solely with the acoustic mode.

2.2 Formulation of the problem

The two-dimensional interaction of a shock wave with a plane vorticity-entropy wave is schematically illustrated in Figure 1. The two-dimensional problem will be extended to describe the interaction of the shock with a three-dimensional field of turbulence in Section 7. Note that the shock wave is stationary in the mean. The variables $U, P, \overline{p}, \overline{T}$ and M denote the mean velocity, pressure, density, temperature and Mach number respectively and subscripts 1 and 2 denote the upstream and downstream states. The flow upstream

of the shock wave is perturbed by the weak disturbance field of the incident vorticity-entropy wave which is assumed to be a plane wave that makes angle ψ_1 with the x axis. The variables u, v, p, ρ and T represent the fluctuating velocities, pressure, density and temperature. The incident field has the following form:

$$\frac{u_1'}{U_1} = lA_v \; e^{ik(mx+ly-U_1mt)} \tag{2a}$$

$$\frac{v_1'}{U_1} = -mA_v \; e^{ik(mx+ly-U_1mt)} \tag{2b}$$

$$\frac{\rho_1'}{\overline{\rho}_1} = A_e \; e^{ik(mx+ly-U_1mt)} \tag{2c}$$

$$\frac{T_1'}{\overline{T}_1} = -\frac{\rho_1'}{\overline{\rho}_1} \tag{2d}$$

$$p_1' = 0 \tag{2e}$$

where the variables $m = \cos\psi_1$ and $l = \sin\psi_1$. The shock wave deforms in response to the incident disturbance; the displacement is denoted by $x = \xi(y,t)$.

The analysis involves solution of a boundary-value problem for the shock displacement and the flow field behind the shock wave. The governing equations behind the shock wave are the Euler equations that are linearized about the uniform flow behind the shock. Boundary conditions are imposed at $x = 0$ (the mean position of the shock wave) by linearizing the Rankine Hugoniot equations in a frame of reference that moves at the instantaneous speed of the shock wave. The equations are solved in consonance with the boundary conditions to yield the flow behind the shock wave and the distortion of the shock front.

The solution could be obtained by superposing the solutions to the interaction of the shock with a vorticity and entropy wave independently. Rather than use results of different workers (Ribner; 1953, Chang; 1957), we solve the above set of equations. Comparison will reveal our method of solution to be much simpler. In the process, the independent interaction of the shock with vorticity and entropy waves become special cases of our analysis and will be used as baseline cases for comparison. Our solution in these limiting cases is of course identical to that of the above workers.

2.3 The solution behind the shock wave

Details of the analysis are presented in Appendix A. The solution behind the shock wave has two different regimes that differ in the nature of the pressure field. The incidence angle of the disturbance ψ_1 and the Mach number of the shock wave M_1 determine the

regime of the solution. For a given Mach number, the two regimes are demarcated by a critical angle of incidence denoted by ψ_c. If $0 < \psi_1 < \psi_c$, the pressure field behind the shock wave (and hence its associated velocity and thermodynamic field) is a plane wave. If however, $\psi_c < \psi_1 < \pi/2$, the pressure field behind the shock wave corresponds to an evanescent wave and decays exponentially. The vorticity and entropy fields behind the shock wave correspond to plane waves over both regimes. The critical angle ψ_c is a root of the following equation:

$$\cot^2 \psi_c = \left(\frac{a_2^2}{U_1^2} - \frac{U_2^2}{U_1^2} \right) \tag{3}$$

Note that ψ_c is a function of the Mach number of the shock wave. The existence of two regimes of the pressure field is a common feature of problems involving acoustic wave propagation. Classical examples include the scattering of sound by a vortex sheet and the propagation of sound generated by a flexural wall.

The solution behind the shock wave may be represented as a superposition of vortical, acoustic and entropic components. It has the following dimensionless form:

$$\frac{1}{A_v} \frac{u_2'}{U_1} = \widetilde{F} \, e^{i\widetilde{k}x} e^{ik(ly - mU_1 t)} + \widetilde{G} \, e^{ik(mrx + ly - mU_1 t)}$$

$$\frac{1}{A_v} \frac{v_2'}{U_1} = \widetilde{H} \, e^{i\widetilde{k}x} e^{ik(ly - mU_1 t)} + \widetilde{I} \, e^{ik(mrx + ly - mU_1 t)}$$

$$\frac{1}{A_v} \frac{p_2'}{P_2} = \widetilde{K} \, e^{i\widetilde{k}x} e^{ik(ly - mU_1 t)} \tag{4}$$

$$\frac{1}{A_v} \frac{\rho_2'}{\overline{\rho}_2} = \frac{\widetilde{K}}{\gamma} \, e^{i\widetilde{k}x} e^{ik(ly - mU_1 t)} + \widetilde{Q} \, e^{ik(mrx + ly - mU_1 t)}$$

$$\frac{1}{A_v} \frac{T_2'}{\overline{T}_2} = \frac{\gamma - 1}{\gamma} \widetilde{K} \, e^{i\widetilde{k}x} e^{ik(ly - mU_1 t)} - \widetilde{Q} \, e^{ik(mrx + ly - mU_1 t)}$$

The boundary conditions across the shock wave yield the following expressions for the velocity and slope of the shock front:

$$\frac{1}{A_v} \frac{\xi_t}{U_1} = \widetilde{L} \, e^{ik \, (ly - mU_1 t)}; \qquad \frac{1}{A_v} \xi_y = -\frac{l}{m} \widetilde{L} \, e^{ik \, (ly - mU_1 t)} \tag{5}$$

The variable r denotes the mean density ratio $\overline{\rho}_2/\overline{\rho}_1$ across the shock wave. As indicated in Appendix A, $\widetilde{k}(M_1, \psi_1)$ is the streamwise wavenumber of the acoustic component behind the shock wave. It is real in the propagating regime and complex in the decaying regime. The coefficients $\widetilde{F}, \widetilde{H}$ and $\widetilde{K}$ are associated with the acoustic component. The vortical component is represented by $\widetilde{G}$ and $\widetilde{I}$ while $\widetilde{Q}$ represents the entropy component. The coefficients $\widetilde{F}, \widetilde{H}, \widetilde{K}, \widetilde{G}, \widetilde{I}$ and $\widetilde{Q}$ are functions of M_1, ψ_1 and the amplitude ratio and phase difference between the vorticity and entropy waves (A_e/A_v).

3. Results

Expressions are now derived to describe the streamwise evolution of statistics behind the shock wave. Consider for example the streamwise component of velocity. The kinetic energy associated with this component is denoted by $\overline{u_2'^2} = \overline{u_2' u_2'^*}$ where the overbar implies averaging over the transverse direction and time and the asterisk denotes the complex conjugate. The following expression is obtained for $\overline{u_2'^2}$ from equation (4):

$$\frac{\overline{u_2'^2}}{U_1^2} = [\ |\widetilde{F}|^2\ e^{i(\widetilde{k}-\widetilde{k}^*)x} + |\widetilde{G}|^2 + \widetilde{F}\widetilde{G}^* e^{i(\widetilde{k}-kmr)x} + \widetilde{F}^*\widetilde{G} e^{-i(\widetilde{k}^*-kmr)x}\ ]\ |A_v|^2 \qquad (6)$$

The spatial variation of $\overline{u_2'^2}$ is different over the two regimes. The wavenumber $\widetilde{k}$ is real over the propagating regime and hence

$$\frac{\overline{u_2'^2}}{U_1^2} = [\ |\widetilde{F}|^2 + |\widetilde{G}|^2 + 2(\widetilde{F}_r\widetilde{G}_r + \widetilde{F}_i\widetilde{G}_i)\cos(\widetilde{k} - kmr)x$$
$$- 2(\widetilde{F}_i\widetilde{G}_r - \widetilde{F}_r\widetilde{G}_i)\sin(\widetilde{k} - kmr)x]\ |A_v|^2 \qquad (7)$$

where the subscripts 'r' and 'i' denote the real and imaginary parts respectively. The kinetic energy thus has spatially uniform contributions from the vortical and acoustic modes of the velocity field and an oscillating component whose argument is the phase difference between them. Similar expressions may be written for quantities such as $\overline{v_2'^2}$, density and temperature in the propagating regime. Variables such as vorticity, dilatation and pressure that depend on only one mode are of course spatially uniform. *eg.*,

$$\frac{\overline{p_2'^2}}{P_2^2} = |\widetilde{K}|^2\ |A_v|^2 \qquad (8)$$

The evolution of $\overline{u_2'^2}$ over the decaying regime may be shown to be given by:

$$\frac{\overline{u_2'^2}}{U_1^2} = [\ e^{-2\widetilde{k}_i x}|\widetilde{F}|^2 + |\widetilde{G}|^2 + 2e^{-\widetilde{k}_i x}(\widetilde{F}_r\widetilde{G}_r + \widetilde{F}_i\widetilde{G}_i)\cos(\widetilde{k}_r - kmr)x$$
$$- 2e^{-\widetilde{k}_i x}(\widetilde{F}_i\widetilde{G}_r - \widetilde{F}_r\widetilde{G}_i)\sin(\widetilde{k}_r - kmr)x]\ |A_v|^2 \qquad (9)$$

The corresponding equation for pressure is:

$$\frac{\overline{p_2'^2}}{P_2^2} = e^{-2\widetilde{k}_i x}|\widetilde{K}|^2\ |A_v|^2 \qquad (10)$$

The kinetic energy over this regime is seen to have a spatially uniform vortical component, an acoustic component that decays exponentially behind the shock wave and a damped

oscillating component due to the correlation between the acoustic and vortical modes that the shock wave introduces. In describing the flow-field behind the shock wave, $x = 0$ is referred to as the 'near-field' and $x \to \infty$ is called the 'far-field'. We will see that the far-field values are attained over a distance comparable to the lengthscale of the incident disturbance. As a result, it is the far-field values that are of practical importance.

The analysis is now applied to the interaction of a vorticity-entropy wave with a Mach 1.5 shock wave. Incidence angles of 45° and 75° are considered so that behavior over both regimes is illustrated. (The critical angle is 61.36°). The objective here is to demonstrate the influence of entropy fluctuations and their correlation with the incident vorticity fluctuations. The interaction of the vorticity-entropy waves is therefore contrasted with the independent interaction of the shock with a vorticity wave and entropy wave at the same angle of incidence. These two limiting cases are referred to as the 'pure vorticity' and 'pure entropy' limits.

The normalization of the curves in the pure entropy limit deserves clarification. There is no incident velocity field in the pure entropy limit; *i.e.*, $q_1^2 = \overline{\omega_1'^2} = 0$. The appropriate normalization in this limit is $(q_2^2 / U_1^2)/(\overline{\rho_1'^2}/\overline{\rho}_1^2)$. We set the intensity $\rho_1'/\overline{\rho}_1$ in the pure entropy limit to equal its value in the vorticity-entropy wave; *i.e.*, $(\rho_1'/\overline{\rho}_1)_{\text{pure ent.}} = A_r (\sqrt{q_1^2}/U_1)_{\text{vort.–ent.}}$. This allows a consistent comparison between the pure entropy limit and the other curves.

Figure 2 shows the evolution of kinetic energy behind the shock wave over the propagating regime ($\psi_1 = 45°$). All three curves are normalized by the incident kinetic energy. The presence of entropy fluctuations is seen to significantly affect the amplification of kinetic energy across the shock wave. The evolution of q^2 is strongly affected by both the amplitude ratio and phase difference between the vorticity and entropy waves. Dependence upon the amplitude is monotonic. Entropy fluctuations that are in phase with the vorticity fluctuations (u_1' and T_1' are negatively correlated) enhance the amplification of kinetic energy. Suppression of amplification is observed when u_1' and T_1' are positively correlated. The pressure fluctuations behind the shock wave are similarly affected.

The decaying regime ($\psi_1 = 75°$) as shown in Figure 3 displays similar influence of the entropy fluctuations. Both near-field and far-field levels of kinetic energy are affected. The dependence upon amplitude ratio and phase difference is identical to that seen in the propagating regime. Also note that the curves asymptote to the far-field levels within a wavelength of the incident disturbance.

This influence of the entropy fluctuations is not limited to the two angles considered above; it extends over all angles of incidence. This is illustrated in Figure 4 where the far-field levels of amplification of q^2 are plotted against the angle of incidence. The Mach

number of the shock wave is 1.5. Note that the notion of far-field is introduced into the propagating regime by ignoring the oscillating component in equation (9). Reason for this neglect is statistical cancellation of this component in the far-field for an incident turbulent field. Also shown in Figure 5 is the amplification of vorticity across the shock wave. Negative correlation between u' and T' is clearly seen to increase the amplification while positive correlation suppresses it.

4. Comparison to numerical computation

The analysis is evaluated by comparison to numerical solution of the interaction of a sinusoidal vorticity-entropy wave with a Mach 1.5 shock wave. The governing equations are the two-dimensional unsteady compressible Navier Stokes equations which are discretized using the sixth order Pade scheme (Lele; 1992) and the third order Runge Kutta scheme (Wray; 1986). Details of the computation are discussed by Mahesh, Lele and Moin (1994c). The shock wave is stationary at the center of the domain in the mean. The shock structure is a result of molecular viscosity; no shock capturing or shock -fitting is used. A structured mesh that is non-uniform in the streamwise direction is used to resolve the shock wave. About 7 mesh points are located inside the shock wave.

Periodic boundary conditions are imposed transverse to the shock. The disturbance field corresponding to a vorticity-entropy wave is superposed onto the supersonic mean flow at the inflow boundary. Approximately non-reflecting boundary conditions (Poinsot and Lele; 1990) are used at the outflow boundary. The initial condition is a numerically computed steady shock wave. The vorticity-entropy wave is then introduced through the inflow boundary condition. The transients set up by the initial period of adjustment are allowed to exit the domain. Statistics are then gathered over a period of the inflow disturbance.

The computations examine the dependence of the interaction upon the incidence angle of the disturbance. The incidence angle was varied from 0 to 90 degrees while the amplitudes A_v and A_e were fixed at 0.05. We compare in Figure 6 the computed values of amplification of vorticity fluctuations to the linear analysis predictions. Good agreement is seen away from the critical angles inspite of the computations solving the viscous equations. Deviation is seen around the critical angle. This behavior is consistent with the interaction of a shock with an acoustic wave (Zang *et al*; 1984, Mahesh *et al*; 1994b).

As noted by Ribner (1953) and Chang (1954), within linear analysis the *unsteady* interaction of an oblique wave with a normal shock may be transformed into the *steady* interaction of an oblique wave with an oblique shock. The transformation involves defining the coordinates $x_s = x, y_s = y - U_1 t \cot \psi_1$. The governing equations in the transformed coordinates are the steady Euler equations linearized about uniform mean flow at a Mach

number:

$$M_e^2 = \frac{U_2^2 + \cot^2 \psi_1 U_1^2}{a_2^2} \tag{11}$$

M_e^2 equals unity at the critical angle whose vicinity therefore corresponds to transonic mean flow in transformed coordinates. We believe (Mahesh *et al*, 1994b) that the inconsistency of linear equations in the transonic regime causes the deviation between computation and linear analysis around the critical angle.

5. A simple explanation

An explanation is provided for the influence of entropy fluctuations on the evolution of a turbulent flow across a shock wave. Consider the following idealization of the mean field associated with the shock:

$$U = U(x); \quad P = P(x); \quad \bar{\rho} = \bar{\rho}(x) \tag{12}$$

Linearization of the Euler equations about the above mean flow yields the following governing equations for the fluctuations:

$$\bar{\rho}\,(u_t' + U u_x' + u' U_x) + \rho'\,U\,U_x = -p_x' \tag{13}$$

$$\bar{\rho}\,(v_t' + U v_x') = -p_y' \tag{14}$$

Denoting the fluctuating vorticity by ω', the following equation may be derived for ω':

$$\omega_t' + U\omega_x' = -\omega' U_x - \frac{\rho_y'}{\bar{\rho}^2}\,P_x + \frac{p_y'}{\bar{\rho}^2}\,\bar{\rho}_x \tag{15}$$

The above set of equations represents the effects of bulk change across the shock wave. Effects due to shock distortion are absent. The motivation to examine the above set of equations is provided by the fact that shock distortion effects are secondary to bulk effects especially in the propagating regime. Also, though the interaction of a vortical field with a shock wave generates acoustic waves, the contribution of these acoustic waves to the downstream kinetic energy is not significant; amplification and generation of vortical fluctuations accounts for most of the kinetic energy behind the shock wave.

The evolution of the vorticity fluctuations can therefore be related to that of kinetic energy. Equation (15) shows three terms that modify the vorticity field. The first term $(-\omega' U_x)$ represents the effect of bulk compression. The drop in mean velocity across the shock wave indicates that this term would enhance vorticity fluctuations. The second and third terms in equation (15) represent baroclinic contributions to the change in vorticity across the shock wave.

If the incident disturbance comprises of vorticity and entropy fluctuations, then $p' = 0$ in the incident field and hence,

$$\omega'_t + U\omega'_x = -\omega' \, U_x - \frac{\rho'_y}{\bar{\rho}^2} \, P_x \tag{16}$$

The incident vorticity fluctuations are thus enhanced by bulk compression. The incident entropy fluctuations produce vorticity at the shock wave through the baroclinic term. The baroclinic contribution can enhance or oppose the effect of bulk compression. The phase difference between the vorticity and entropy waves determines whether enhancement or opposition is observed.

Consider for example the plane vorticity-entropy wave represented by equation (2). It is easily shown that

$$-\omega'U_x - \frac{\rho'_y}{\bar{\rho}^2} \, P_x \sim A_v \, UU_x - A_e \, l\frac{P_x}{\bar{\rho}} \tag{17}$$

Since U_x is negative and P_x is positive across a shock wave, the two sources of vorticity are of the same sign if A_e and A_v are of the same sign. They oppose each other if A_e and A_v are of opposite sign. Thus, if u' and T' are negatively correlated the entropy field enhances the amplification of fluctuating vorticity. On the other hand, a positive correlation between u' and T' suppresses the amplification of vorticity across the shock wave.

Further insight is gained from a schematic illustration of this effect. Figure 7 shows a fluid element of circular cross-section passing through a shock wave. The geometric center of this element is denoted by C_F while the variable C_M is used to represent the center of mass. The disturbance field associated with the fluid element is that of a vorticity-entropy wave. The element therefore exhibits solid body rotation with associated vorticity ω' which is assumed positive in the direction shown. Also, the density field associated with the entropy wave causes the centre of mass to differ from the centre of force (the geometric centre).

Bulk compression compresses the element in the streamwise direction thereby enhancing the rotation. In addition, the shock wave exerts a pressure force (associated with the adverse pressure gradient) on the fluid element passing through the geometric centre as shown. The non-coincidence of C_F and C_M would cause this pressure force to exert a torque about the centre of mass. It is this torque that manifests itself as the baroclinic source of vorticity. Note that if C_M is above C_F the baroclinic rotation is in the same direction as ω'. The reverse is true if C_M is below C_F. The correlation between u' and T' over the fluid element determines the location of C_M with respect to C_F and thereby the relative sense of rotation that baroclinic torque produces.

6. Scaling of the evolution of vorticity across a shock wave

The simplicity of equation (16) motivates its use to derive formulae that approximate the evolution of vorticity fluctuations across a shock wave. The performance of the formulae may be evaluated by comparison to results of the linear analysis. Equation (16) may be rewritten as:

$$D_t(U\omega') = -\frac{\rho'_y}{\bar{\rho}^2}\, UP_x \tag{18}$$

where D_t denotes the material derivative $\partial/\partial t + U\partial/\partial x$. Use of the relation $P_x = -\bar{\rho}UU_x$ in the above equation yields:

$$D_t(U\omega') = \frac{\rho'_y}{\bar{\rho}}\, U^2 U_x = \frac{\rho'_y}{3\bar{\rho}}\,(U^3)_x \tag{19}$$

Approximation of the shock wave as a discontinuity allows $(U^3)_x$ to be expressed as $\Delta U^3\delta(x)$ where $\Delta(U^3)$ represents the difference in U^3 across the shock wave. The term ρ'_y is set to equal its upstream value to allow integration of the above equation. Transforming coordinates to $x' = x - Ut, \tau = t$ and integrating yields the following expression for the change in vorticity across the shock wave:

$$U_2\omega'_2 - U_1\omega'_1 \sim \frac{ikl}{3} A_e \frac{(U_2^3 - U_1^3)}{U_1} \tag{20}$$

which yields:

$$\omega'_2 \sim r\omega'_1 + \frac{ikl}{3}\, A_e\, U_1\, \frac{1-r^3}{r^2} \tag{21}$$

The above equation suggests that the amplification of incident vortical fluctuations equals the mean density ratio across the shock wave while the production of vorticity by entropy fluctuations scales as $kA_e l(1 - r^3)/r^2$.

The ability of these formulae to predict the evolution of vorticity is evaluated in Figures 8 and 9. Figure 8 considers the amplification of vorticity in the interaction of a pure vorticity wave with a shock. Mean Mach numbers from 1.25 to 2.5 are considered. Both scaled and unscaled values of *rms* vorticity behind the shock wave are plotted as a function of incident angle. The scaling is seen to work quite well especially in the propagating regime. A systematic deviation is seen with increasing Mach number.

The interaction of a pure entropy wave with a shock is examined in Figure 9. Once again the proposed scaling seems to yield reasonable collapse of the curves. The agreement in the absence of effects of shock distortion is quite encouraging.

7. Interaction of a shock wave with an isotropic field of vorticity-entropy waves

The analysis is extended to describe the evolution of a turbulent flow across a shock wave. In light of Morkovin's hypothesis, the turbulence is represented as a random three-dimensional field of vorticity-entropy waves. For reasons of generality, the turbulent field is assumed to be isotropic. It will be seen however, that the procedure is easily extended to consider anisotropic turbulence.

The incident turbulent field is represented as a superposition of plane vorticity-entropy waves (Fourier modes) in three dimensions. Each of these waves would interact independently with the shock wave under linear analysis. For a given upstream spectrum, the interaction of each of these waves with the shock wave is predicted. Integration over all waves behind the shock wave yields turbulence statistics behind the shock.

The three dimensional problem is related to the two dimensional analysis of the preceding section as follows. Consider an incident plane wave in three dimensions. As shown in Figure 10, the wavenumber vector of the wave lies in a plane that makes angle ϕ with the y axis. In this plane which we call the $x - x_r$ plane, the wave makes angle ψ_1 with the x axis. It is readily seen that the $x - x_r$ plane is identical to the plane of interaction in the two-dimensional problem.

The solenoidal nature of the incident velocity field requires the velocity vector of the wave to be normal to the wavenumber vector. The velocity field may therefore be expressed as a sum of two components: one normal to the wavenumber vector in the $x - x_r$ plane and the other normal to the $x - x_r$ plane (the ϕ direction). It is intuitively clear that the ϕ component of velocity would pass unchanged through the shock wave. As a result, the three dimensional problem may be solved using results of the two dimensional analysis in the $x - x_r$ plane. The subscripts 'r' and 'ϕ' are used to denote the components in the x_r and ϕ directions respectively. Equations (4) and (6) allow the following expressions to be written for the components of kinetic energy behind the shock wave:

$$\frac{E_{11}}{U_1^2} = [\ |\widetilde{F}|^2 + |\widetilde{G}|^2 + \widetilde{F}\widetilde{G}^* e^{i(\widetilde{k}-k_{mr})x} + \widetilde{F}^*\widetilde{G} e^{-i(\widetilde{k}-k_{mr})x}\ ]\ |A_v|^2 \tag{22}$$

$$\frac{E_{rr}}{U_1^2} = [\ |\widetilde{H}|^2 + |\widetilde{I}|^2 + \widetilde{H}\widetilde{I}^* e^{i(\widetilde{k}-k_{mr})x} + \widetilde{H}^*\widetilde{I} e^{-i(\widetilde{k}-k_{mr})x}\ ]\ |A_v|^2 \tag{23}$$

Recall that the variables in parentheses depend upon $M_1, \psi_1, A_e/A_v$ and k. The term $|A_v|$ represents the magnitude of the velocity vector *in the $x - r$ plane*. Figure 10 shows that $|A_v| = |u_1|/l$ which implies:

$$|A_v|^2 = \frac{E_{11}^{(1)}}{l^2} = \frac{E(k)}{4\pi k^2} \tag{24}$$

where the superscript '1' denotes the state upstream of the shock and $E_{11}^{(1)}$ is obtained from the following expression for the isotropic energy spectrum tensor:

$$E_{ij}^{(1)} = \frac{E(k)}{4\pi k^2}\left(\delta_{ij} - \frac{k_i k_j}{k^2}\right) \tag{25}$$

where $E(k)$ is the three dimensional energy spectrum tensor such that $\int E(k)\,dk = q_1^2/2$ and the wavenumbers in cartesian coordinates are given by:

$$k_1 = k\cos\psi_1; \quad k_2 = k\sin\psi_1\cos\phi; \quad k_3 = k\sin\psi_1\sin\phi \tag{26}$$

E_{11} and E_{rr} behind the shock wave will be completely determined once $E(k)$ and A_e/A_v are specified. We use the following form for $E(k)$:

$$E(k) \sim \left(\frac{k}{k_0}\right)^4 e^{-2\left(\frac{k}{k_0}\right)^2} \tag{27}$$

The quantity A_e/A_v may be represented as $A_r e^{i\phi_r}$ where A_r and ϕ_r are both functions of the wavenumber vector. Appropriate functional dependencies may be assumed depending upon the flow being considered. In the interests of generality, this paper assumes A_r and ϕ_r to be *independent* of the wavenumber vector. Also, the results presented consider the limiting cases of $\phi_r = 0$ and π. For these angles it is easily shown that

$$A_r = \sqrt{2}\frac{\rho_1'/\overline{\rho_1}}{\sqrt{q_1^2/U_1}} \tag{28}$$

Once $E(k)$ and A_e/A_v are specified, equations (22) and (23) are used to obtain E_{11} and E_{rr} behind the shock wave. Also Fig. 9 may be useed to show that:

$$E_{22} + E_{33} = E_{rr} + E_{\phi\phi} \tag{29}$$

Recognizing that turbulence behind the shock wave will be axisymmetric, we solve for $E_{22} + E_{33}$. $E_{\phi\phi}$ was noted to remain unchanged across the shock wave and hence is equated to its upstream value. The upstream value of $E_{\phi\phi}$ is given by:

$$E_{\phi\phi}^{(1)} = E_{nn}^{(1)} - |A_v|^2 = \frac{E(k)}{4\pi k^2} \tag{30}$$

The spectra are then integrated over all wavenumbers to obtain statistics as a function of distance behind the shock wave. The elemental volume of integration is given by the expression:

$$d^3\mathbf{k} = k^2\sin\psi_1\,d\psi_1\,d\phi\,dk \tag{31}$$

where k varies from 0 to ∞, ψ_1 varies from $-\pi/2$ to $\pi/2$ and ϕ varies from 0 to 2π.

The following expressions are obtained for the streamwise variation of kinetic energy behind the shock wave:

$$\frac{\overline{u_2'^2}}{U_1^2} = \int_{k=0}^{\infty}\int_{\psi_1=-\pi/2}^{\pi/2}\int_{\phi=0}^{2\pi} E_{11}\ k^2 \sin\psi_1\ \mathrm{d}\phi\ \mathrm{d}\psi_1\ \mathrm{d}k = 4\pi\int_{k=0}^{\infty}\int_{\psi_1=0}^{\pi/2} E_{11}\ k^2 \sin\psi_1\ \mathrm{d}\psi_1\ \mathrm{d}k$$

$$(32)$$

since the problem is symmetric about $\psi_1 = 0$ and the transfer functions that yield E_{11} are independent of ϕ. The integration over k and ψ_1 is performed numerically. Similar expressions are obtained for the transverse components of kinetic energy. *i.e.*,

$$\frac{\overline{v_2'^2}}{U_1^2} = \frac{\overline{w_2'^2}}{U_1^2} = \frac{4\pi}{2}\int_{k=0}^{\infty}\int_{\psi_1=0}^{\pi/2}\left[E_{rr} + \frac{E(k)}{4\pi k^2}\right] k^2 \sin\psi_1\ \mathrm{d}\psi_1\ \mathrm{d}k \qquad (33)$$

The evaluation of scalar quantities behind the shock wave is considerably simpler. For example the pressure field behind the shock is given by the following expression (equations 8 and 10) :

$$\frac{\overline{p_2'^2}}{P_2^2} = 4\pi\int_{k=0}^{\infty}\int_{\psi_1=0}^{\pi/2} E_{pp}\ k^2 \sin\psi_1\ \mathrm{d}\psi_1\ \mathrm{d}k \qquad (34)$$

where $E_{pp} = |\widetilde{K}|^2|A_v|^2$ in the propagating regime and $e^{-2k_i x}|\widetilde{K}|^2|A_v|^2$ in the decaying regime respectively.

8. Results

8.1 The spatial evolution of kinetic energy

The variation of q^2 with distance behind a Mach 1.5 shock wave is plotted in Figure 11. The combined interaction of vorticity and entropy fluctuations is compared to that of vorticity and entropy fluctuations alone. As mentioned before, two representative cases of combined interaction are considered: one where u' and T' are negatively correlated upstream of the shock ($A_r = 0.58, \phi_r = 0$) and the other where u' and T' are positively correlated ($A_r = 0.58, \phi_r = \pi$). The value of 0.58 was (arbitrarily) chosen to satisfy Morkovin's hypothesis at a Mach number of 1.35. All four curves are normalized with the incident value of q^2. As discussed in Section 3, q_2^2/q_1^2 in the pure entropy limit corresponds to $0.17\ (q_2^2/U_1^2)/(\overline{\rho_1'^2}/\overline{\rho_1^2})$ where the factor 0.17 equals $(\overline{\rho_1'^2}/\overline{\rho_1^2})/(q_1^2/U_1^2)$ for $A_r = 0.58$.

Similar spatial variation is exhibited by all three curves. Amplification of q^2 across the shock wave is followed by rapid drop and rise immediately downstream of the shock wave. Temperature fluctuations that are negatively correlated with u' yield higher levels of kinetic

energy at all streamwise locations while positively correlated temperature fluctuations have the opposite effect.

The rapid variation of kinetic energy behind the shock wave is a fundamental feature of shock/turbulence interaction. DNS of isotropic vortical fluctuations interacting with a shock wave (Lee, Lele and Moin, 1993) exhibits this feature, as does linear analysis of acoustic fluctuations (Mahesh, Lee, Lele and Moin, 1994b) interacting with a shock. The discussion (Section 3) of single vorticity-entropy waves interacting with a shock shows that waves incident at angles greater than the critical angle (decaying regime) produce this rapid variation through the damped oscillatory correlation between acoustic and vortical fluctuations behind the shock wave.

This correlation was overlooked by Lee, Lele and Moin (1993) in their linear analysis of a shock wave interacting with isotropic vortical fluctuations. This led them to erroneously conclude that linear analysis could not reproduce this rapid variation of kinetic energy seen in their computations. This error was subsequently corrected by them (Lee, Lele and Moin, 1994). Equations (7) and (9) suggest that q^2 behind the shock wave may be decomposed into four components: a spatially uniform vortical component, an acoustic component that decays exponentially and non-monotonic components corresponding to the correlation between acoustic and vortical fluctuations over both regimes of the solution. This decomposition, was performed by Mahesh, Lee, Lele and Moin (1994b) in their analysis of acoustic fluctuations interacting with a shock wave. The correlation between acoustic and vortical fluctuations produced by waves in the decaying regime of the solution were seen to produce the rapid variation of kinetic energy.

The variation of kinetic energy behind the shock wave may be further clarified by examination of the equations governing its evolution. Rearrangement of the linearized Euler equations (Appendix A) shows that the quantity

$$I_{\text{total}} = \frac{\gamma M}{2} \left[\frac{q^2}{a^2} + \frac{\overline{p'^2}}{\gamma^2 P^2} \right] + \frac{\overline{p'u'}}{Pa} \tag{35}$$

is conserved along a mean streamline. I_{total} changes across the shock wave and remains constant downstream. As will be seen in the next section, $\overline{p'^2}$ decays exponentially behind the shock wave. The rapid non-monotonic variation of q^2 may therefore be explained as a result of partitioning between potential and kinetic energy brought about by the correlation between acoustic fluctuations and the shock-normal component of fluctuating velocity. This is illustrated in Figure 12 where the terms in equation (35) are plotted.

The $\overline{p'u'}$ correlation may be decomposed into two components as follows:

$$\overline{p'u'} = \overline{p'u'}_{\text{prop}} + \overline{p'u'}_{\text{decay}} \tag{36}$$

where the subscripts 'prop' and 'decay' refer to the propagating and decaying regimes respectively. The above decomposition is performed by Mahesh, Lele and Moin (1994c) and reveals that the correlation between acoustic fluctuations and the velocity field in the decaying regime causes the rapid variation of q^2 behind the shock wave.

8.2 Far-field kinetic energy

The influence of entropy fluctuations on far-field levels of kinetic energy amplification is examined as a function of mean Mach number. If A_e/A_v is independent of k, it is easily shown that turbulent statistics in the far-field are independent of the upstream energy spectrum. Equation (32) outlined the expression for $\overline{u_2'}^2$. Substituting for E_{11} from equations (7) and (9) into equation (32), the following expression is obtained:

$$\left(\frac{\overline{u_2'}^2}{\overline{U_1^2}}\right)_{\text{far-field}} = \left[\int_0^{\psi_c} (|\widetilde{F}|^2 + |\widetilde{G}|^2)\sin\psi_1\,\mathrm{d}\psi_1 + \int_{\psi_c}^{\pi/2} |\widetilde{G}|^2 \sin\psi_1\,\mathrm{d}\psi_1\right] \int_0^\infty E(k)\,\mathrm{d}k \quad (37)$$

In writing the above expression, use is made of the fact that the correlation term in the propagating regime integrates to zero in the far-field. Since $\int_0^\infty E(k)\mathrm{d}k = q_1^2/2$, the above expression is independent of the upstream energy spectrum. The above discussion holds also for the other components of kinetic energy and the thermodynamic fluctuations. Thus if A_e/A_v is independent of k, the far-field levels depend only upon M_1 and A_e/A_v.

The far-field levels of kinetic energy amplification are plotted in Figures 13 and 14 respectively. The presence of entropy fluctuations is seen to significantly influence the levels of kinetic energy behind the shock wave. Recall that the far-field kinetic energy may be decomposed into vortical and acoustic components. Such decomposition reveals that while acoustic waves are generated at the shock wave, their contribution to the far-field kinetic energy is not very significant; amplification and generation of vortical fluctuations accounts for most of the kinetic energy behind the shock wave.

Entropy fluctuations also influence the anisotropy of the turbulence behind the shock. As shown in Figure 15, negatively correlated fluctuations of u' and T' upstream of the shock wave increase the fraction of energy in the streamwise direction behind the shock. Positively correlated fluctuations have the opposite effect.

8.3 Statistics of the shock front

The oscillation of the shock wave is considerably affected by the presence of entropy fluctuations in the incident field of disturbances. Results for the velocity and amplitude of oscillation of the shock front are presented below.

From equation (5), the *rms* level of the oscillation velocity is given by:

$$\frac{\overline{\xi_t^2}}{U_1^2} = 4\pi \int_{k=0}^\infty \int_{\psi_1=0}^{\pi/2} |\widetilde{L}|^2\,|A_v|^2\,k^2 \sin\psi_1\,\mathrm{d}k\,\mathrm{d}\psi_1 = \int_{\psi_1=0}^{\pi/2} |\widetilde{L}|^2 \sin\psi_1\,\mathrm{d}\psi_1 \int_{k=0}^\infty E(k)\,\mathrm{d}k \quad (38)$$

i.e., the *rms* velocity of oscillation of the shock wave is independent of the incident energy spectrum if A_e/A_v does not depend upon k. The influence on incident entropy fluctuations on the *rms* level of ξ_t is illustrated in Figure 16. The oscillation velocity is seen to be of the order of the incident velocity fluctuation. Entropy fluctuations with negatively correlated u' and T' enhance the oscillation velocity of the shock wave. Positively correlated fluctuations are observed to suppress it.

The amplitude of oscillation of the shock wave is similarly affected. Integration of equation (5) yields the following expression for the *rms* oscillation amplitude:

$$\overline{\xi^2} = 4\pi \int_{k=0}^{\infty} \int_{\psi_1=0}^{\pi/2} \frac{|\widetilde{L}|^2}{m^2 k^2} |A_v|^2 k^2 \sin\psi_1 \, dk \, d\psi_1 = \int_{\psi_1=0}^{\pi/2} \frac{|\widetilde{L}|^2}{m^2} \sin\psi_1 \, d\psi_1 \int_{k=0}^{\infty} \frac{E(k)}{k^2} \, dk \tag{39}$$

Unlike the oscillation velocity, the amplitude of oscillation is dependent upon the incident spectrum. As shown in Figure 17, the oscillation amplitude is increased by the incidence of temperature fluctuations that are negatively correlated with u'. Decrease in the amplitude of oscillation is observed when u' and T' in the incident field are positively correlated.

8.4 Thermodynamic fluctuations

The streamwise variation of pressure, density and temperature fluctuations behind a Mach 1.5 shock wave is shown in Figure 18. The incident field comprises of vorticity and entropy fluctuations ($A_r = 0.58, \phi_r = 0$). Pressure fluctuations decay exponentially behind the shock wave while density and temperature fluctuations exhibit non-monotonic behavior. The pressure fluctuations in the near-field are seen to be intense while the far-field intensity is smaller than those of density and temperature.

The preceding sections showed how entropy fluctuations affect the vortical part of the flow-field. Figure 19 shows that this influence extends to the acoustic component. The far-field intensity of pressure is plotted as a function of Mach number. The combined interaction of vorticity and entropy fluctuations is compared to that of vortical fluctuations alone. Fluctuations with a negative correlation between u' and T' are seen to increase the level of sound in the far-field while positively correlated fluctuations suppress it. Over the range of Mach numbers shown, this difference in sound level is calculated to be between 4 and 5 decibels.

8.5 Morkovin's hypothesis across a shock wave

The applicability of Morkovin's hypothesis (equation 1) across a shock wave is examined in this section. The incident field of vorticity and entropy fluctuations is constrained to

satisfy Morkovin's hypothesis *i.e.*, A_r is chosen such that the relation

$$\frac{\rho_1'}{\bar{\rho}_1} = (\gamma - 1)M_1^2 \frac{u_1'}{U_1} \tag{40}$$

is satisfied at every wavenumber. The fluctuations in the far-field behind the shock are then examined to see if the hypothesis holds. The results (Figure 20) show that the first part of the hypothesis *i.e.*, $\rho'/\bar{\rho} = -T'/\bar{T}$ is still a good approximation behind the shock wave especially if the mean Mach number is less than 2. However the part of the hypothesis that relates T' to u' does not seem to hold behind the shock wave. This behavior is explained below.

The equation $\rho'/\bar{\rho} = -T'/\bar{T}$ is obtained by setting p' to zero in the linearized equation of state. It amounts to neglecting the acoustic mode in comparison to the entropy mode. As seen from equation (2d) it is an identity as far as the initial disturbance field is concerned. Upon interaction with the shock, the incident field of vorticity and entropy fluctuations generate acoustic waves. The generation of acoustic waves is however accompanied by amplification of the incident entropy fluctuations. Also a fraction of the acoustic waves decays behind the shock. As a result the acoustic contribution in the far-field to the thermodynamic fluctuations becomes significant only at the larger Mach numbers. The first part of Morkovin's hypothesis is therefore a good approximation behind shock waves of moderate strength.

The relation,

$$\frac{T'}{\bar{T}} = -(\gamma - 1)M^2 \frac{u'}{U} \tag{41}$$

is obtained by assuming negligible fluctuations in stagnation temperature in the linear limit. Denoting the stagnation temperature by T_0,

$$T_0 = \bar{T} + T' + \frac{(U + u')^2 + v'^2 + w'^2}{2C_p} \tag{42}$$

Linearizing the above equation yields the following expression for fluctuations in stagnation temperature:

$$T_0' = T' + \frac{Uu'}{C_p} \tag{43}$$

Setting T_0' to zero and rearranging yields equation (41).

The Rankine Hugoniot equations may be used to show that equation (41) cannot be valid behind a shock wave if it is assumed to hold upstream of the shock. The energy equation requires the stagnation temperature to be constant across the shock in a frame of reference that moves at the instantaneous speed of the shock wave. *i.e.*,

$$\bar{T}_1 + T_1' + \frac{(U_1 + u_1' - \xi_t)^2 + v_1'^2 + w_1'^2}{2C_p} = \bar{T}_2 + T_2' + \frac{(U_2 + u_2' - \xi_t)^2 + v_2'^2 + w_2'^2}{2C_p} \tag{44}$$

Linearizing the above equation and constraining the incident fluctations to satisfy equation (41) yields (Mahesh, Lele and Moin; 1994c):

$$T_2' + \frac{U_2 u_2'}{C_p} = -\frac{\xi_t}{C_p}(U_1 - U_2) \tag{45}$$

i.e., the fluctuations of stagnation temperature are not zero behind the shock wave. Dividing through by $\overline{T}_2$ and rearranging, we get:

$$\frac{T_2'}{\overline{T}_2} + (\gamma - 1)M_2^2 \frac{u_2'}{U_2} = -(\gamma - 1)M_2 \left(\frac{U_1}{U_2} - 1\right)\frac{\xi_t}{a_2} \tag{46}$$

The applicability of Morkovin's hypothesis behind the shock wave requires that

$$(\gamma - 1)M_2 \left(\frac{U_1}{U_2} - 1\right)\frac{\xi_t}{a_2} \sim 0 \tag{47}$$

As shown in Figure 20, the above term is not negligible, leading to inapplicability of the hypothesis behind the shock wave.

9. Summary

Inviscid linear analysis was used to study the simultaneous interaction of vorticity and entropy fluctuations with a shock wave. The two-dimensional interaction of a shock wave with a plane vorticity-entropy wave was initially considered. Expressions were derived for the flow-field behind the shock and the displacement of the shock front. The statistics of kinetic energy and thermodynamic fluctuations behind the shock wave were examined. The amplitude ratio and phase difference between the incident entropy and vorticity fluctuations were shown to significantly influence the statistics. Dependence upon the amplitude ratio was monotonic. Entropy fluctuations in phase with the incident vorticity fluctuations (u' and T' negatively correlated) were observed to enhance levels of kinetic energy and thermodynamic fluctuations behind the shock. Positively correlated fluctuations were observed to have a suppressing effect.

An explanation was provided to explain these trends. The evolution of fluctuating vorticity across the shock wave was noted to have two important contributions: bulk compression of incident vorticity and baroclinic production of vorticity through the incident entropy fluctuations. The upstream correlation between vorticity and entropy fluctuations was shown to determine whether these two sources of vorticity enhance or oppose each other thereby determining kinetic energy levels behind the shock wave. A scaling was then proposed for the evolution of vorticity across the shock wave.

The analysis was extended to consider the interaction of a shock wave with an isotropic field of vorticity and entropy fluctuations. Both spatial variation behind the shock and far-field levels of turbulent statistics were examined. The presence of entropy fluctuations was shown to significantly affect the levels of kinetic energy, vorticity and thermodynamic fluctuations behind the shock. Higher levels of kinetic energy and vorticity were observed when u' and T' in the incident fluctuations were negatively correlated. Positive correlation had the opposite effect. Acoustic waves were produced through the interaction. The level of sound behind the shock wave was enhanced by the incidence of fluctuations with negative correlation between u' and T'. Suppression of sound level was observed if the incident fluctuations were positively correlated. The incidence of entropy fluctuations was observed to affect the oscillation of the shock front. Negatively correlated fluctuations of u' and T' increased the velocity and amplitude of oscillation while positively correlated fluctuations suppressed it.

The applicability of Morkovin's hypothesis behind a shock wave was examined. Statistics in the far-field indicate that neglect of the acoustic mode is a good approximation in the far-field of shock waves of moderate strength ($M_1 < 2$). The part of the hypothesis relating u' and T' was seen to be invalid behind the shock. Non-negligible oscillation of the shock front was shown to be responsible.

The results indicate the considerable importance of entropy fluctuations in the evolution of the turbulent fluctuations in a compressible boundary layer upon its interaction with a shock wave.

Appendix A

The procedure for analysis of the two-dimensional interaction of a shock wave with a plane vorticity-entropy wave is summarized below. A more detailed description is furnished by Mahesh, Lele and Moin (1994c).

A.1. The governing equations

The governing equations behind the shock wave are the Euler equations that are linearized about the uniform flow behind the shock. *i.e.*,

$$\rho'_t + U \rho'_x = -\bar{\rho} \left(u'_x + v'_y \right) \tag{A.1a}$$

$$u'_t + U u'_x = -\frac{1}{\bar{\rho}} p'_x \tag{A.1b}$$

$$v'_t + U v'_x = -\frac{1}{\bar{\rho}} p'_y \tag{A.1c}$$

$$s'_t + U s'_x = 0 \tag{A.1d}$$

Also,

$$\frac{p'}{P} = \frac{\rho'}{\bar{\rho}} + \frac{T'}{\bar{T}} \quad \text{and} \quad \frac{s'}{C_p} = \frac{p'}{\gamma P} - \frac{\rho'}{\bar{\rho}} \tag{A.1e}$$

The variables s' and C_p in the above equations represent entropy fluctuations and the specific heat at constant pressure respectively.

Linearizing the Rankine Hugoniot equations yields the following relations that the disturbance field must satisy at the mean position of the shock front $(x = 0)$.

$$\frac{u'_2 - \xi_t}{U_1} = \frac{(\gamma - 1)M_1^2 - 2}{(\gamma + 1)M_1^2} \left(\frac{u'_1 - \xi_t}{U_1} \right) + \frac{2}{(\gamma + 1)M_1^2} \left(\frac{T'_1}{\bar{T}_1} \right) \tag{A.2a}$$

$$\frac{v'_2}{U_1} = \frac{v'_1}{U_1} + \frac{2(M_1^2 - 1)}{(\gamma + 1)M_1^2} \xi_y \tag{A.2b}$$

$$\frac{\rho'_2}{\bar{\rho}_2} = \frac{4}{(\gamma - 1)M_1^2 + 2} \left(\frac{u'_1 - \xi_t}{U_1} \right) - \frac{(\gamma - 1)M_1^2 + 4}{(\gamma - 1)M_1^2 + 2} \left(\frac{T'_1}{\bar{T}_1} \right) \tag{A.2c}$$

$$\frac{p'_2}{P_2} = \frac{4\gamma M_1^2}{2\gamma M_1^2 - (\gamma - 1)} \left(\frac{u'_1 - \xi_t}{U_1} \right) - \frac{2\gamma M_1^2}{2\gamma M_1^2 - (\gamma - 1)} \left(\frac{T'_1}{\bar{T}_1} \right) \tag{A.2d}$$

A.2 The two regimes behind the shock wave

The solution behind the shock wave was noted to have two different regimes that differed in the nature of the pressure field. The existence of the two regimes is illustrated as follows. The pressure field behind the shock wave satisfies the wave equation; *i.e.*,

$$p'_{tt} + 2U_2 p'_{xt} - (a_2^2 - U_2^2) p'_{xx} - a_2^2 p'_{yy} = 0 \tag{A.3}$$

Continuity at the shock wave requires that the solution behind the shock wave have the same transverse wave number and frequency as the incident disturbance. The pressure may therefore be expressed as ,

$$p' = F(x) \, e^{ik(ly - mU_1 t)} \tag{A.4}$$

Substituting the above expression for pressure into equation (A.3) yields the following equation for F.

$$\left[\frac{a_2^2}{U_1^2} - \frac{U_2^2}{U_1^2}\right] F'' + i \, 2km \frac{U_2}{U_1} \, F' + k^2 \left[m^2 - l^2 \frac{a_2^2}{U_1^2}\right] F = 0 \tag{A.5}$$

The solution to the above equation is of the form $F \sim e^{i\widetilde{k}x}$. Substitution into equation (A.5) yields the following equation for $\widetilde{k}$.

$$\left[\frac{a_2^2}{U_1^2} - \frac{U_2^2}{U_1^2}\right] \widetilde{k}^2 + 2km \frac{U_2}{U_1} \, \widetilde{k} - k^2 \left[m^2 - l^2 \frac{a_2^2}{U_1^2}\right] = 0 \tag{A.6}$$

The discriminant of the above quadratic equation determines if $\widetilde{k}$ is real or imaginary. A real valued $\widetilde{k}$ would imply that the pressure field is a plane wave. The discriminant is given by the following expression:

$$\text{Discriminant} = 2kl \frac{a_2}{U_1} \sqrt{\frac{m^2}{l^2} - \left(\frac{a_2^2}{U_1^2} - \frac{U_2^2}{U_1^2}\right)} \tag{A.7}$$

Recall that $m = \cos \, \psi_1$ and $l = \sin \, \psi_1$. The requirement for real $\widetilde{k}$ is therefore,

$$\cot^2 \, \psi_1 > \left(\frac{a_2^2}{U_1^2} - \frac{U_2^2}{U_1^2}\right) \tag{A.8}$$

i.e., $0 < \psi_1 < \psi_c$ where ψ_c is a root of

$$\cot^2 \, \psi_c = \left(\frac{a_2^2}{U_1^2} - \frac{U_2^2}{U_1^2}\right) \tag{A.9}$$

Note that ψ_c is a function of the Mach number of the shock wave. If the incident angle exceeds ψ_c, $\widetilde{k}$ becomes imaginary. Denoting the real and imaginary parts of $\widetilde{k}$ by $\widetilde{k}_r$ and and $\widetilde{k}_i$ respectively, the function F is now given by,

$$F \sim e^{-\widetilde{k}_i x} \, e^{i\widetilde{k}_r x} \tag{A.10}$$

i.e. the pressure field decays exponentially behind the shock wave.

A.3 The solution behind the shock wave

The arguments of the vorticity, entropy and acoustic modes over both regimes of the solution are derived below. The flow-field may then be expressed as a superposition of vortical, acoustic and entropic components.

It was noted that the vorticity and entropy fluctuations were plane waves over both regimes. Since vorticity and entropy fluctuations are both convected by the mean flow, they are of the same form which is given by:

$$e^{i\overline{k}x}e^{ik(ly-mU_1t)} \tag{A.11}$$

Note that the transverse wavenumber and frequency have been matched to that of the incident disturbance. The variable $\overline{k}$ is obtained as follows. Convection by the mean flow requires that the vorticity and entropy fluctuations have the following dispersion relation:

$$\omega = U_1km = U_2\overline{k}$$

i.e.,

$$\overline{k} = km\frac{U_1}{U_2} = kmr \tag{A.12}$$

The vorticity and entropy fields are therefore of the form:

$$e^{ik(mrx+ly-mU_1t)} \tag{A.13}$$

The form of the pressure field was derived in the previous section. However, explicit expressions were not derived for the variables $\widetilde{k}, \widetilde{k}_i$ and $\widetilde{k}_r$. Evaluation of these variables would completely determine the functional form of the pressure field. Recall that $\widetilde{k}$ was defined as the root of equation $(A.6)$; *i.e.*,

$$
\begin{aligned}
\frac{\widetilde{k}}{k} &= \frac{-m\frac{U_2}{U_1} + l\frac{a_2}{U_1}\sqrt{\frac{m^2}{l^2} - \left(\frac{a_2^2}{U_1^2} - \frac{U_2^2}{U_1^2}\right)}}{\left(\frac{a_2^2}{U_1^2} - \frac{U_2^2}{U_1^2}\right)} \\
&= \frac{U_1}{U_2}\frac{M_2}{1-M_2^2}\left[-mM_2 + l\sqrt{\frac{m^2}{l^2} - \frac{U_2^2}{U_1^2}\left(\frac{1}{M_2^2} - 1\right)}\right] \tag{A.14}
\end{aligned}
$$

The other root is rejected on the grounds that it leads to a physically unacceptable solution that grows exponentially behind the shock wave. The above expression is real

only if $0 < \psi_1 < \psi_c$. If the angle of incidence exceeds ψ_c, $\widetilde{k}$ is complex. Equation $(A.14)$ shows that the real and imaginary parts of $\widetilde{k}$ are given by:

$$\frac{\widetilde{k}_r}{k} = -m\frac{U_2}{U_1}\frac{1}{\left(\frac{a_2^2}{U_1^2} - \frac{U_2^2}{U_1^2}\right)} = -m\frac{U_1}{U_2}\frac{M_2^2}{1 - M_2^2} \qquad (A.15)$$

$$\frac{\widetilde{k}_i}{k} = \frac{l\frac{a_2}{U_1}\sqrt{\left(\frac{a_2^2}{U_1^2} - \frac{U_2^2}{U_1^2}\right) - \frac{m^2}{l^2}}}{\left(\frac{a_2^2}{U_1^2} - \frac{U_2^2}{U_1^2}\right)} = l\frac{U_1}{U_2}\frac{M_2}{1 - M_2^2}\sqrt{\frac{U_2^2}{U_1^2}\left(\frac{1}{M_2^2} - 1\right) - \frac{m^2}{l^2}} \qquad (A.16)$$

The argument of the vorticity, entropy and acoustic modes behind the shock wave are now completely determined over both regimes of the solution. Expressions for the velocity and thermodynamic field as given by equation (4) follow.

A.4 Expressions for the coefficients

The coefficients $\widetilde{F}, \widetilde{G}, \widetilde{H}, \widetilde{I}, \widetilde{K}, \widetilde{Q}$ and $\widetilde{L}$ are obtained by substituting the solution into the governing equations behind the shock wave and the boundary conditions at the mean position of the shock front ($x = 0$). Since the argument of the solution has been matched to that of the incident disturbance this yields a set of equations relating the coefficients. This system of equations is then solved thereby completing the solution.

The governing equations and boundary conditions yield the following set of equations (Mahesh, Lele and Moin; 1994c):

$$\widetilde{F} = \alpha\widetilde{K} \qquad (A.17a)$$

$$\widetilde{H} = \beta\widetilde{K} \qquad (A.17b)$$

$$\widetilde{I} = -\frac{mr}{l}\widetilde{G} \qquad (A.17c)$$

$$\widetilde{F} + \widetilde{G} - \widetilde{L} = B_1(l - \widetilde{L}) - B_2\frac{A_e}{A_v} \qquad (A.17d)$$

$$\frac{\widetilde{K}}{\gamma} + \widetilde{Q} = C_1(l - \widetilde{L}) - C_2\frac{A_e}{A_v} \qquad (A.17e)$$

$$\widetilde{K} = D_1(l - \widetilde{L}) - D_2\frac{A_e}{A_v} \qquad (A.17f)$$

$$\widetilde{H} + \widetilde{I} = -m - E_1\frac{l}{m}\widetilde{L} \qquad (A.17g)$$

The variables α and β are defined as:

$$\alpha = \frac{a_2^2}{\gamma U_1^2} \frac{\frac{\widetilde{k}}{k}}{m - \frac{\widetilde{k}}{kr}} ; \qquad \beta = \frac{a_2^2}{\gamma U_1^2} \frac{l}{m - \frac{\widetilde{k}}{kr}}$$

The variables $B_1, B_2, C_1, C_2, D_1, D_2$ and E_1 in the above equations correspond to the following compact representation of the boundary conditions and may be obtained by comparison to Equations $(A.2)$:

$$\frac{u_2' - \xi_t}{U_1} = B_1 \frac{u_1' - \xi_t}{U_1} + B_2 \frac{T_1'}{\overline{T_1}} \qquad (A.18a)$$

$$\frac{\rho_2'}{\overline{\rho_2}} = C_1 \frac{u_1' - \xi_t}{U_1} + C_2 \frac{T_1'}{\overline{T_1}} \qquad (A.18b)$$

$$\frac{p_2'}{P_2} = D_1 \frac{u_1' - \xi_t}{U_1} + D_2 \frac{T_1'}{\overline{T_1}} \qquad (A.18c)$$

$$\frac{v_2'}{U_1} = \frac{v_1'}{U_1} + E_1 \, \xi_y \qquad (A.18d)$$

Equations $(A.17)$ are solved for the coefficients. Details of the solution are provided by Mahesh, Lele and Moin (1994c). The variable $\widetilde{L}$ is first solved for and has the following form:

$$\widetilde{L} = \frac{-m - \beta(D_1 l - D_2 \frac{A_e}{A_v}) + \frac{mr}{l}[-\alpha(D_1 l - D_2 \frac{A_e}{A_v}) + B_1 l - B_2 \frac{A_e}{A_v}]}{E_1 \frac{l}{m} - \beta D_1 - \frac{mr}{l}(1 - B_1 + \alpha D_1)} \qquad (A.19)$$

Once $\widetilde{L}$ is known, the other coefficients are easily obtained using equations $(A.17)$. This completes the solution.
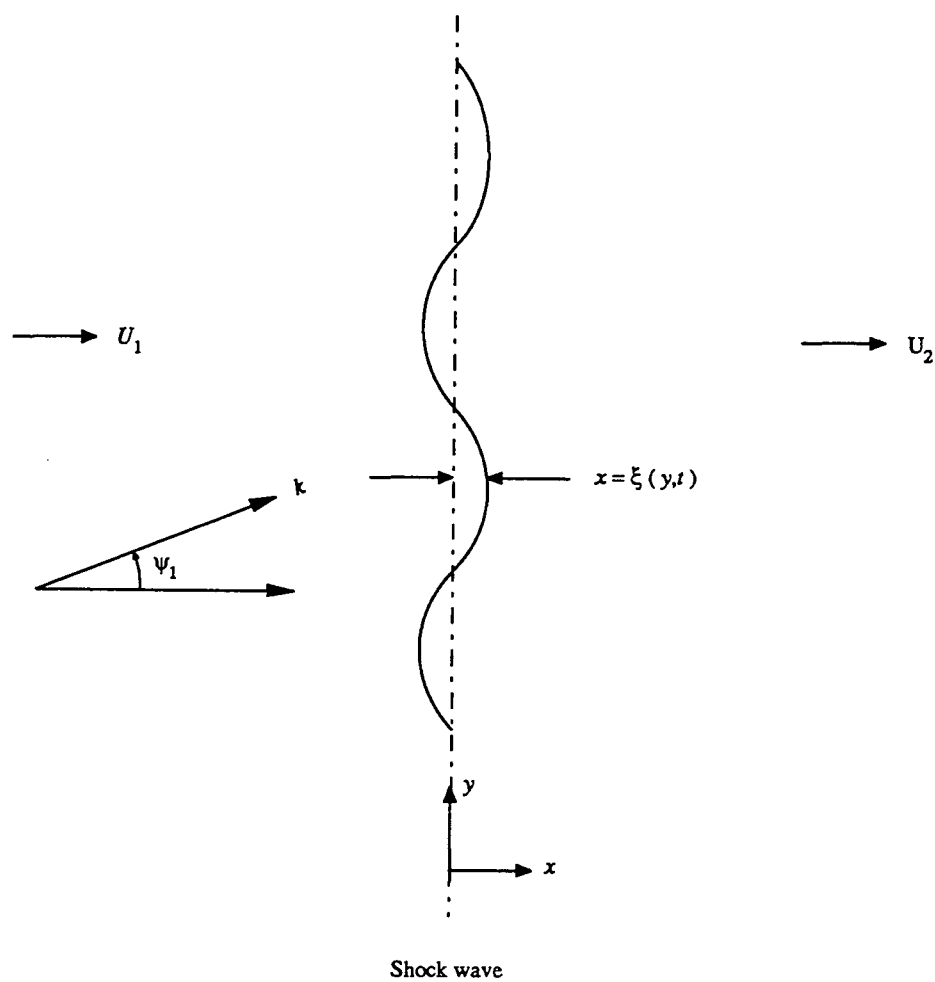
FIG. 1. Schematic of the interaction of a vorticity-entropy wave with a shock wave.
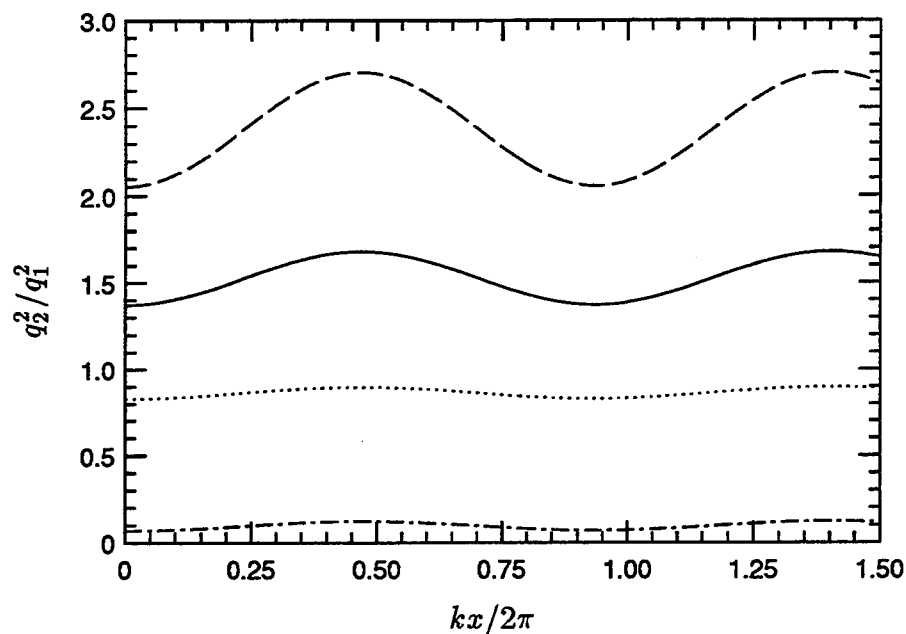
FIG. 2. Evolution of q^2 behind the shock wave in the propagating regime. The incident angle is 45° and the mean Mach number is 1.5. ——— (Pure vorticity), - - - - ($A_r = 1; \phi_r = 0$), ········ ($A_r = 1; \phi_r = 180°$), —-—- (Pure entropy).
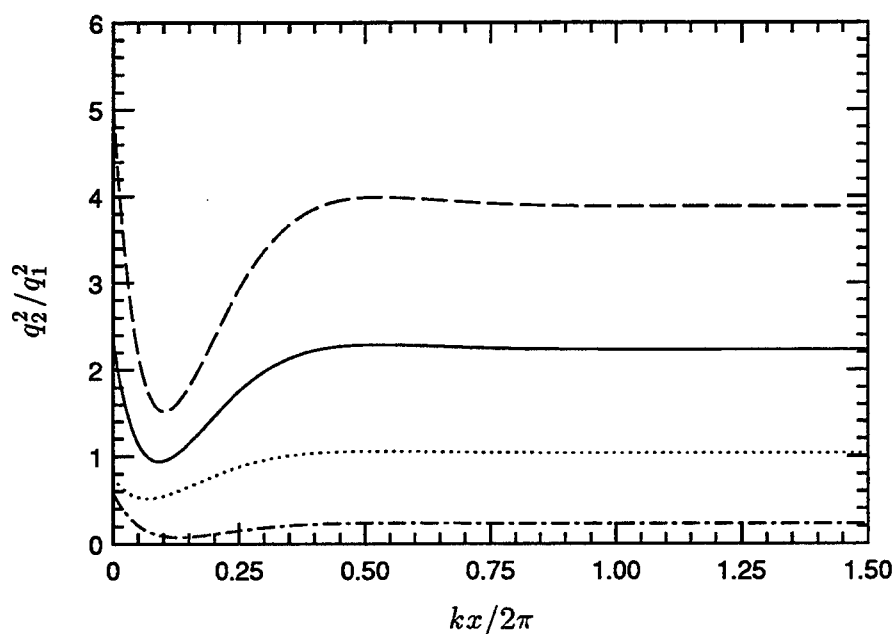

FIG. 3. Evolution of q^2 behind the shock wave in the decaying regime. The incident angle is 75° and the mean Mach number is 1.5. ——— (Pure vorticity), - - - - ($A_r = 1; \phi_r = 0$), ········ ($A_r = 1; \phi_r = 180°$), —-—- (Pure entropy).
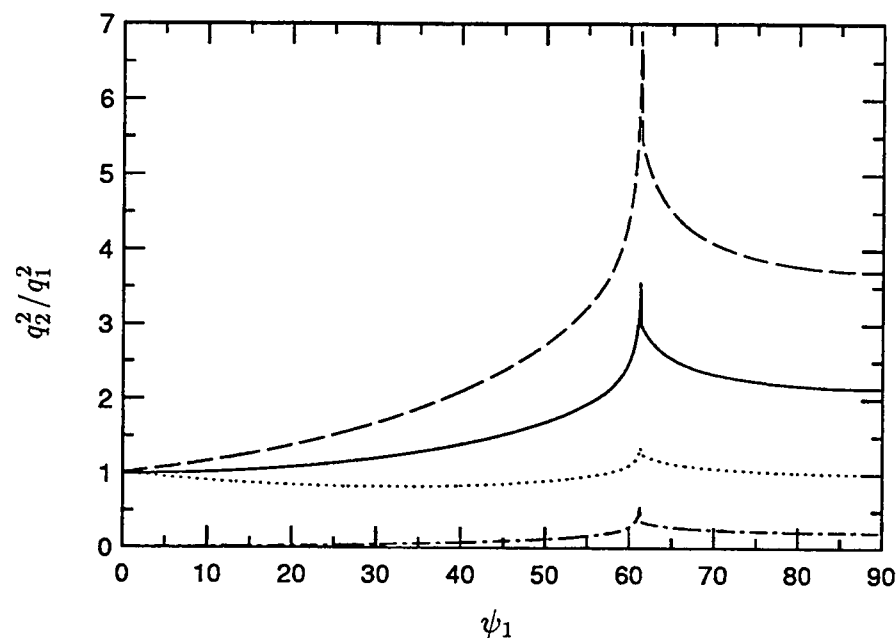
FIG. 4. The amplification of kinetic energy across the shock wave as a function of the angle of
incidence. Far-field kinetic energy levels are plotted and the mean Mach number is 1.5.
———— (Pure vorticity), – – – – $(A_r = 1; \phi_r = 0)$, ········ $(A_r = 1; \phi_r = 180°)$, — – — (Pure
entropy).
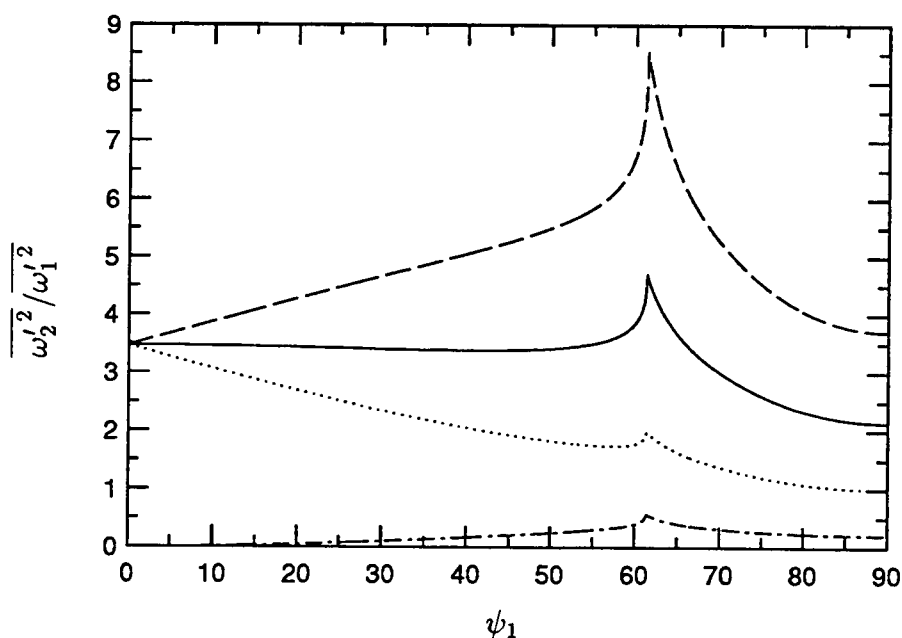
FIG. 5. The amplification of vorticity across the shock wave as a function of the angle of inci-
dence. The mean Mach number is 1.5. ———— (Pure vorticity), – – – – $(A_r = 1; \phi_r = 0)$,
········ $(A_r = 1; \phi_r = 180°)$,— – — (Pure entropy).
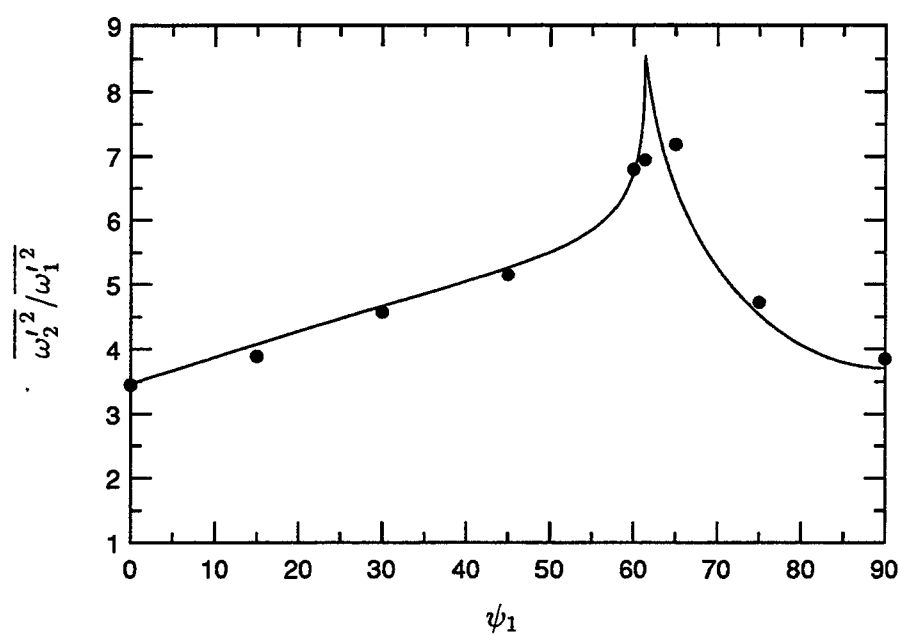
FIG. 6. The amplification of vorticity across the shock wave as a function of the angle of incidence. The mean Mach number is 1.5. The line corresponds to linear analysis while the symbols are from numerical computation.
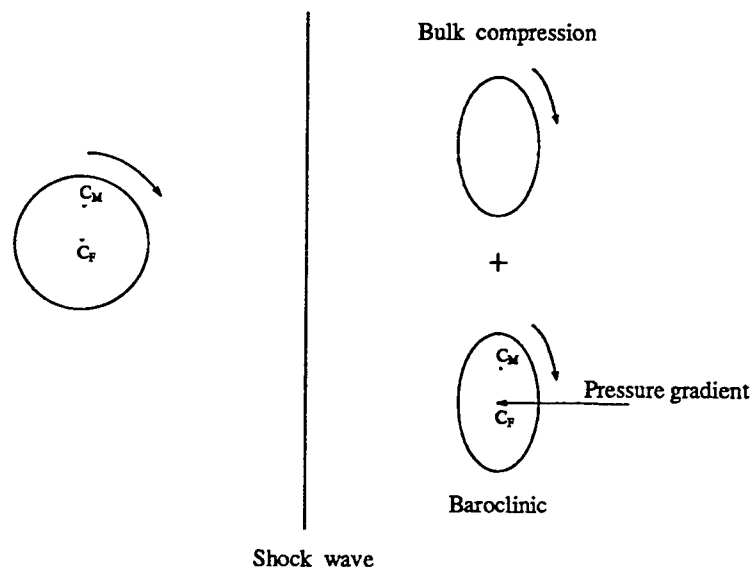
(a)
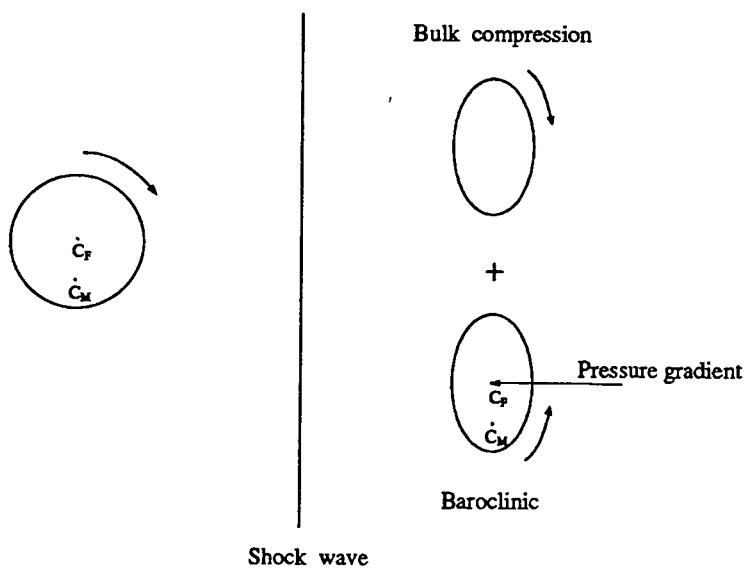
(b)

FIG. 7. A spherical element of fluid passing through a shock wave. The effects of bulk compression and baroclinic vorticity production are shown. u' and T' are negatively correlated upstream of the shock wave in (a) while (b) corresponds to positive correlation between u' and T'.
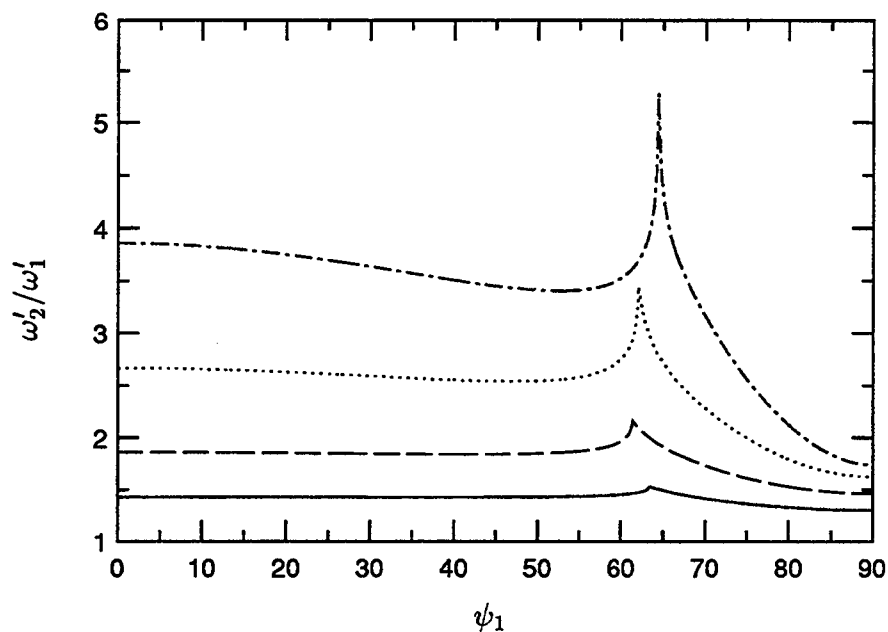
FIG. 8a. Unscaled amplification of the *rms* level of vorticity in the interaction of a vorticity wave with a shock wave. ——— ($M_1 = 1.25$), – – – – ($M_1 = 1.5$), ········ ($M_1 = 2$), — · — ($M_1 = 2.5$).
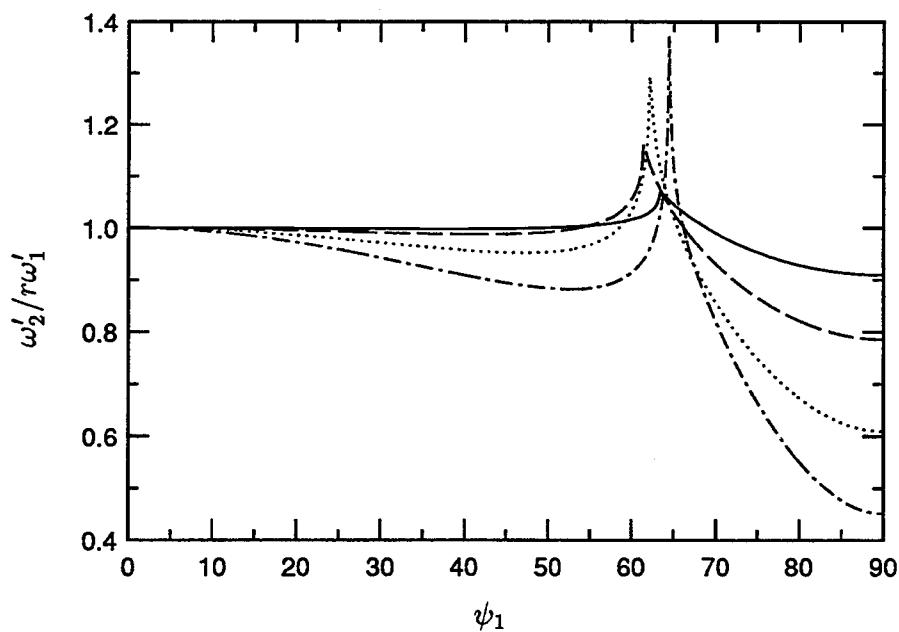
FIG. 8b. Scaled amplification of the *rms* level of vorticity in the interaction of a vorticity wave with a shock wave. ——— ($M_1 = 1.25$), – – – – ($M_1 = 1.5$), ········ ($M_1 = 2$), — · — ($M_1 = 2.5$).
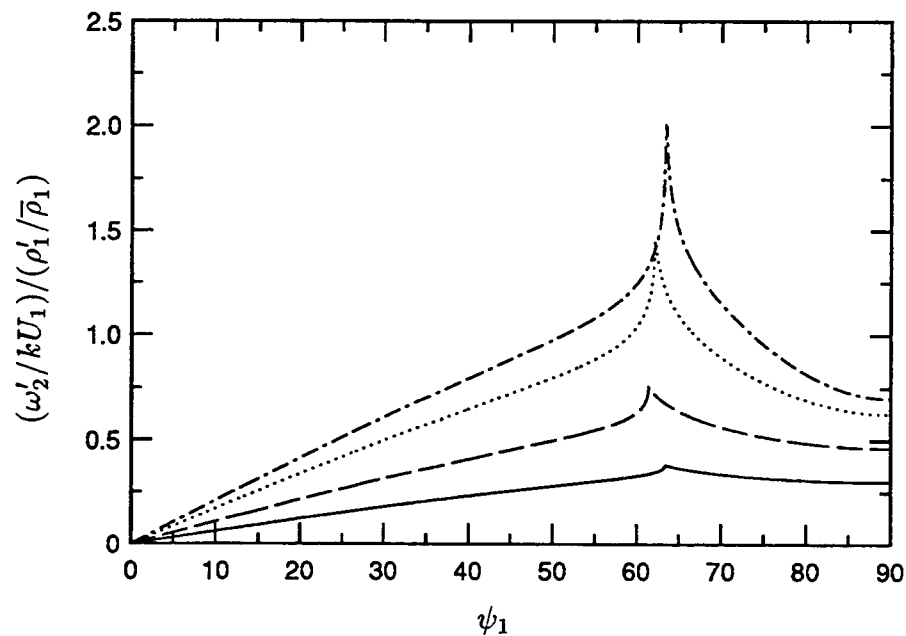
FIG. 9a. Unscaled *rms* level of vorticity produced in the interaction of an entropy wave with a shock wave. ——— ($M_1 = 1.25$), ---- ($M_1 = 1.5$), ········ ($M_1 = 2$), ——- ($M_1 = 2.5$).
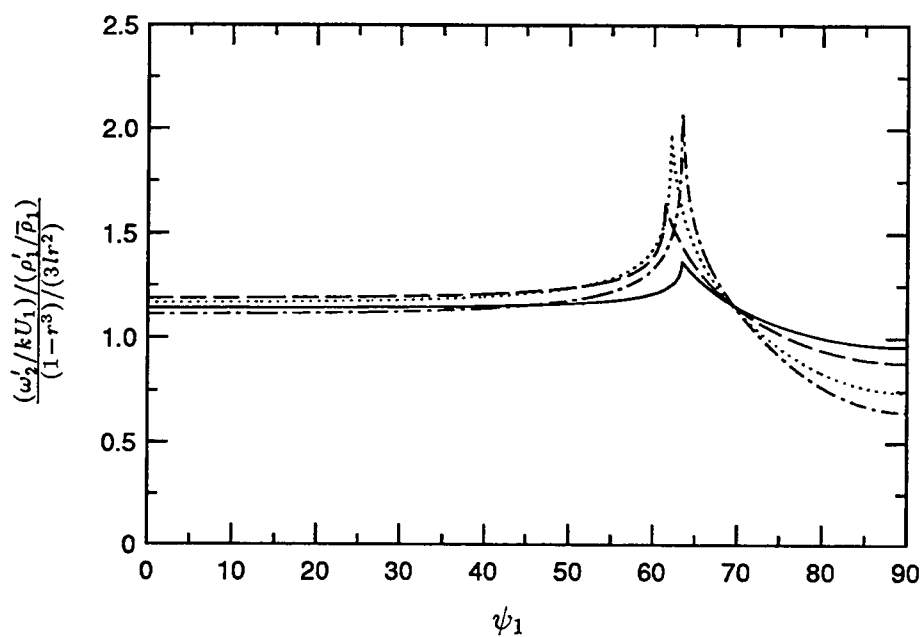
FIG. 9b. Scaled *rms* level of vorticity produced in the interaction of an entropy wave with a shock wave. ——— ($M_1 = 1.25$), ---- ($M_1 = 1.5$), ········ ($M_1 = 2$), ——- ($M_1 = 2.5$).
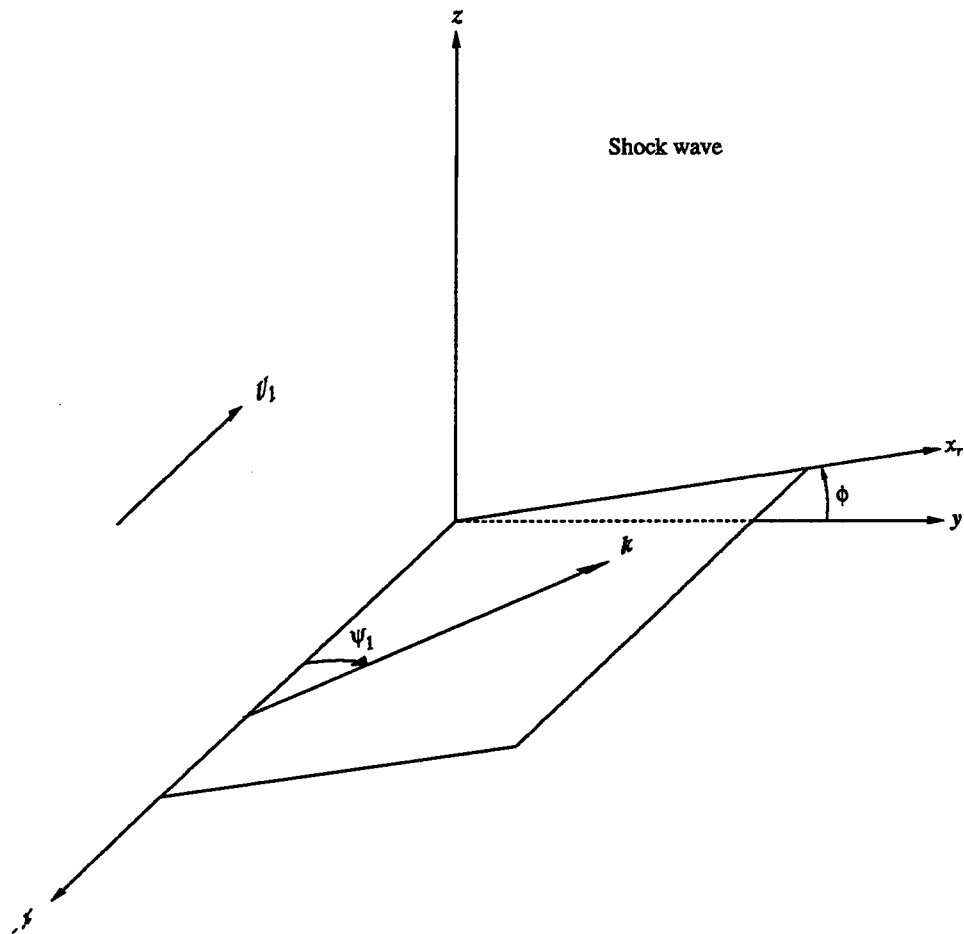
FIG. 10. Coordinate system used in the interaction of isotropic turbulence with a shock wave.
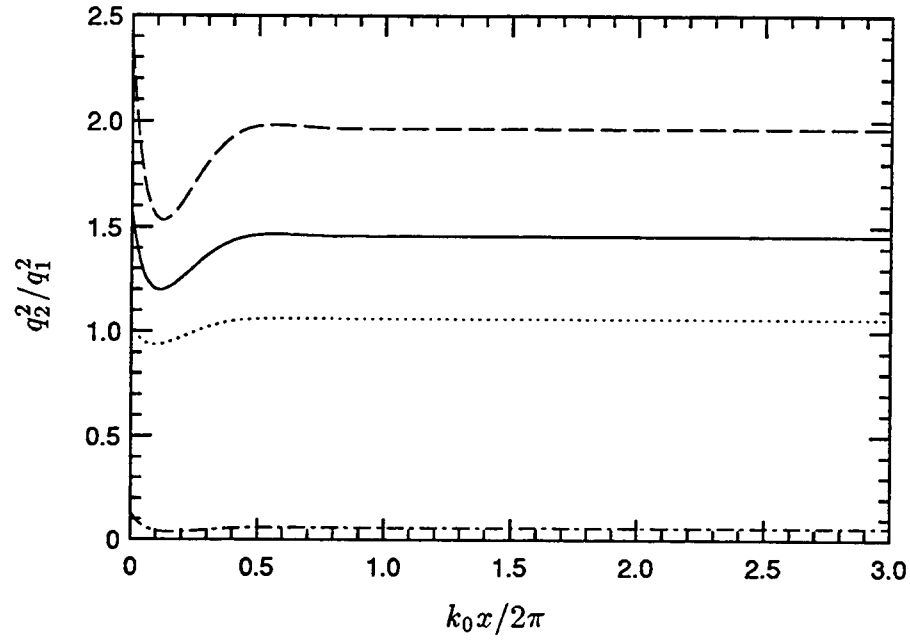
FIG. 11. Evolution of q^2 behind a Mach 1.5 shock wave. ——— (Pure vorticity), ———— ($A_r =$ 0.58; $\phi_r = 0$), ········ ($A_r = 0.58$; $\phi_r = 180°$), —·—·— (Pure entropy).
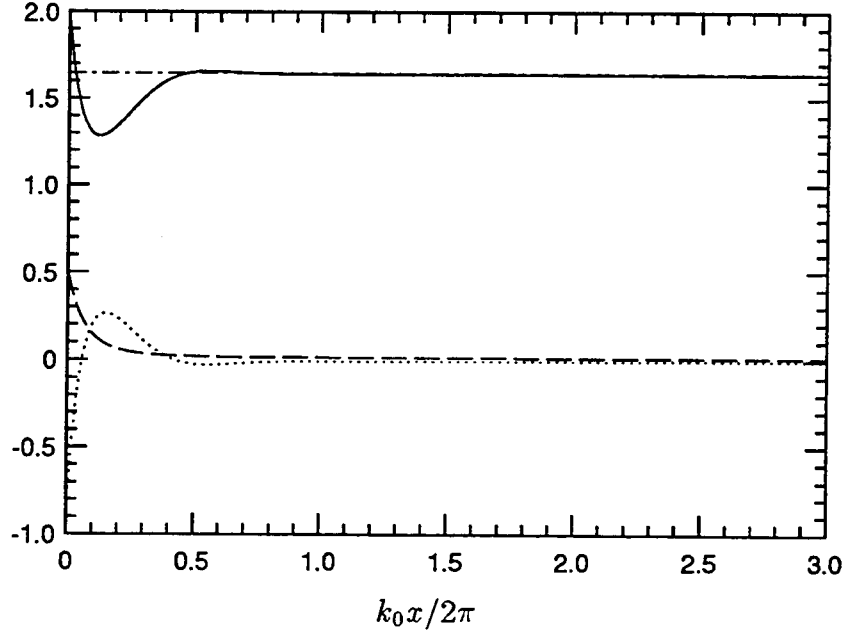
FIG. 12. The streamwise variation of terms in Equation 3.57 behind a Mach 1.5 shock wave. The incident fluctuations correspond to $A_r = 0.58$ and $\phi_r = 0$. All terms are non-dimensionalized as indicated in Equation 3.57 and normalized with $\sqrt{q_1^2}/U_1$. ——— (q^2), ———— ($\overline{p'^2}$), ········ ($\overline{p'u'}$), —·—·— (I_{total}).
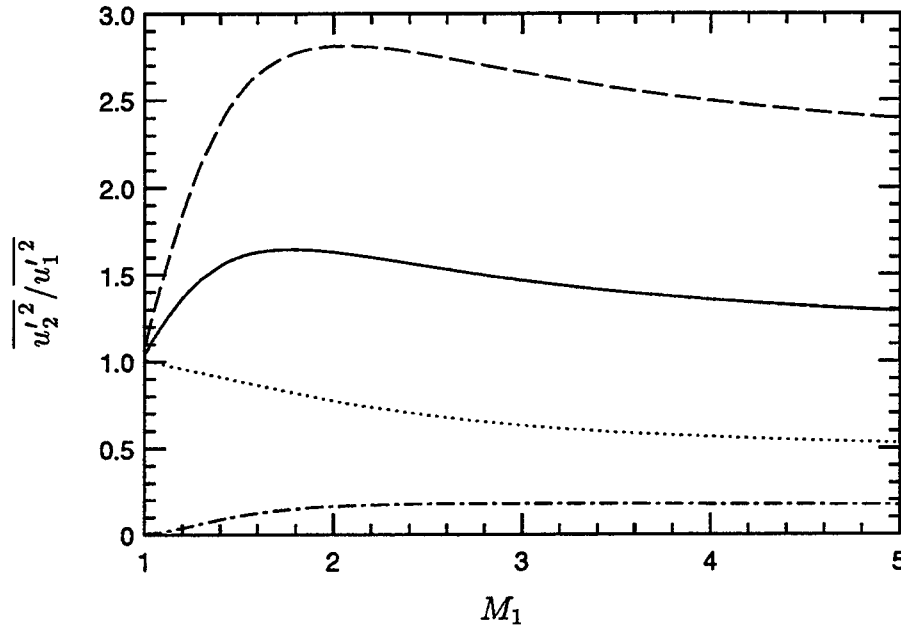
FIG. 13. The amplification of $\overline{u'^2}$ across the shock wave in the far-field. ——— (Pure vorticity), ———— $(A_r = 0.58; \phi_r = 0)$, ········ $(A_r = 0.58; \phi_r = 180°)$,——— (Pure entropy).
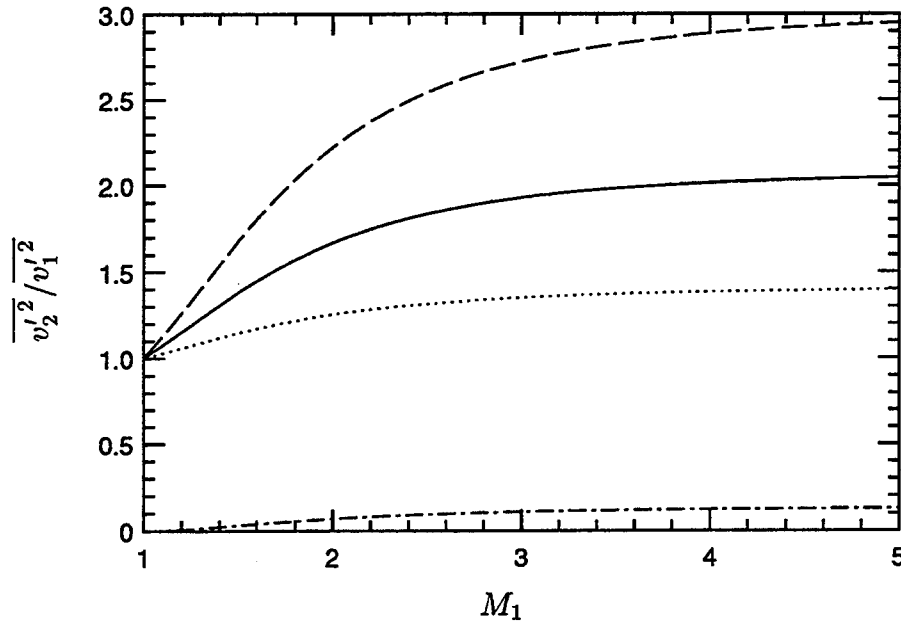
FIG. 14. The amplification of $\overline{v'^2}$ across the shock wave in the far-field. ——— (Pure vorticity), ———— $(A_r = 0.58; \phi_r = 0)$, ········ $(A_r = 0.58; \phi_r = 180°)$,——— (Pure entropy).
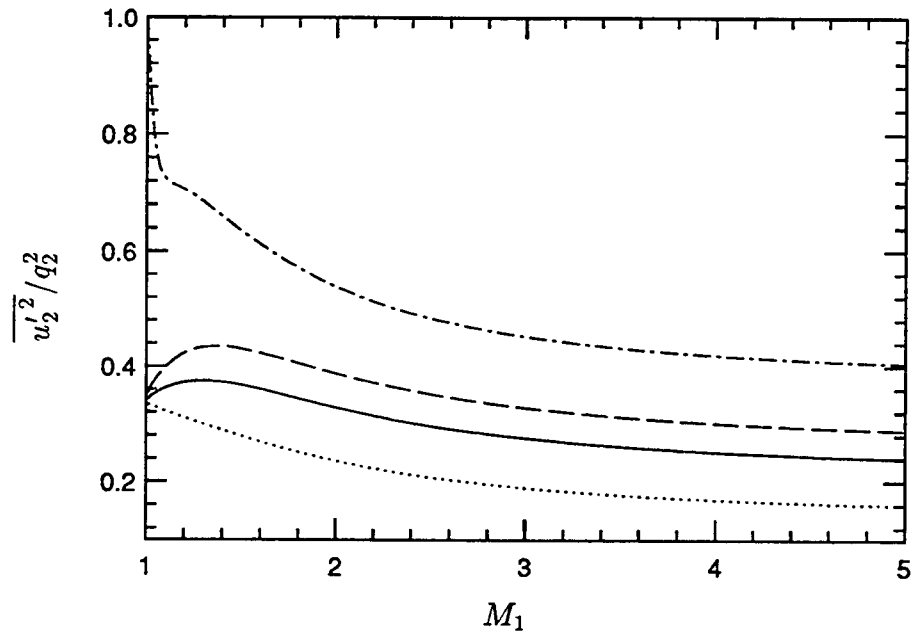
FIG. 15. Far-field values of $\overline{u'^2}/q^2$ behind the shock wave. —— (Pure vorticity), — — — ($A_r = 0.58; \phi_r = 0$), ········ ($A_r = 0.58; \phi_r = 180°$),— - — (Pure entropy).
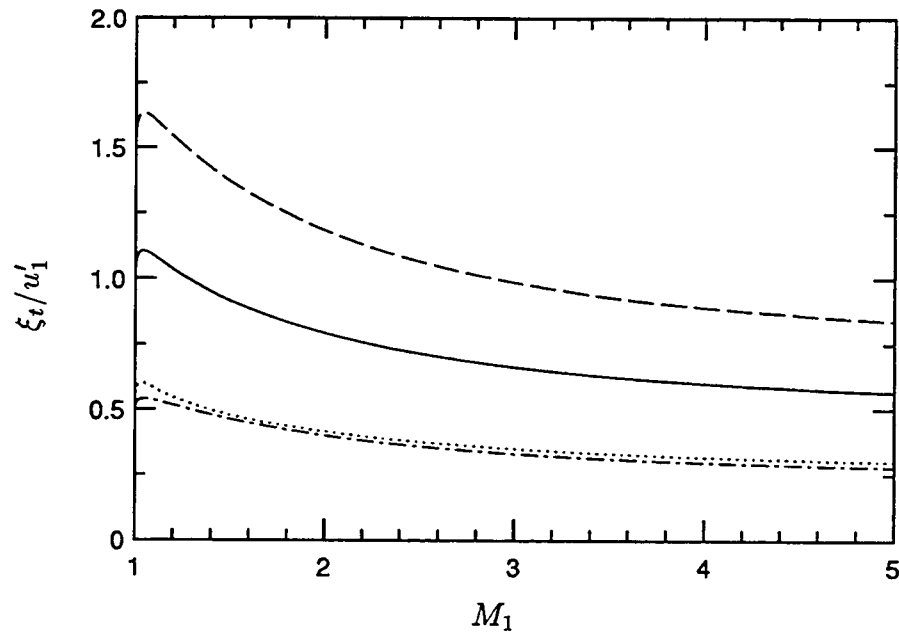
FIG. 16. The *rms* level of fluctuations in shock speed. —— (Pure vorticity), — — — ($A_r = 0.58; \phi_r = 0$), ········ ($A_r = 0.58; \phi_r = 180°$), — - — (Pure entropy).
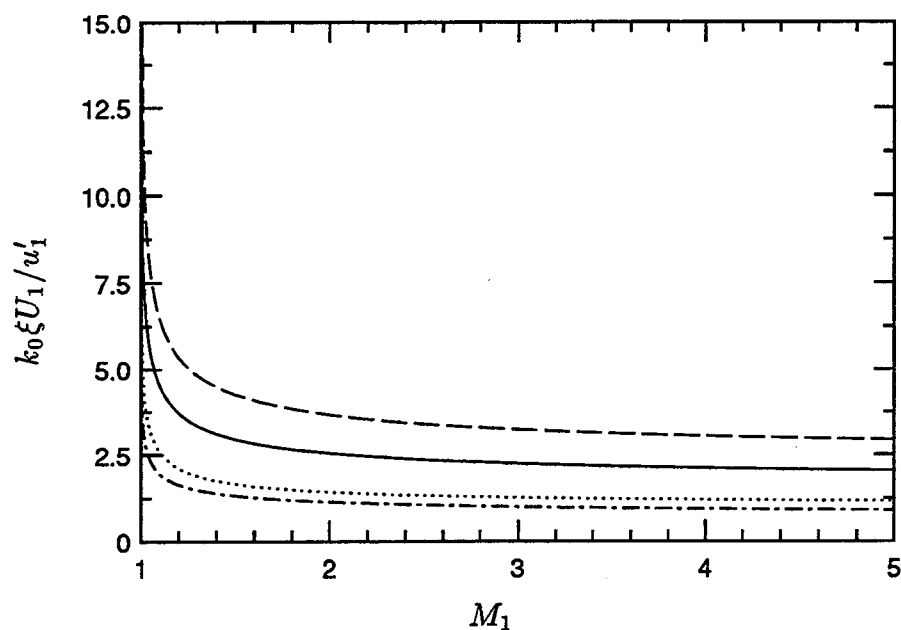
FIG. 17. The *rms* level of displacement of the shock front. ——— (Pure vorticity), ——— ($A_r = 0.58; \phi_r = 0$), ········ ($A_r = 0.58; \phi_r = 180°$), —·—· (Pure entropy).
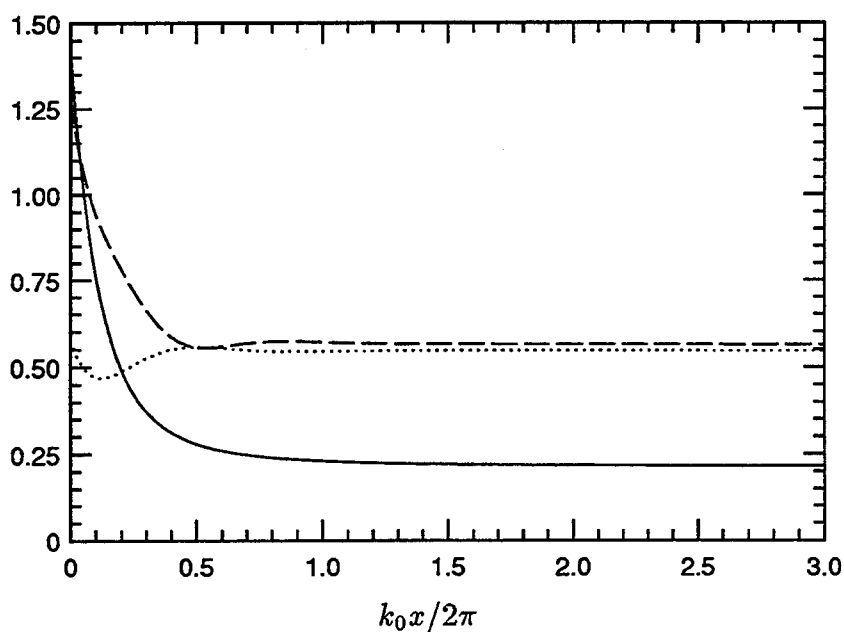

FIG. 18. The variation of thermodynamic fluctuations behind a Mach 1.5 shock wave. The incident fluctuations correspond to $A_r = 0.58$ and $\phi_r = 0$. All three curves are normalized with $\sqrt{q_1^2}/U_1$. ——— (p_2'/P_2), ——— ($\rho_2'/\bar{\rho}_2$), ········ ($T_2'/\bar{T}_2$).
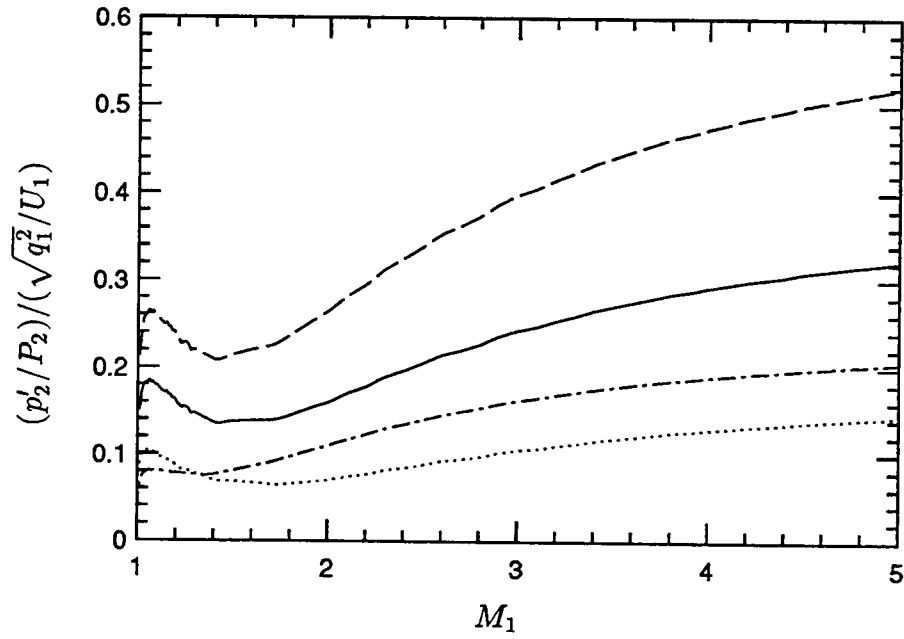
FIG. 19. The intensity of far-field pressure fluctuations behind the shock wave. ———— (Pure vorticity), ———— $(A_r = 0.58; \phi_r = 0)$, ········ $(A_r = 0.58; \phi_r = 180°)$,——— (Pure entropy).
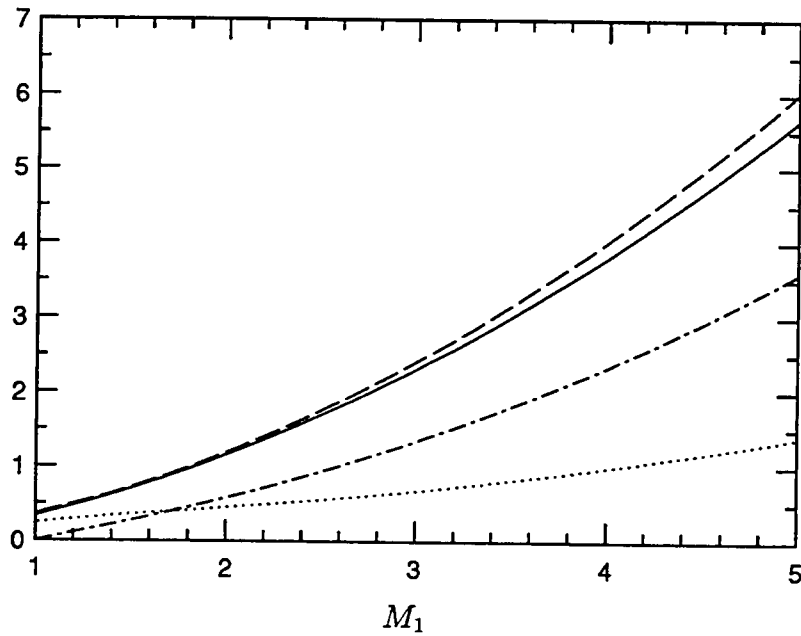

FIG. 20. Evaluation of Morkovin's hypothesis in the far-field of the shock wave. ———— $(\rho_2'/\bar{\rho}_2)$, ———— $(T_2'/\bar{T}_2)$, ········ $(\gamma-1)M_2^2 u_2'/U_2$, ——— $(\gamma-1)M_2(U_1/U_2-1)\xi_t/a_2$.

REFERENCES

BRADSHAW, P. 1977 Compressible turbulent shear layers. *Annu. Rev. Fluid Mech.* **9**, 33-54.

CHANG, C.T. 1957 Interaction of a plane shock and oblique plane disturbances with special reference to entropy waves. *J. Aero. Sci.* **24**, 675-682.

CUADRA, E. 1968 Flow perturbations generated by a shock wave interacting with an entropy wave. *AFOSR-UTIAS Symposium on Aerodynamic Noise,*Toronto, pp. 251-271.

DOLLING, D.S. 1993 Fluctuating loads in shock wave/turbulent boundary layer interaction: tutorial and update. *AIAA Paper,*93-0284.

FERNHOLZ, H.H. & FINLEY, P.J. 1981 A further compilation of compressible boundary layer data with a survey of turbulence data. *AGARDograph 263.*

GREEN, J.E. 1970 Interaction between shock waves and turbulent boundary layers. *Prog. Aerosp. Sci.* **11**, 235-340.

HANNAPPEL, R. & FRIEDRICH, R. 1994 DNS of a M=2 shock interacting with isotropic turbulence. In *Proc. First ERCOFTAC Workshop on DNS and LES*, Guildford, Surrey, U.K.

HESSELINK, L. & STURTEVANT, B. 1988 Propagation of weak shocks through a random medium. *J. Fluid Mech.* **196**, 513-553.

HONKAN, A. & ANDREOPOULOUS, J. 1992 Rapid compression of grid-generated turbulence by a moving shock wave. *Phys. Fluids A.* **4**, 2562-2572.

KELLER,J. & MERZKIRCH, W. 1990 Interaction of a normal shock wave with a compressible turbulent flow. *Exp. Fluids.* **8**, 241-248.

KOVASZNAY, L.S.G. 1953 Turbulence in supersonic flow. *J. Aero. Sci.* **20**, 657-682.

LEE, S., LELE, S.K. & MOIN, P. 1993 Direct numerical simulation of isotropic turbulence interacting with a weak shock wave. *J. Fluid Mech.* **251**, 533-562.

LEE, S. LELE, S.K. & MOIN, P. 1994 Interaction of isotropic turbulence with a strong shock wave. *AIAA Paper,* 94-0311.

LELE, S.K. 1992 Compact finite difference schemes with spectral-like resolution. *J. Comput. Phys.* **103**, 16-42.

LELE, S.K. 1994 Compressibility Effects on Turbulence. *Annu. Rev. Fluid Mech.* **26**, 211-254.

MAHESH, K., LELE, S.K. & MOIN, P. 1994a The response of anisotropic turbulence to rapid homogeneous one-dimensional compression. *Phys. Fluids.* **6,** 1052-1062.

MAHESH, K., LEE, S., LELE, S.K. & MOIN, P. 1994b The interaction of an isotropic field of acoustic waves with a shock wave. *Submitted to J. Fluid Mech.*

MAHESH, K., LELE, S.K. & MOIN, P. 1994c The interaction of a shock wave with a turbulent shear flow. PhD Thesis in preparation, Stanford University, Stanford, California.

MOORE, F.K. 1954 Unsteady Oblique Interaction of a Shock Wave with a Plane Disturbance. *NACA TN 2879.*

MORKOVIN, M.V. 1960 Note on the assessment of flow disturbances at a blunt body traveling at supersonic speeds owing to flow disturbances in the free stream. *J. App. Mech.,* ASME Trans., No. 60-APM-10.

MORKOVIN, M.V. 1961 Effects of compressibility on turbulent flows. In *Mecanique de la Turbulence* ed. A. Favre, pp. 367-380.

POINSOT, T.J. & LELE, S.K. 1990 Bounary conditions for direct simulation of compressible viscous reacting flow. *Center for Turbulence Research Manuscript 102,* Stanford University/NASA Ames, CA.

RIBNER, H.S. 1953 Convection of a Pattern of Vorticity through a Shock Wave. *NACA TN 2864.*

RIBNER, H.S. 1954 Shock-Turbulence Interaction and the Generation of Noise. *NACA TN 3255.*

RIBNER, H.S. 1969 Acoustic energy flux from shock-turbulence interaction. *J. Fluid Mech.* **35,** 299-310.

RIBNER, H.S. 1987 Spectra of noise and amplified turbulence emanating from shock-turbulence interaction. *AIAA Journal.* **25,** 436-442.

SETTLES, G.S. & DODSON, L.J. 1994 Supersonic and hypersonic shock/boundary-layer interaction database. *AIAA Journal.* **32,** 1377-1383.

WRAY, A.A. 1986 Very low storage time-advancement schemes. *Internal Rep.* NASA-Ames Research Center, Moffett Field, CA.

YANG, J., KUBOTA, T. & ZUKOSKI, E.E. 1994 A model for characterization of a vortex pair formed by shock passage over a light-gas inhomogeneity. *J. Fluid Mech.* **258,** 217-244.

ZANG, T.A., HUSSAINI, M.Y. & BUSHNELL, D.M. 1984 Numerical computations of turbulence amplification in shock-wave interactions. *AIAA Journal.* **22,** 13-21.

PART FOUR

THE INTERACTION OF AN ISOTROPIC FIELD
OF ACOUSTIC WAVES WITH A SHOCK WAVE

B.1 Introduction

This section uses linear analysis to study the interaction of a shock wave with an isotropic field of acoustic waves. The analysis aims at characterizing the effect of compressibility in the interaction of a compressible turbulent flow with a shock wave. Within the linear framework, a field of acoustic waves would correspond to the dilatational component of a compressible turbulent flow. As discussed in Chapter 3, there is evidence to suggest that compressible effects are negligible in non-hypersonic turbulent boundary layers. However shear flows such as the mixing layer and supersonic jet are known to be significantly affected by compressibility.

The increased level of compressibility of these flows (parametrized by the ratio of kinetic energy in solenoidal and dilatational components) suggests that effects due to the dilatational component would be important in their interaction with a shock wave. Past analytical work related to shock/turbulence interaction (Chapter 1) has considered the interaction of a shock wave with a plane acoustic wave. To the best of our knowledge, the interaction of a field of acoustic waves with a shock wave has not been analyzed before. Our analysis is based upon Moore's (1954) study of the interaction of a shock with a plane acoustic wave. Moore's analysis is extended to study the evolution of an isotropic field of acoustic waves across a shock. The results are then applied to predict the response of a compressible isotropic turbulent flow to a shock.

This section is organized as follows. Section B.2 formulates the problem of a plane acoustic wave interacting with a shock. The results are evaluated by comparison to DNS. The analysis is then extended to examine the evolution of an isotropic field of acoustic waves across a shock. The statistics of turbulent kinetic energy and thermodynamic fluctuations behind the shock wave are described in Section B.3. A brief discussion including description of shock wave/compressible turbulence interaction is presented in Section B.4. Summary of the study in Section B.5 is followed by the concluding section (B.6) where some of the details of Moore's analysis are outlined.

Parallel may be drawn between Part 3 and the following analysis. The notation used below might differ from that in Part 3; we have retained Moore's notation and method of analysis for consistency. The work described below is discussed by Mahesh, Lee, Lele and Moin (1994c).

B.2 Formulation of the problem

B.2.1 The interaction of an acoustic wave with a shock wave

Figure B.1 shows a schematic of the problem. A normal shock propagates at speed V into fluid that is at rest in the mean. The mean velocity behind the shock is denoted by U. The subscripts 1 and 2 denote the fluid in front and behind the shock respectively. The fluid at rest is assumed to be perturbed by the weak field of a plane acoustic wave that is incident at angle ψ_1 to the shock. The flow field associated with the acoustic wave is given by:

$$\frac{u_1}{V} = A_1 f\left(\frac{mx_1 - ly + a_1 t}{\lambda_1}\right) \qquad (B.1a)$$

$$\frac{v_1}{V} = A_2 f\left(\frac{mx_1 - ly + a_1 t}{\lambda_1}\right) \qquad (B.1b)$$

$$\frac{p_1}{P_1} = A_3 f\left(\frac{mx_1 - ly + a_1 t}{\lambda_1}\right) \qquad (B.1c)$$

$$\frac{\rho_1}{R_1} = A_4 f\left(\frac{mx_1 - ly + a_1 t}{\lambda_1}\right). \qquad (B.1d)$$

Here, P_1, R_1 and a_1 are the mean pressure, density and sound speed in the fluid ahead of the shock while u_1 and v_1 are the disturbance velocities in the x_1 and y directions respectively. The pressure and density fluctuations associated with the incident acoustic wave are denoted by p_1 and ρ_1. The variables l and m are related to the direction of propagation by $l = \sin\psi_1$ and $m = \cos\psi_1$ and λ_1 represents the lengthscale of the disturbance. Note that the coordinate system is fixed in the fluid that is at rest, yielding $x_1 = Vt$ at the mean position of the shock wave. The amplitudes of velocity, pressure and density are related through the governing equations for an acoustic wave; *i.e.*,

$$lA_1 = -mA_2; \qquad A_3 = \gamma A_4; \qquad A_1 = -\frac{m}{\gamma M}A_3 \qquad (B.2)$$

$M = V/a_1$ is the mean Mach number of the shock wave and γ is the ratio of specific heats. Incidence of the acoustic wave causes the shock wave to deform with a profile that matches the profile of the incident wave. The linearized Rankine-Hugoniot equations are used to describe the jump of the disturbance across the disturbed shock. This yields boundary conditions for the flow behind the shock which is described by the Euler equations linearized about the uniform mean flow. The linearized Euler equations are solved in consonance with the boundary conditions to calculate the displacement of the shock wave and the flow field downstream of the shock.

The flow behind the shock wave has two distinct regimes depending upon the angle of incidence of the acoustic wave. The two regimes differ in the nature of the pressure field (and hence, its associated velocity, temperature and density field) behind the shock wave. Over a range of incident angles $0 \leq \psi_1 < \psi_{cl}$ or $\psi_{cu} < \psi_1 \leq \pi$, the pressure field behind the shock is a freely propagating plane acoustic wave. However, if $\psi_{cl} < \psi_1 < \psi_{cu}$, the pressure field behind the shock corresponds to an evanescent wave and decays exponentially. Over both these regimes, the vorticity and entropy waves propagate without decaying. ψ_{cl} and ψ_{cu} are roots of the following equation (Moore, 1954):

$$\left(\frac{a_2}{V}\right)^2 - \left(1 - \frac{U}{V}\right)^2 = \left(\cot\psi_c + \frac{a_1}{V}\csc\psi_c\right)^2. \qquad (B.3)$$

Note that ψ_{cl} and ψ_{cu} depend only on the mean Mach number. The displacement of the shock front has a certain speed of propagation along the shock front due to the unsteady nature of the incident field. Analogous to the classical flexural wall problem in acoustics, (Pierce, 1981) the nature of the downstream pressure field is determined by how the speed of the disturbance compares with the mean speed of sound and velocity downstream of the shock. Moore (1954) illustrates the two regimes geometrically. Ribner (1953) provides an equivalent explanation by noting that the unsteady interaction of an oblique wave with a normal shock can be transformed into the steady interaction of an oblique wave with an oblique shock. In the transformed coordinates, depending upon the incident angle of the wave, the flow behind the oblique shock is either supersonic or subsonic (yielding either a wave equation or Poisson equation for the pressure), which corresponds to the two regimes mentioned above. Alternatively, arguments similar to those in Chapter 3 could be used to demonstrate the existence of two regimes.

The method for solution of the downstream flow field is given by Moore. In the interests of clarity, we reproduce his results at the end of the Appendix in Section B.6. Apart from the existence of two different regimes, note that the velocity field is a linear superposition of acoustic and vortical components. Similarly, the density and temperature fields are superpositions of acoustic and entropic components. The pressure field is associated solely with the acoustic component.

B.2.2 Comparison of linear analysis to numerical solution

We compare results of the linear analysis to numerical computations of the interaction of a normal shock wave with a plane acoustic wave that is incident from upstream. The computation solves the two-dimensional compressible Navier-Stokes equations in a frame of reference that moves at the mean speed of the shock wave. The sixth order Pade scheme (Lele, 1992) is used to compute spatial derivatives and the third order Runge Kutta (Wray, 1986) is used to integrate in time. No shock-capturing or shock-fitting is used to treat the shock wave; its structure is resolved by a non-uniform mesh.

This comparison is intended to complement that by Zang *et al* (1984) who compared the predictions of McKenzie and Westphal's (1968) linear analysis to their numerical solution of the two-dimensional Euler equations using a shock-fitting scheme. Zang *et al* examined the effect of incident angle, shock-strength and the amplitude of the incident disturbance in the interaction of acoustic and vorticity waves with a shock wave. Results were presented only in the freely propagating regime. The dependence on incident angle was examined in the interaction of disturbances of amplitude 0.1% and 10% with a shock wave of Mach number 8. Good agreement was seen away from the critical angle; divergence from the linear analysis prediction was seen within about 20° of the critical angle. The linear analysis predictions were quite robust in terms of dependence on shock strength and disturbance amplitude. For an incident angle of 30°, the linear predictions were valid for disturbance amplitudes as high as 25% for acoustic waves and 100% for vorticity waves and shock waves whose Mach number was close to unity.

We present results of the interaction of a plane acoustic wave ($p_1/P_1 = 2.5\%$) interacting with a shock wave of Mach number 1.5. The Mach number of 1.5 was chosen to be representative of experiments on the shock/turbulence interaction. In the context of Zang *et al*'s results, we only present the dependence on the incident angle. Results are presented in both freely propagating and decaying regimes. Figure B.2 compares the computed values of *rms* dilatation and vorticity with predictions of the linear analysis. Note that ψ_{cl} and ψ_{cu} have values of 97.16° and 154.45° respectively for $M = 1.5$. Excellent agreement is seen except for a region within 25 degrees of the critical angles. As noted by Zang *et al* (for the shock wave of Mach number 8), a decaying pressure field is observed downstream of the shock wave before the critical angle is reached.

A possible reason for deviation of the computed result from the linear analysis around the critical angle is as follows. Within linear analysis, the unsteady interaction of a plane disturbance with a normal shock wave may be transformed into the *steady* interaction of

the disturbance with an oblique shock wave. This transformation is an integral part of Ribner's (1953) and Chang's (1957) analysis of the interaction of a shock with a vorticity and entropy wave respectively. While Moore does not employ this transformation, it exists and involves defining coordinates x' and y' such that

$$x' = x - Vt; \qquad y' = y - \frac{a_1 + mV}{l}t$$

i.e., the flow is observed from a frame of reference that moves at the mean shock speed in the x direction and at speed $(a_1 + mV)/l$ in the y direction. In these transformed coordinates, the governing equations behind the shock wave are the steady Euler equations that are linearized about uniform mean flow at an equivalent Mach number M_e that is given by the relation:

$$M_e^2 = \frac{l^2(V - U)^2 + (a_1 + mV)^2}{a_2^2 l^2}$$

This equivalent Mach number depends upon the Mach number of the normal shock wave and the incident angle of the disturbance and equals unity at the critical angle. As a result, incident angles close to the critical angle correspond to steady transonic flow downstream of the shock wave in the transformed coordinates. It is well known that the linear approximation is inconsistent in the transonic regime. We believe that use of the transonic small disturbance equations are necessary to accurately represent the interaction around the critical angle.

Further indication of this is provided in Figure B.3, where the dependence of the interaction upon the amplitude of the incident disturbance is examined. The interaction away from the critical angle ($\psi_1 = 60°$) is compared to that close to the critical angle ($\psi_1 = 100°$). The *rms* intensity (p_{rms}/P) of the incident pressure fluctuation is varied from 0.14% to 14% in both cases. The vorticity (normalized by the incident dilatation) behind the shock wave is plotted against the amplitude of the incident disturbance in Figure B.3. The variation with the incident amplitude is negligible away from the critical angle. However, significant dependence upon the incident amplitude is seen close to the critical angle. This non-linear behavior around the critical angle is in accordance with the expectation that the transonic small disturbance equations are needed to describe the interaction in that range.

B.2.3 The interaction of a field of acoustic waves with a shock wave

Moore's analysis is now extended to describe the interaction of an isotropic field of acoustic waves with the shock wave. The problem is convenient to analyze in cylindrical coordinates. Figure B.4 shows a schematic of the problem in a frame of reference that

moves at the speed of the undisturbed shock. The $y - z$ plane corresponds to the shock wave, while the acoustic wave lies in the $x_1 - r$ plane that makes an angle ϕ with the y axis. Irrotationality precludes any component of velocity outside this plane. In the $x_1 - r$ plane, the acoustic wave makes an angle ψ_1 with the x_1 axis. The $x_1 - r$ plane is equivalent to the $x_1 - y$ plane used in Moore's analysis. It is seen from Figure B.4 that

$$u_r = \frac{v}{\cos\phi} = \frac{w}{\sin\phi}; \quad u_\phi = 0. \tag{B.4}$$

Moore's results are used to obtain the following relations describing the amplitude of the fluctuating field behind the shock for a plane incident wave. Note that we transform to a coordinate system that moves at the mean speed of the shock i.e., our streamwise coordinate becomes $\eta_2 = -[x_2 - (V - U)t]$.

For $0 \le \psi_1 < \psi_{cl}$ or $\psi_{cu} < \psi_1 \le \pi$,

$$\frac{|\widehat{p}_2|^2}{P_2{}^2} = \widetilde{K}^2 \frac{|\widehat{p}_1|^2}{P_1{}^2} \tag{B.5a}$$

$$\frac{|\widehat{u}_2|^2}{V^2} = \left[\widetilde{F}^2 + \widetilde{G}^2 + 2\widetilde{F}\widetilde{G}\cos\left(\frac{1}{\lambda_2}\frac{a_2}{V}\frac{\eta_2}{1-r}\right)\right]\frac{|\widehat{p}_1|^2}{P_1{}^2} \tag{B.5b}$$

$$\frac{|\widehat{u}_{r2}|^2}{V^2} = \left[\widetilde{H}^2 + \widetilde{I}^2 + 2\widetilde{H}\widetilde{I}\cos\left(\frac{1}{\lambda_2}\frac{a_2}{V}\frac{\eta_2}{1-r}\right)\right]\frac{|\widehat{p}_1|^2}{P_1{}^2} \tag{B.5c}$$

$$\frac{|\widehat{\rho}_2|^2}{R_2{}^2} = \left[\left(\frac{\widetilde{K}}{\gamma}\right)^2 + \widetilde{Q}^2 + 2\frac{\widetilde{K}\widetilde{Q}}{\gamma}\cos\left(\frac{1}{\lambda_2}\frac{a_2}{V}\frac{\eta_2}{1-r}\right)\right]\frac{|\widehat{p}_1|^2}{P_1{}^2} \tag{B.5d}$$

The constants $\widetilde{K}, \widetilde{F}$ and $\widetilde{H}$ are associated with the acoustic component of the flow field. Similarly, $\widetilde{G}$ and $\widetilde{I}$ are associated with the vortical component and $\widetilde{Q}$ corresponds to the entropic component.

If $\psi_{cl} < \psi_1 < \psi_{cu}$, the amplitudes behind the shock are given by:

$$\frac{|\widehat{p}_2|^2}{P_2{}^2} = e^{-2d\eta_2/\lambda_1}\left[\widetilde{K}_{(1)}^2 + \widetilde{K}_{(2)}^2\right]\frac{|\widehat{p}_1|^2}{P_1{}^2} \tag{B.6a}$$

$$\frac{|\widehat{u}_2|^2}{V^2} = \left[T_1 + T_2 + T_3\right]\frac{|\widehat{p}_1|^2}{P_1{}^2} \tag{B.6b}$$

where,

$$T_1 = \widetilde{G}_{(1)}^2 + \widetilde{G}_{(2)}^2; \quad T_2 = e^{-2d\eta_2/\lambda_1}\left[\widetilde{F}_{(1)}^2 + \widetilde{F}_{(2)}^2\right]$$

$$T_3 = 2e^{-d\eta_2/\lambda_1} \left[\left(\widetilde{F}_{(1)}\widetilde{G}_{(1)} + \widetilde{F}_{(2)}\widetilde{G}_{(2)} \right) \cos\delta - \left(\widetilde{F}_{(2)}\widetilde{G}_{(1)} - \widetilde{F}_{(1)}\widetilde{G}_{(2)} \right) \sin\delta \right]; \quad \delta = \frac{c\eta_2}{\lambda_1} \frac{1}{1-r}$$

The amplitude of u_{r2}/V may be obtained from the expression for u_2/V by replacing $\widetilde{F}_{(1)}, \widetilde{G}_{(1)}, \widetilde{F}_{(2)}$ and $\widetilde{G}_{(2)}$ by $\widetilde{H}_{(1)}, \widetilde{I}_{(1)}, \widetilde{H}_{(2)}$ and $\widetilde{I}_{(2)}$ respectively. The amplitude of ρ_2/R_2 may be obtained from the expression for u_2/V by replacing $\widetilde{F}_{(1)}, \widetilde{G}_{(1)}, \widetilde{F}_{(2)}$ and $\widetilde{G}_{(2)}$ by $\widetilde{K}_{(1)}/\gamma, \widetilde{Q}_{(1)}, \widetilde{K}_{(2)}/\gamma$ and $\widetilde{Q}_{(2)}$ respectively.

Analogous to the propagating regime, the constants $\widetilde{K}_{(\alpha)}, \widetilde{F}_{(\alpha)}$ and $\widetilde{H}_{(\alpha)}$ are associated with the acoustic component of the flow field. $\widetilde{G}_{(\alpha)}$ and $\widetilde{I}_{(\alpha)}$ are associated with the vortical component and $\widetilde{Q}_{(\alpha)}$ corresponds to the entropic component.

Note that the solution downstream of the shock wave requires the spectrum of pressure fluctuations ahead of the shock. We assume the incident acoustic field to be isotropic. This combined with the condition of irrotationality requires the upstream spectrum of the velocity fluctuations to be of the form:

$$E_{ij}(\mathbf{k}) = \frac{E(k)}{8\pi k^2} \frac{k_i k_j}{k^2}$$

where $E_{ij}(\mathbf{k})$ is the energy spectrum tensor and $E(k)$ is the three-dimensional energy spectrum. Using the acoustic relation, $A_3 = \gamma M A_1 / \cos\psi_1$, and the above expression for the energy spectrum tensor, we get,

$$\frac{|\widehat{p}_1|^2(\mathbf{k})}{P_1{}^2} = \left(\frac{\gamma M}{V} \right)^2 \frac{E(k)}{4\pi k^2} \tag{B.7}$$

Substituting for $|\widehat{p}_1|^2(\mathbf{k})/P_1{}^2$ and integrating over wavenumber space at every streamwise location (η_2), we get the streamwise evolution of statistics downstream of the shock wave. This integration is done in polar coordinates in the wave number space:

$$k_1 = k\cos\psi_1, \quad k_2 = k\sin\psi_1\cos\phi, \quad k_3 = k\sin\psi_1\sin\phi, \quad \mathrm{d}^3\mathbf{k} = k^2\sin\psi_1\,\mathrm{d}\psi_1\,\mathrm{d}\phi\,\mathrm{d}k$$

where, $k = |\mathbf{k}|$ varies from 0 to ∞, ψ_1 from 0 to π and ϕ varies from 0 to 2π. Since the coefficients in the above equations are independent of ϕ, the integration over ϕ can be done analytically for isotropic initial spectra. For example,

$$\frac{v_2^2(\eta_2)}{V^2} = \int \cos^2\phi \, \frac{|\widehat{u}_{r2}(\eta_2, k, \psi_1)|^2}{V^2} \, \mathrm{d}^3\mathbf{k} = \pi \iint_{k,\psi_1} \frac{|\widehat{u}_{r2}|^2}{V^2} \, k^2\sin\psi_1\,\mathrm{d}\psi_1\,\mathrm{d}k$$

94

The integration over k and ψ_1 is performed numerically at every streamwise location. Note that the results depend upon the three dimensional energy spectrum, $E(k)$. We assume the following form for $E(k)$:

$$\frac{E(k)}{V^2} \sim \left(\frac{k}{k_0}\right)^4 e^{-2(\frac{k}{k_0})^2}$$

This form of the spectrum was used by Lee *et al.* (1993,1994*b*) in their analysis of the interaction of isotropic vortical turbulence with a shock wave. There is no data that suggests the chosen spectral dependency for an isotropic field of sound waves. However, only the inhomogeneous part of the flow-field behind the shock wave is dependent upon the energy spectrum of the incident waves; the far-field ($\eta_2 \to \infty$) values are *independent* of the shape of the spectrum. We choose the same spectrum as Lee *et al* to allow direct comparison to ther results of the inhomogeneous near-field behind the shock wave. Since the inhomogeneous component of the flow-field exponentially decays behind the shock wave, it is the far-field that is of importance and will be examined in detail.

B.3 Results

B.3.1 Spatial variation of kinetic energy

The evolution of the kinetic energy behind the shock wave is shown in Figure B.5, where $q^2 = R_{ii}$ is plotted as a function of downstream distance. The inhomogeneous nature of the velocity field is apparent immediately downstream of the shock. Note that the curves for $M = 1.2$ and $M = 2$ are qualitatively different. While q^2 decays monotonically for $M = 1.2$, it exhibits rapid nonmonotonic variation for $M = 2$. A similar rapid variation of kinetic energy was observed in the interaction of vortical fluctuations with a shock wave by Lee *et al* (1993). However, in the shock wave/vortical turbulence interaction problem, this variation was observed at all Mach numbers considered.

Equations (5) and (6) are used to show that this variation of kinetic energy behind the shock wave is a consequence of the acoustic waves that are incident at $\psi_{cl} < \psi_1 < \psi_{cu}$. Recall that the downstream pressure field and hence the velocity field set up by these waves decayed exponentially. Equation (6*b*) shows that the downstream kinetic energy over this regime has three components: a homogeneous component associated with the vorticity waves (T_1), a monotonically decreasing component due to acoustic waves (T_2) and a non-monotonic component due to the correlation between the vorticity and acoustic waves (T_3). Upon integration over all the incident waves, these components combine to produce the

rapid evolution immediately downstream of the shock. As seen from equations (5a) and (5b), the kinetic energy associated with waves incident outside this range has homogeneous vortical and acoustic components and a nonmonotonic inhomogeneous component due to the correlation between them. When integrated over all incident waves, this correlation term is however, much smaller than the other components. This is illustrated in Figure B.6 where the kinetic energy is decomposed into four components (vortical, acoustic, correlation term for $\psi_{cl} < \psi_1 < \psi_{cu}$ and correlation term outside this regime) for $M = 2.0$. The correlation term associated with waves incident at $\psi_{cl} < \psi_1 < \psi_{cu}$ is seen to produce the rapid nonmonotonic evolution downstream.

A similar decomposition for the $M = 1.2$ shock showed the correlation term to be insignificant resulting in the monotonic evolution of Figure B.5. In our linear analysis calculations, the nonmonotonic downstream variation was observed for shocks whose Mach number exceeded 1.5. In studying the interaction of vortical disturbances with the shock wave, Lee *et al* (1993) erroneously concluded that linear analysis could not reproduce this trend which they had found in the DNS. This error was subsequently corrected and explained by them (Lee *et al*, 1994a,1994b).

The equation governing the evolution of kinetic energy downstream of the shock wave provides further insight into the spatial evolution of kinetic energy. The Euler equations linearized about uniform mean flow may be rearranged to show that the quantity,

$$I_{\text{total}} = \frac{\gamma M}{2}\left[\frac{q^2}{a^2} + \frac{p^2}{\gamma^2 P^2}\right] + \frac{\overline{pu}}{Pa} \qquad (B.8)$$

is conserved along a mean streamline. I_{total} changes across the shock wave and remains unchanged downstream. The $\overline{pu}$ correlation determines the partitioning of I_{total} between potential and kinetic energy. The spatial uniformity of I_{total} and the exponential decay of p^2 behind the shock wave show that the rapid evolution of q^2 behind the shock wave is a result of the rapid change in the partitioning of I_{total} through the correlation between pressure and the shock-normal component of fluctuating velocity. Decomposition of the $\overline{pu}$ correlation reveals that the rapid evolution of kinetic energy behind the shock wave is produced by the waves that are incident at $\psi_{cl} < \psi_1 < \psi_{cu}$. The far-field values of kinetic energy and pressure are however, determined by the correlation between pressure fluctuations and the *acoustic* component of the velocity field in the *propagating* regime.

B.3.2 Far-field kinetic energy

As seen from Figure B.5, after a distance that is comparable to the lengthscale (taken as $2\pi/k_0$) of the incident acoustic waves, the kinetic energy asymptotes to its far-field

96

value. The far-field values are independent of the upstream energy spectrum since the inhomogeneous terms drop out in the far-field. As a result, the integration over k can be performed independently of ψ_1 and ϕ to give $\int E(k)\,dk = q_0^2/2$. To gauge the effect of shock strength upon the interaction, we examine (Figure B.7) the far-field kinetic energy (normalized with the upstream kinetic energy) as a function of the Mach number of the shock wave. Note that the shock-normal component of kinetic energy is larger than the transverse components for all Mach numbers shown. An interesting feature of the evolution of kinetic energy is that kinetic energy *decreases* slightly across the shock wave over a range of Mach number from 1.25 to 1.80. The transverse components decrease across the shock wave over a wider range of the Mach number. This decrease in kinetic energy across the shock wave is peculiar to the acoustic wave/shock interaction problem. It is not observed in the interaction of vortical fluctuations with the shock wave where under linear analysis, kinetic energy increases across the shock wave for all shock strengths. Also, for $M > 3$, the amplification of kinetic energy is significantly higher than amplification levels seen in the interaction of vortical fluctuations with the shock wave.

The decrease in kinetic energy across the shock wave may be explained by decomposing (Figure B.8) the far-field energy into acoustic and vortical components and examining their dependence on Mach number. Both components are normalized with the upstream kinetic energy. This decomposition of kinetic energy is possible since the correlation between vortical and acoustic components falls to zero in the far-field. Note that the kinetic energy associated with the vortical component increases monotonically with Mach number and *exceeds* the upstream kinetic energy beyond a Mach number of about 2.25. The kinetic energy associated with the acoustic component, however *decreases* across the shock wave for Mach numbers exceeding about 1.2. These two components compete in determining the overall evolution of kinetic energy. For lower Mach numbers, the acoustic component dominates since not enough vorticity is generated downstream, causing the overall kinetic energy to drop. At higher Mach number, the vortical component dominates due to increased generation of vortical fluctuations and the overall kinetic energy rises across the shock. The vortical component of energy exceeds the acoustic component for Mach number exceeding 2.

The decrease of the far-field acoustic kinetic energy with Mach number is explained as follows. As the Mach number increases, $\psi_{cu} - \psi_{cl}$ increases (see Figure B.4 of Moore) and hence a larger fraction of incident waves lie in the range $\psi_{cl} < \psi_1 < \psi_{cu}$. Recall that these waves make no contribution to the far-field acoustic kinetic energy. The only contribution to the far-field acoustic kinetic energy comes from waves incident outside this

range whose amplification increases upon increasing the Mach number. Upon integrating over all incident waves, the net result of these competing factors is to produce (as seen in Figure B.8) a slow decrease (for $M < 3.5$) in the the far-field acoustic kinetic energy. Note that the variation of ψ_{cl} and ψ_{cu} with Mach number is most rapid at lower Mach numbers; in the limit of infinite Mach number, ψ_{cl} and ψ_{cu} are symmetrical about 90° and (for $\gamma = 1.4$), have values of 67.8° and 112.2° respectively.

B.3.3 The production of turbulence

Having observed the generation of vortical fluctuations - 'turbulence' behind the shock wave, we examine in Figure B.9, the intensity of the turbulence relative to the intensity of the incident pressure fluctuations. Note that $(q_{\text{vort.}}/U_2)/(p_1/P_1)$ is of the order 1 for most of the Mach numbers shown. ($U_2 = V - U$ is the mean velocity behind the shock wave if the shock were stationary in the mean) This suggests an interesting possibility in turbulent flows involving multiple shock waves (eg. unadapted supersonic jets). It is known that upon interaction with a shock wave, turbulence generates intense sound. For isotropic turbulence, the intensity of the sound generated (p_2/P_2) scales with the intensity of the incident turbulence (q_1/U_1). In turbulent flows involving multiple shock waves, it is reasonable to expect the generated sound waves to interact with the subsequent shock waves. If this happens, Figure B.9 suggests that these acoustic waves can generate significant levels of turbulence through the interaction. We do not mean to suggest that our homogeneous analysis is directly applicable to flows involving shock cells, which are quite inhomogeneous. However, our results suggest that acoustic wave/ shock wave interaction may be a significant generator of turbulence in these flows.

B.3.4 Thermodynamic fluctuations

Interaction with the shock wave is seen to significantly increase sound levels. Figure B.10 shows the intensity (p_2/P_2) of the far-field pressure fluctuations normalized with the intensity of pressure fluctuations upstream of the shock. Note that the intensity drops, although pressure fluctuations actually amplify across the shock wave. The rise across the shock wave of the far-field sound pressure level (SPL) and the level of acoustic intensity (AIL) in decibels is shown in Figure B.11. We define,

$$\text{SPL} = 10 \log \left[\frac{p^2}{p_r{}^2} \right], \quad \text{AIL} = 10 \log \left[\frac{p^2/Ra}{p_r{}^2/R_r a_r} \right] \quad (B.9)$$

where the subscript r denotes reference values. The rise in the level of sound across the shock wave is independent of the reference values. The increase in sound pressure level varies from 5 to 20 decibels while the rise in acoustic intensity varies from 2 to 10

decibels over the range of Mach numbers shown. Figure B.10 also shows the nature of the thermodynamic fluctuations in the far-field. The density and temperature fluctuations are normalized such that the three curves would collapse if the fluctuations were isentropic. We see that the isentropic relations hold until a Mach number of 1.5, beyond which the entropy fluctuations that are generated at the shock wave become significant relative to the acoustic fluctuations. The increasing importance of the entropy fluctuations in the far-field is due to two factors: increased production of entropy fluctuations at the shock wave and the decrease with Mach number of the far-field intensity of pressure fluctuations. Asymptotically, $(s_2/C_p)/(p_2/P_2)$ equals 1.47 ($\gamma = 1.4$) where s_2 is the *rms* entropy behind the shock wave and C_p is the specific heat at constant pressure.

B.3.5 Asymptotic behaviour

Another feature that distinguishes the interaction of sound waves with a shock wave is the asymptotic behavior with respect to Mach number. Linear analysis shows that for incident acoustic waves, quantities such as the ratio of fluctuating kinetic energy, pressure and temperature fluctuations across the shock wave are not bounded but increase as M^2. This is easily seen from equations (5) and (6). The constants (*eg.* $\widetilde{K}$) in the equations have finite values in the limit of infinite Mach number and hence the intensities of velocity, density and pressure fluctuations are bounded for finite intensity of incident pressure fluctuations. However, for a given intensity of pressure fluctuations the incident kinetic energy decreases as $1/M^2$ causing the amplification of kinetic energy to vary as M^2 for strong shocks. Similarly, since the mean pressure and temperature ratio varies as M^2 for strong shocks, the ratio of pressure and temperature fluctuations are not bounded. Unboundedness of kinetic energy amplification is peculiar to the acoustic wave/shock interaction problem; it is not present when vortical fluctuations interact with the shock wave. We show in Figure B.12 the kinetic energy amplification normalized by M^2. Note that the amplification ratios asymptote to finite values when properly scaled with M^2.

B.4. Discussion

B.4.1 Evaluation of linear analysis

The inviscid linear analysis of Moore (1954) is extended to study the interaction of a three-dimensional isotropic field of acoustic waves with a normal shock wave. The objective of this study is to isolate the effect of acoustic waves on the evolution of a turbulent flow as it interacts with a shock wave. As the level of compressibility of a turbulent flow increases, the effects associated with the acoustic component will become important. Understanding

the interaction of acoustic waves with a shock wave is therefore of fundamental importance. The interaction is likely to be especially important in unbounded turbulent flows.

Our use of linear analysis is prompted by its success in past investigations. In the interaction of a single unsteady disturbance with a shock wave, there appear to be four important factors that could cause deviation from linear behavior: proximity of the incident angle to the critical angle, the amplitude of the disturbance being non-negligible relative to the strength of the shock wave, the mean Mach number being close to unity and finally, viscous effects. Proximity to the critical angle seems to be the most important factor. Our computations of of single acoustic waves interacting with a shock wave disagree with linear analysis around 25 degrees of the critical angle; very good agreement is seen outside this range. Fortunately, in the interaction of a spectrum of waves with a shock wave, the incident waves around the critical angle make only partial contribution to the overall energy. With regard to the amplitude of incident disturbances, results of computations are encouraging. Our computations show good agreement with linear analysis away from the critical angle for disturbance amplitudes varying from 0.14% to 14%. Zang *et al* (1984) show that linear analysis yields good prediction away from the critical angle for acoustic disturbance amplitudes as large as 25%. Meadows *et al* (1994) reach a similar conclusion in their study of the one-dimensional interaction of an acoustic wave with a shock wave. Their comparison of linear analysis to a non-linear Riemann analysis yielded indistinguishable results (to plotting accuracy) for disturbance amplitudes less than 10%. An effect of increasing disturbance amplitude for a fixed shock strength has been documented by Honkan and Andreopoulous (1992) and Lee *et al* (1992) in the interaction of isotropic turbulence with a normal shock. Both studies reported a decrease in the amplification of kinetic energy as the disturbance amplitude was increased. Honkan and Andreopoulous' experimental study had a shock of mean Mach number 1.24 while Lee *et al*'s numerical results were for a shock wave of mean Mach number 1.2.

B.4.2 Combined interaction of vortical and acoustic fluctuations

The linearity of the analysis permits the use of superposition to predict the combined interaction of vortical and acoustic fluctuations with a shock wave. Since sound and vorticity travel at different speeds, the correlation between them can be assumed negligible upstream and in the far-field behind the shock wave. The amplification of kinetic energy across the shock wave can therefore be expressed as,

$$\frac{q^2}{q_0^2} = \frac{q_\omega^2 + q_\theta^2}{(q_\omega^2)_0 + (q_\theta^2)_0} \qquad (B.10)$$

where , the subscript '0' represents conditions upstream of the shock and the subscripts ω and θ represent the vortical and dilatational components respectively. The amplification ratio in the mixed problem may be expressed in terms of the amplification ratios of vortical and acoustic fluctuations as:

$$\frac{q^2}{q_0^2} = (1 - X)f_\omega + Xf_\theta \qquad (B.11)$$

where, $f_\omega = q_\omega^2/(q_\omega^2)_0$, $f_\theta = q_\theta^2/(q_\theta^2)_0$ and $X = (q_\theta^2)_0/q_0^2$. X is the ratio of acoustic to total kinetic energy upstream of the shock wave. Note that as X varies from 0 to 1, q^2/q_0^2 varies from f_ω to f_θ. Available experiments on the shock/turbulence interaction are in the range of Mach numbers for which the kinetic energy of the acoustic component decreases across the shock wave. Our results suggest that the presence of acoustic waves in these experiments will decrease the amplification of kinetic energy. As noted by Jacquin *et al* (1993), wind-tunnel experiments on the shock/turbulence interaction report lower amplification ratios than shock-tube experiments. They suggest that boundary-layer induced oscillation of the shock wave in the wind-tunnel experiments might be responsible (through an unknown mechanism) for this observation. Our results suggest the alternative scenario that the lower kinetic energy amplification is a consequence of a significant amount of acoustic waves in the turbulence ahead of the shock wave. A likely source of these sound waves are the shock waves that are generated at the edges of the grid that generates turbulence in the tunnel. Further data is needed to support or discard this scenario.

According to linear analysis (equation 18), when compressible isentropic turbulence interacts with a shock wave, the evolution of kinetic energy lies between two limits - the pure solenoidal and pure dilatational limits. This behavior is identical to the response of *homogenous* turbulence to one-dimensional compression. As shown by Cambon *et al*, the evolution of kinetic energy when compressible homogeneous turbulence is subjected to one-dimensional compression lies between the solenoidal and the dilatational limits. However an important difference between the shock/turbulence interaction problem and the homogeneous compression problem is the behavior of the turbulence in the dilatational limit. For homogeneous turbulence, Cambon *et al* show that the dilatational limit is characterized by loss of acoustic communication which forces the pressure-strain correlation to zero thereby yielding significantly higher amplification of q^2 as compared to solenoidal turbulence. The compressibility-induced decrease in kinetic energy across the shock wave that is seen in the acoustic wave/shock wave interaction for $1.25 < M < 1.8$ is not observed. This is due to the fundamentally different nature of the pressure fluctuations in the two problems.

The difference between the one-dimensional compression of solenoidal turbulence and

Ribner's (1954,1987) analysis of solenoidal fluctuations interacting with a shock wave were pointed out by Lee *et al* (1993) and underscored by Jacquin *et al* (1993). Results of the two problems agree for small Mach numbers; for large Mach numbers significantly larger amplification is seen in the homogeneous problem. Jacquin *et al* also compare the compression of homogeneous compressible turbulence to Ribner's analysis and note that the difference between the two problems is greater than pointed out by Lee *et al*. A comparison of the compression of dilatational fluctuations to the interaction of solenoidal fluctuations with a shock wave is not appropriate; comparison should be made to the interaction of dilatational fluctuations with the shock wave. Such comparison would reveal disagreement in the dilatational limit over the entire range of Mach numbers. While the homogeneous problem can approximate the evolution of kinetic energy in the interaction of solenoidal fluctuations with a shock wave of moderate strength, it is quite inappropriate as the incident turbulence becomes increasingly compressible.

B.4.3 Comparison to computation

The analysis explains recent observations (Hannapel and Friedrich, 1994) on the interaction of compressible turbulence with a normal shock. Hannapel and Friedrich numerically computed the interaction of low Reynolds number isotropic turbulence ($R_\lambda \sim 4$ upstream of the shock wave) with a normal shock of mean Mach number 2. The fluctuating Mach number was 0.1 at the inflow and the kinetic energy was equally distributed between the vortical and acoustic modes. ($X = 0.5$ in our notation.) They compared this interaction with that of essentially solenoidal turbulence ($X = 0$) of the same fluctuating Mach number. The 'compressible' case displayed increased amplification of vorticity, decreased amplification of velocity components transverse to the shock, decreased reduction of Taylor microscale and decreased amplification of density, temperature and pressure fluctuations across the shock wave.

The computation may suffer from lack of sufficient resolution of the shock front. As a result we do not attempt quantitative comparison. We show that the computation follows the trends predicted by the linear analysis and quote the linear analysis predictions for reference. The higher amplification of the transverse components of vorticity in the compressible case is explained by the generation of vorticity through the acoustic wave/shock wave interaction. Using an expression similar to equation (18), the increase in the amplification of vorticity may be shown to be $3g_\theta(\theta_0{}^2/\omega_0{}^2)$, where $g_\theta = \omega_2{}^2/\theta_0{}^2$ in the acoustic wave/shock wave interaction problem. Similarly, linear analysis predicts the decrease in transverse velocity and reduction in Taylor microscale. For the interaction of vortical fluctuations with a shock wave, Ribner's analysis yields $u^2/u_0^2 = 1.64$ and $v^2/v_0^2 = 1.66$

across a shock wave of Mach number 2. For dilatational fluctuations, our analysis yields values of 1.69 and 0.9 respectively. Using an expression similar to equation (18), we get $u^2/u_0^2 = 1.67$ and $v^2/v_0^2 = 1.28$; *i.e.*, the amplification of u^2 is essentially unchanged while the amplification of the transverse velocity drops.

Linear analysis yields values of 0.53 and 0.77 for $\lambda_1/(\lambda_1)_0$ and $\lambda_2/(\lambda_2)_0$ respectively (λ_i represents the Taylor microscale in the i direction) for the vortical problem. Corresponding values for the compressible problem are 0.66 and 0.94 respectively. The reduced amplification of thermodynamic fluctuations in the compressible problem (an order lower) is a consequence of the fact that in pure vortical turbulence, the absolute level of incident thermodynamic fluctuations is much lower (zero in the linear limit). The level of thermodynamic fluctuations behind the shock wave, however scale with the incident kinetic energy as a result of which the amplification of thermodynamic fluctuations will be quite large (undefined within linear analysis).

B.5. Summary

Inviscid linear analysis was used to study the evolution of fluctuating kinetic energy, sound level and thermodynamic fluctuations in the interaction of an isotropic field of acoustic waves with a normal shock wave. The analysis was an extension of Moore's (1954) study of the interaction of a shock wave with a single acoustic wave. Moore's analysis was evaluated by comparison to numerical computation. Good agreement was seen for angles away from the critical angles. A possible reason for disagreement around the critical angles was proposed. Linear approximation was noted to be inconsistent in this regime; requirement of the transonic small disturbance equations was suggested.

The interaction of an isotropic acoustic field with the shock was noted to be significantly different from that of vortical fluctuations. The kinetic energy of the acoustic fluctuations decreased across the shock wave for Mach numbers between 1.25 and 1.8. For Mach numbers exceeding 3, the kinetic energy amplified by levels that significantly exceeded those found in the interaction of vortical fluctuations with the shock. These trends were explained by decomposing the velocity field into acoustic and vortical components and examining their dependence on the Mach number. Upon interacting with the shock wave, the acoustic waves generated vortical fluctuations whose contribution to the far-field kinetic energy increased with increasing Mach number. The level of sound increased across the shock wave. The rise in the sound pressure level across the shock varied from 5 to 20 decibels for Mach number varying from 1.5 to 5. The fluctuations behind the shock

wave were nearly isentropic for Mach number less than 1.5 beyond which the generation of entropy fluctuations became significant.

Finally the analysis was used to describe the combined interaction of isotropic vortical and acoustic fluctuations with a normal shock wave.

B.6 Details of Moore's analysis

The solution dowstream of the shock wave is given below. The subscript 2 refers to conditions behind the shock wave.

For $0 \leq \psi_1 < \psi_{cl}$ or $\psi_{cu} < \psi_1 \leq \pi$,

$$\frac{1}{A_3} \frac{p_2}{P_2} = \widetilde{K} f\left(\frac{\alpha x_2 + \beta y + a_2 t}{\lambda_2} \right)$$

$$\frac{1}{A_3} \frac{\rho_2}{R_2} = \frac{\widetilde{K}}{\gamma} f\left(\frac{\alpha x_2 + \beta y + a_2 t}{\lambda_2} \right) + \widetilde{Q} f\left(\frac{\frac{m+1/M}{1-r} x_2 - ly}{\lambda_1} \right)$$

$$\frac{1}{A_3} \frac{u_2}{V} = \widetilde{F} f\left(\frac{\alpha x_2 + \beta y + a_2 t}{\lambda_2} \right) + \widetilde{G} f\left(\frac{\frac{m+1/M}{1-r} x_2 - ly}{\lambda_1} \right)$$

$$\frac{1}{A_3} \frac{v_2}{V} = \widetilde{H} f\left(\frac{\alpha x_2 + \beta y + a_2 t}{\lambda_2} \right) + \widetilde{I} f\left(\frac{\frac{m+1/M}{1-r} x_2 - ly}{\lambda_1} \right).$$

The x_2 axis is stationary in a frame of reference that moves with speed U yielding, $x_2 = (V - U)t$ at the mean position of the shock wave. Of the two terms that contribute to the velocity, density and temperature, the unsteady term corresponds to the acoustic wave while the steady term corresponds to the vorticity and entropy waves. The coefficients $\widetilde{K}, \widetilde{Q}, \widetilde{G}, \widetilde{H}$ and $\widetilde{I}$ in the above equations are functions of the Mach number of the shock and the angle of incidence and are given below.

If $\psi_{cl} < \psi_1 < \psi_{cu}$, the solution is a bit more complex and is given by:

$$\frac{1}{A_3} \frac{p_2(\eta, \xi)}{P_2} = \widetilde{K}_{(1)} \Phi_{(1)}(\eta, \xi) + \widetilde{K}_{(2)} \Phi_{(2)}(\eta, \xi)$$

$$\frac{1}{A_3} \frac{\rho_2}{R_2} = \frac{1}{\gamma} \frac{p_2}{P_2} + \widetilde{Q}_{(1)} f\left(\frac{\frac{m+1/M}{1-r} x_2 - ly}{\lambda_1} \right) + \widetilde{Q}_{(2)} g\left(\frac{\frac{m+1/M}{1-r} x_2 - ly}{\lambda_1} \right)$$

$$\frac{1}{A_3} \frac{u_2}{V} = \widetilde{F}_{(1)} \Phi_{(1)}(\eta, \xi) + \widetilde{F}_{(2)} \Phi_{(2)}(\eta, \xi) + \widetilde{G}_{(1)} f\left(\frac{\frac{m+1/M}{1-r} x_2 - ly}{\lambda_1} \right) + \widetilde{G}_{(2)} g\left(\frac{\frac{m+1/M}{1-r} x_2 - ly}{\lambda_1} \right)$$

$$\frac{1}{A_3}\frac{v_2}{V} = \widetilde{H}_{(1)}\Phi_{(1)}(\eta,\xi) + \widetilde{H}_{(2)}\Phi_{(2)}(\eta,\xi) + \widetilde{I}_{(1)}f\left(\frac{\frac{m+1/M}{1-r}x_2 - ly}{\lambda_1}\right) + \widetilde{I}_{(2)}g\left(\frac{\frac{m+1/M}{1-r}x_2 - ly}{\lambda_1}\right).$$

Analogous to the propagating regime, $\widetilde{K}_{(\alpha)}, \widetilde{Q}_{(\alpha)}, \widetilde{G}_{(\alpha)}, \widetilde{H}_{(\alpha)}$ and $\widetilde{I}_{(\alpha)}$ are functions of the Mach number of the shock and the angle of incidence and are given below. Also, η and ξ are related to x_2, y and t by:

$$\eta = -\frac{d}{\lambda_1}[x_2 - (V - U)t]$$

$$\xi = \frac{1}{\lambda_1}(\alpha x_2 + \beta y + cVt).$$

η is thus proportional to the distance behind the shock while ξ=constant represents an oblique plane moving at constant velocity. The functions $g, \Phi_{(1)}$ and $\Phi_{(2)}$ are defined as:

$$g(\eta) = \frac{1}{\pi}\int_{-\infty}^{\infty}\frac{f(\tau)}{\tau - \xi}d\tau$$

$$\Phi_{(1)} = \frac{1}{\pi}\int_{-\infty}^{\infty}f(\tau)\frac{\eta}{\eta^2 + (\tau - \eta)^2}d\tau$$

$$\Phi_{(2)} = \frac{1}{\pi}\int_{-\infty}^{\infty}f(\tau)\frac{\tau - \eta}{\eta^2 + (\tau - \eta)^2}d\tau.$$

Since a homogenous acoustic field may be represented as a superposition of plane waves, we consider $f(x) = e^{ix}$ for which $g, \Phi_{(1)}$ and $\Phi_{(2)}$ are given by:

$$g(\xi) = i\,e^{i\xi}, \quad \Phi_{(1)} = e^{-\eta}e^{i\xi}, \quad \Phi_{(2)} = i\,e^{-\eta}e^{i\xi}$$

Note that if the incident wave is a plane wave, the above equations take on a simple form. The coefficients in the solution are determined as follows.

$$B_1 = -\frac{2}{\gamma + 1}\frac{1}{M^2}\left(1 - \frac{\gamma - 1}{2}M^2\right); \qquad B_2 = \left(\frac{\gamma - 1}{\gamma + 1}\right)\frac{2}{\gamma M^2}$$

$$C_1 = \frac{2}{1 + \frac{\gamma - 1}{2}M^2}; \qquad C_2 = \frac{1}{\gamma}\left(1 - \frac{\gamma - 1}{1 + \frac{\gamma - 1}{2}M^2}\right)$$

$$D_1 = \frac{2\gamma M^2}{\gamma M^2 - \frac{\gamma - 1}{2}}; \qquad D_2 = \frac{M^2 - \frac{\gamma - 1}{2}}{\gamma M^2 - \frac{\gamma - 1}{2}}$$

$$l = \sin\psi_1; \quad m = \cos\psi_1; \quad n = \tan\psi_1$$

$$r = \frac{2}{\gamma + 1}\left(1 - \frac{1}{M^2}\right); \qquad \left(\frac{a_2}{V}\right)^2 = (1 - r)\left(1 + \frac{\gamma - 1}{2}r\right); \qquad \sigma = \frac{n(1 - r)}{1 + \frac{1}{Mm}}.$$

For $0 \le \psi_1 < \psi_{cl}$ or $\psi_{cu} < \psi_1 \le \pi$,

$$\chi = \left[1 - \frac{r(\gamma+1)(1+\sigma^2)}{2+(\gamma-1)r}\right]^{\frac{1}{2}}$$

$$\widetilde{L} = -\frac{m}{\gamma M}\frac{\left[1+\frac{\gamma+1}{4}\frac{M}{m}\left(\frac{3-\gamma}{\gamma+1}+\frac{\gamma-1}{2}r\right)\right]\chi + \frac{\gamma+1}{4}\left[1-2\frac{\gamma-1}{\gamma+1}\frac{n}{\sigma}-\frac{n\sigma}{1-r}\right](1-r)}{1+\chi-\frac{\gamma+1}{4}r\left(1+\frac{\sigma^2}{1-r}\right)}$$

$$\widetilde{K} = D_1\left(\widetilde{L}+\frac{m}{\gamma M}\right) + D_2$$

$$\widetilde{Q} = C_1\left(\widetilde{L}+\frac{m}{\gamma M}\right) + C_2 - \frac{\widetilde{K}}{\gamma}$$

$$m\frac{\lambda_2}{\lambda_1} = \frac{\frac{a_2}{V}(1+\frac{1}{mM})}{(1+\frac{1}{mM})^2+n^2(1-r)^2}\left[1+\sqrt{1-r\frac{1+n^2(1-r)^2/(1+\frac{1}{mM})^2}{1-\frac{\gamma-1}{\gamma+1}(1-r)}}\right]$$

$$\alpha = \frac{1}{1-r}\left[\frac{\lambda_2}{\lambda_1}\left(m+\frac{1}{M}\right)-\frac{a_2}{V}\right]; \qquad \beta = -l\frac{\lambda_2}{\lambda_1}$$

$$\widetilde{F} = -\frac{a_2}{\gamma V}\widetilde{K}\alpha; \qquad \widetilde{H} = -\frac{a_2}{\gamma V}\widetilde{K}\beta$$

$$\widetilde{G} = \widetilde{L} - \widetilde{F} - B_1\left(\widetilde{L}+\frac{m}{\gamma M}\right) - B_2; \qquad \widetilde{I} = \frac{1+1/Mm}{n(1-r)}\widetilde{G}.$$

For $\psi_{cl} \le \psi_1 \le \psi_{cu}$, the coefficients are as follows.

$$c = \frac{m+1/M}{1-V^2(1-r)^2/a_2^2}; \qquad \alpha = -\frac{V^2}{a_2^2}(1-r)c; \qquad \beta = -l; \qquad d = \sqrt{\frac{\alpha^2+l^2-V^2c^2/a_2^2}{1-V^2(1-r)^2/a_2^2}}$$

$$h_1 = -\frac{1-r}{r}\frac{1}{\sigma}\left[\frac{l}{\gamma M}+\left(\frac{m}{\gamma M}B_1+B_2\right)\frac{1}{\sigma}\right]$$

$$h_2 = 1 - \frac{1-r}{r}\frac{1-B_1}{\sigma^2}; \qquad h_3 = -\frac{2d(1-r)}{l\sigma(1+\frac{\gamma-1}{2}r)}$$

$$\widetilde{L}_{(1)} = \frac{h_1h_2-(\frac{m}{\gamma M}+\frac{D_2}{D_1})h_3^2}{h_2^2+h_3^2}; \qquad \widetilde{L}_{(2)} = h_3\frac{h_1+(\frac{m}{\gamma M}+\frac{D_2}{D_1})h_2}{h_2^2+h_3^2}$$

$$h_4 = \frac{4}{\gamma+1}\frac{\sigma^2}{1+\sigma^2}; \qquad h_5 = \frac{2rd\sigma(1-r)}{l(1+\sigma^2)}\frac{V^2}{a_2^2}$$

$$\widetilde{F}_{(1)} = h_4\left(\widetilde{L}_{(1)}+\frac{m}{\gamma M}+\frac{D_2}{D_1}\right) - h_5\widetilde{L}_{(2)}; \qquad \widetilde{F}_{(2)} = h_5\left(\widetilde{L}_{(1)}+\frac{m}{\gamma M}+\frac{D_2}{D_1}\right) + h_4\widetilde{L}_{(2)}$$

$$\widetilde{H}_{(1)} = \frac{h_4}{\sigma}\left(\widetilde{L}_{(1)} + \frac{m}{\gamma M} + \frac{D_2}{D_1}\right) + \sigma h_5 \widetilde{L}_{(2)}; \qquad \widetilde{H}_{(2)} = -\sigma h_5\left(\widetilde{L}_{(1)} + \frac{m}{\gamma M} + \frac{D_2}{D_1}\right) + \frac{h_4}{\sigma}\widetilde{L}_{(2)}$$

$$\widetilde{K}_{(1)} = D_1\left(\widetilde{L}_{(1)} + \frac{m}{\gamma M}\right) + D_2; \qquad \widetilde{K}_{(2)} = D_1 \widetilde{L}_{(2)}$$

$$\widetilde{Q}_{(1)} = C_1\left(\widetilde{L}_{(1)} + \frac{m}{\gamma M}\right) + C_2 - \frac{\widetilde{K}_{(1)}}{\gamma}; \qquad \widetilde{Q}_{(2)} = C_1 \widetilde{L}_{(2)} - \frac{\widetilde{K}_{(2)}}{\gamma}$$

$$\widetilde{G}_{(1)} = \widetilde{L}_{(1)} - \widetilde{F}_{(1)} - B_1\left(\widetilde{L}_{(1)} + \frac{m}{\gamma M}\right) - B_2; \qquad \widetilde{G}_{(2)} = \widetilde{L}_{(2)}(1 - B_1) - \widetilde{F}_{(2)}$$

$$\widetilde{I}_{(1)} = \frac{1 + \frac{1}{mM}}{n(1-r)}\widetilde{G}_{(1)}; \qquad \widetilde{I}_{(2)} = \frac{1 + \frac{1}{mM}}{n(1-r)}\widetilde{G}_{(2)}.$$

The expression for $\widetilde{H}_{(1)}$ in Moore's paper contains a typographical error; $\widetilde{L}_{(1)} + \frac{m}{\gamma M} + \frac{D_2}{D_1}$ should be replaced by $\widetilde{L}_{(1)} + \frac{n}{\gamma M} + \frac{D_2}{D_1}$. Also, the plots of the constants when $\psi_{cl} \leq \psi_1 \leq \psi_{cu}$ do not agree with the formulae. After repeating Moore's analysis, we conclude that the formulae are correct.
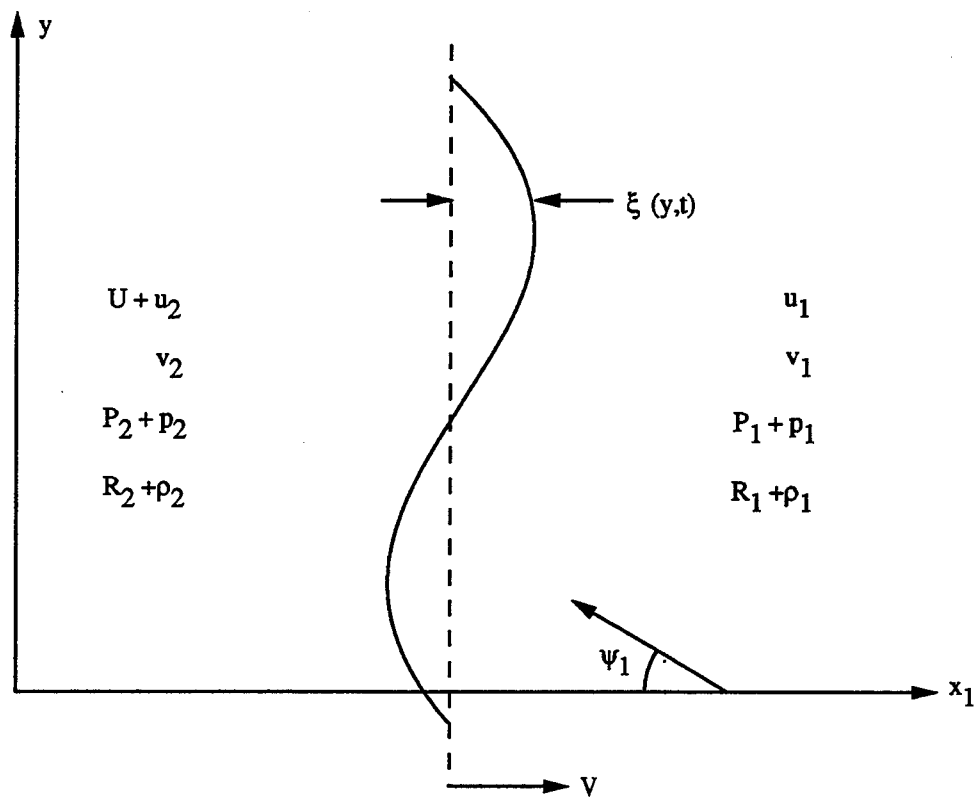
FIG. B.1. Schematic of the interaction of a shock wave with an acoustic wave that is incident from upstream.
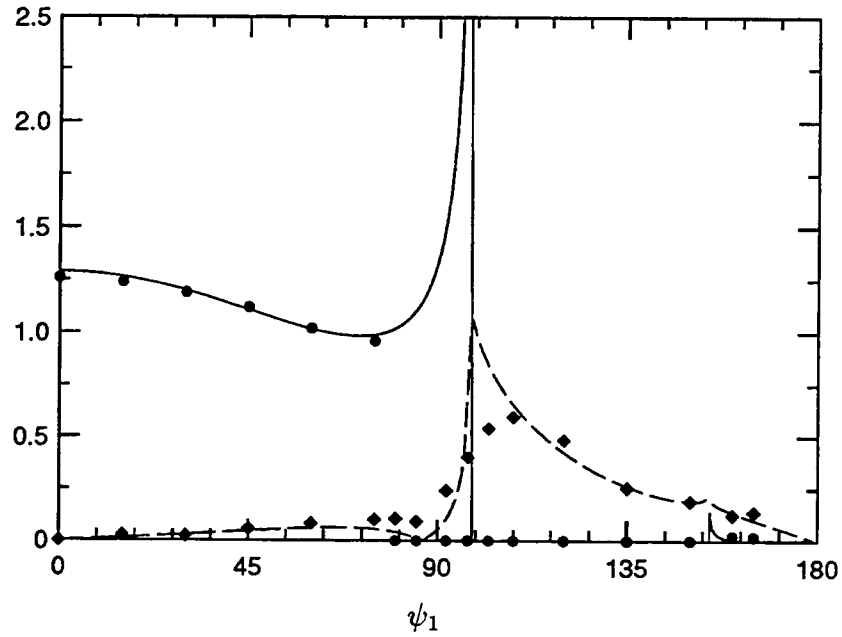
FIG. B.2. Comparison of the predictions of the linear analysis to computed results. The lines are values obtained from analysis while the symbols represent computed values. All quantities are normalized by p_1/P_1. —— (θ_2/θ_1), - - - - (ω_2/θ_1). θ_2 and ω_2 denote the *rms* dilatation and vorticity behind the shock wave respectively.
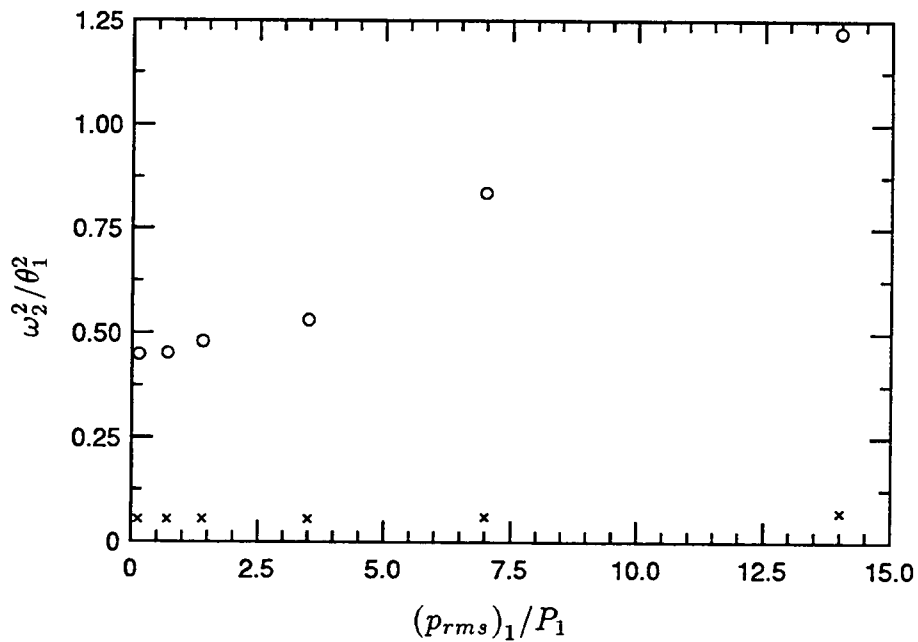
FIG. B.3. Computed values of the vorticity behind the shock wave as a function of the amplitude of the incident disturbance. The mean Mach number is 1.5. o $(\psi_1 = 100°)$, × $(\psi_1 = 60°)$

109
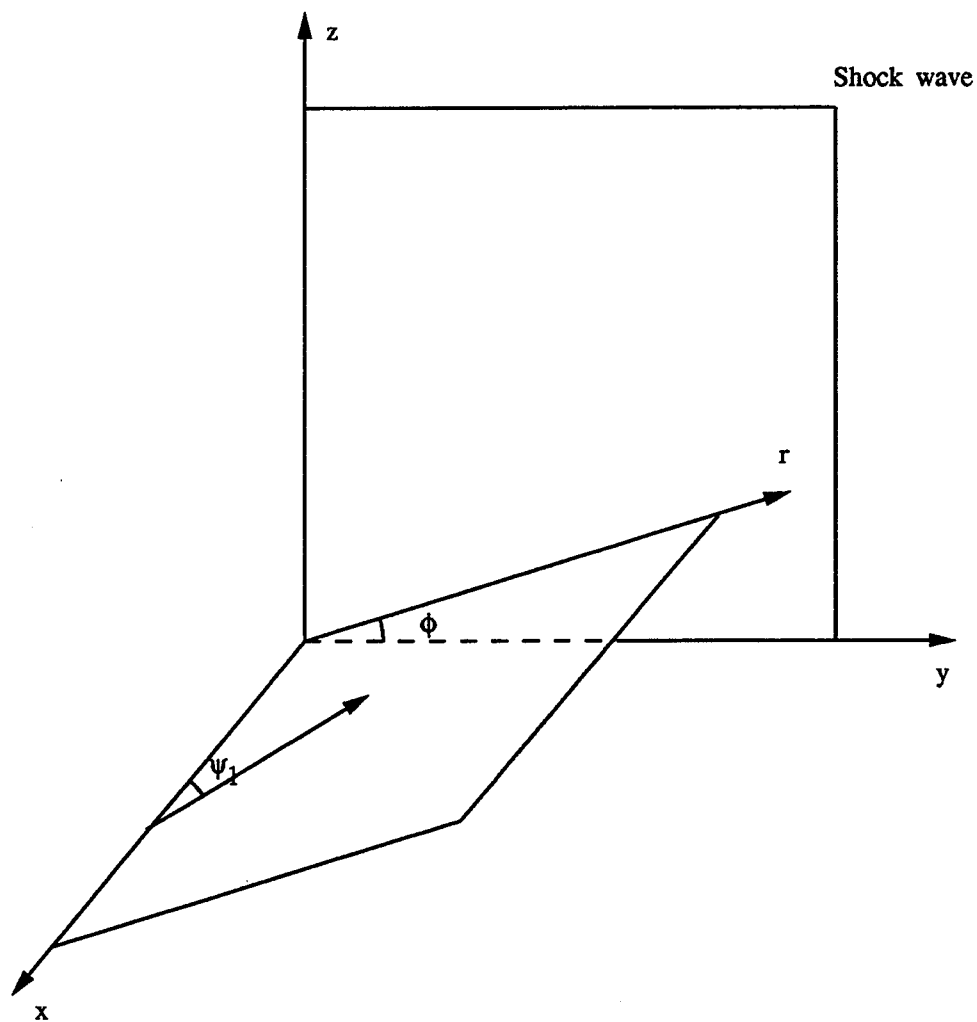
FIG. B.4. Coordinate system used in analysis of the interaction of a shock wave with an isotropic field of acoustic waves that are incident from upstream.
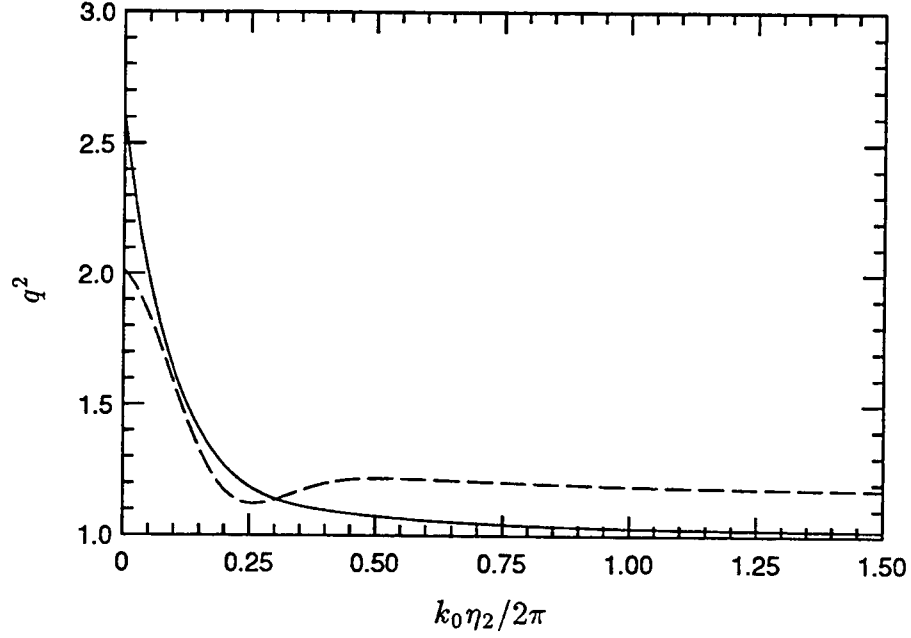
FIG. B.5. Evolution of q^2 behind the shock wave as predicted by linear analysis. q^2 is normalized with its upstream value. —— $(M = 1.2)$, ---- $(M = 2.0)$.
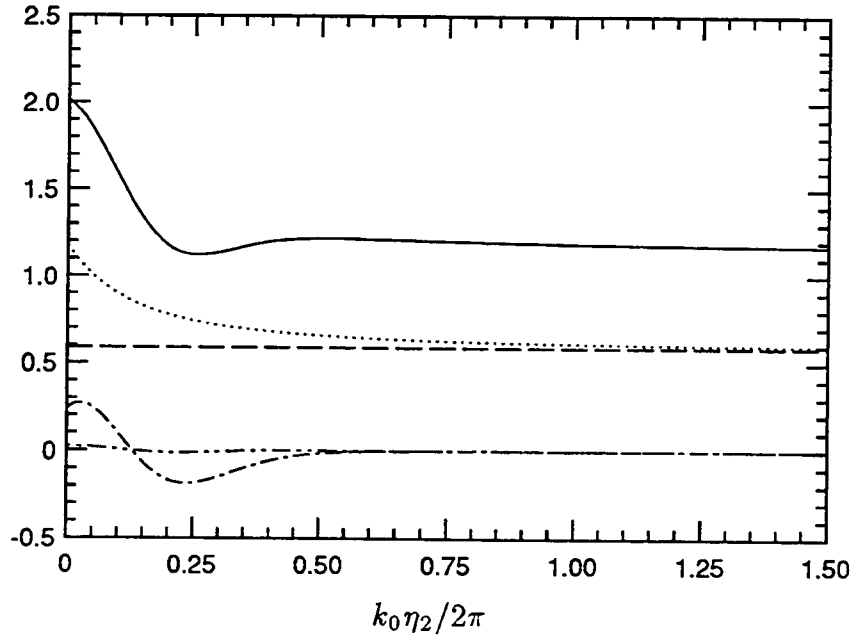
FIG. B.6. Decomposition of q^2 behind the shock wave under linear analysis. The Mach number is 2 and all components are normalized with the upstream value of q^2. —— (Total), ---- (Vortical), ········ (Acoustic), —·— (Correlation for $\psi_{cl} < \psi_1 < \psi_{cu}$), —··— (Correlation for $0 \leq \psi_1 < \psi_{cl}, \psi_{cu} < \psi_1 \leq \pi$).

111
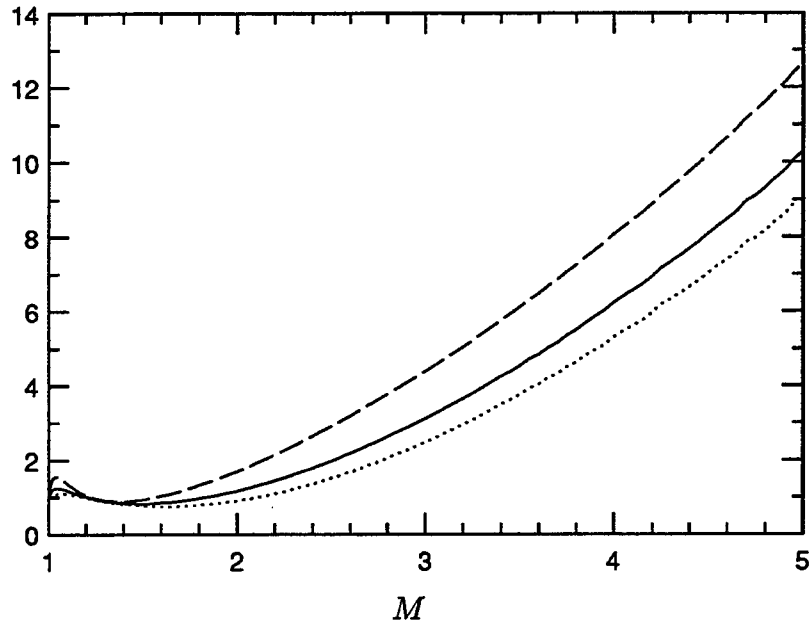
FIG. B.7. Far-field kinetic energy as a function of Mach number. All components are normalized with their upstream value. $----$ $(\overline{u^2})$, $\cdots\cdots$ $(\overline{v^2} = \overline{w^2})$, —— (q^2).
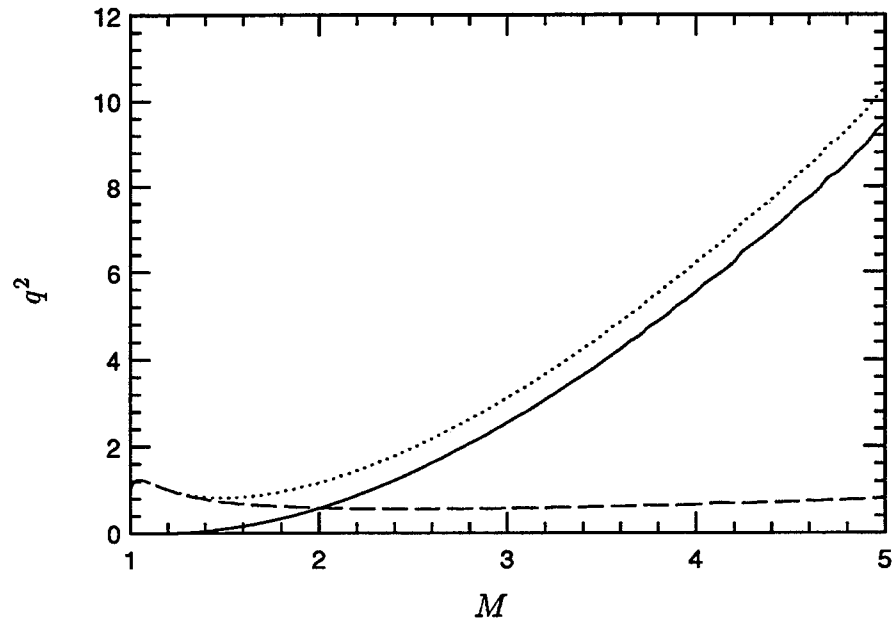
FIG. B.8. The far-field kinetic energy decomposed into acoustic and vortical components. Both components are normalized with the upstream value of q^2. $\cdots\cdots$ (Total), —— (Vortical), $----$ (Acoustic).
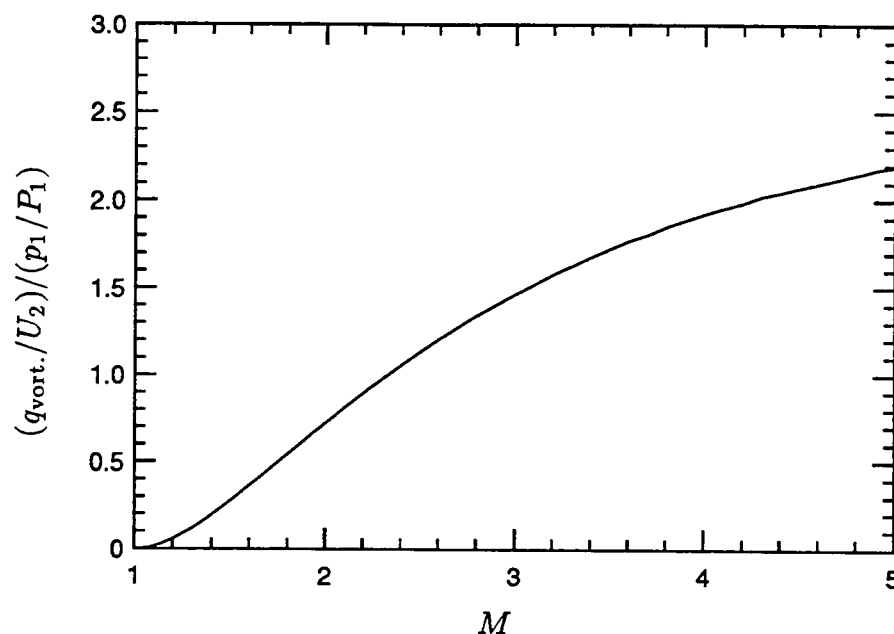
FIG. B.9. The far-field 'turbulent' intensity compared to the intensity of incident pressure fluctuations. The curve asymptotes to 2.75 ($\gamma = 1.4$).
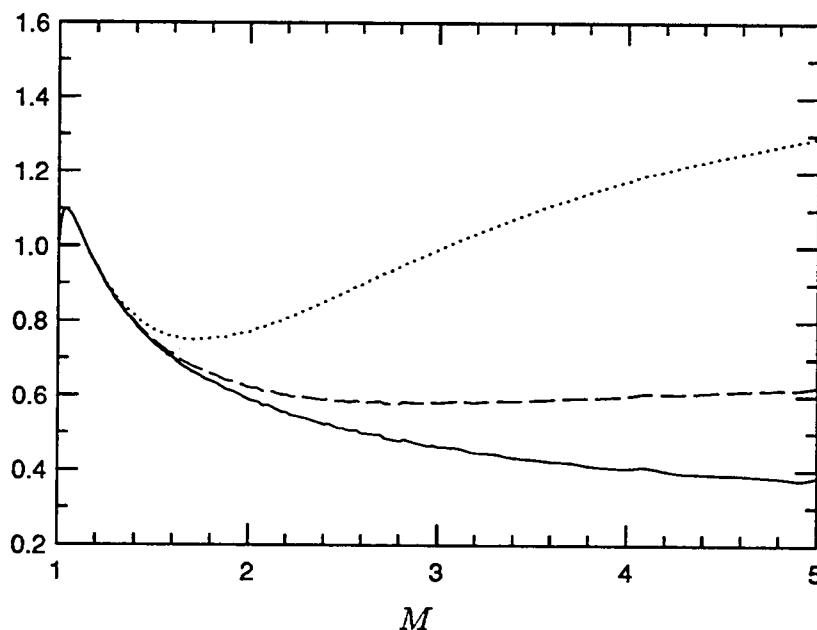
FIG. B.10. The intensity of pressure, density and temperature fluctuations in the far-field compared to the intensity of incident pressure fluctuations. ——— (p_2/P_2), - - - - $\gamma(\rho_2/R_2)$, $\cdots\cdots$ $\gamma/(\gamma-1)(\theta_2/T_2)$. θ_2 and T_2 are the rms and mean temperature behind the shock wave respectively. The three curves are normalized with p_1/P_1 and asymptote to 0.29, 0.67 and 1.54 respectively ($\gamma = 1.4$).

113
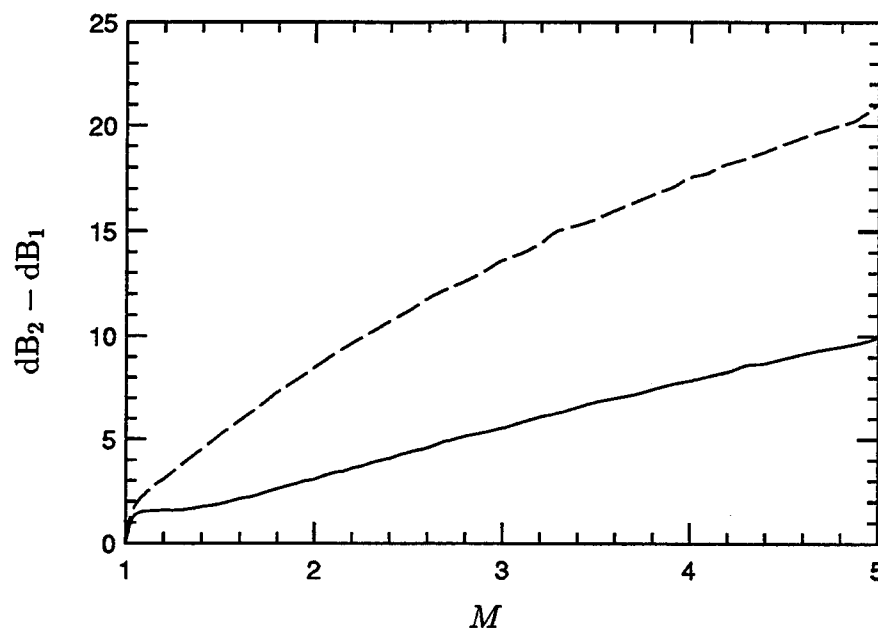
FIG. B.11. The level of far-field sound behind the shock wave compared to the incident sound level. ---- Sound pressure level, —— Level of acoustic intensity.
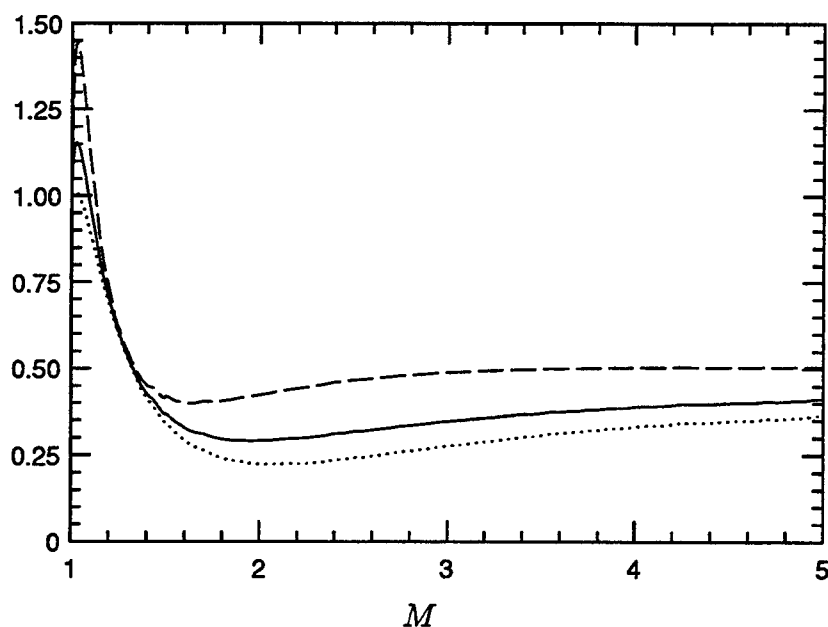

FIG. B.12. Far-field kinetic energy as a function of Mach number. All components are normalized with the incident energy and M^2. ---- $(\overline{u^2}/M^2\ \overline{u_0^2})$, ········ $(\overline{v^2}/M^2\ \overline{v_0^2} = \overline{w^2}/M^2\ \overline{w_0^2})$, —— $(\overline{q^2}/M^2\ \overline{q_0^2})$. The three curves asymptote to 0.49, 0.40 and 0.43 respectively $(\gamma = 1.4)$.

114

PART FIVE

AIAA 94-0311
Interaction of Isotropic Turbulence with a Strong Shock Wave

S. Lee, S.K. Lele, and P. Moin
Stanford University
Stanford, CA 94305-3030

32nd Aerospace Sciences
Meeting & Exhibit
January 10-13, 1994 / Reno, NV

INTERACTION OF ISOTROPIC TURBULENCE WITH A *STRONG* SHOCK WAVE

Sangsan Lee, Sanjiva K. Lele*, and Parviz Moin†
Center for Turbulence Research
Stanford University, Stanford, CA 94305-3030

Abstract

Direct numerical simulation (DNS) and linear analysis (LIA) of isotropic turbulence interacting with a shock wave are performed for several upstream shock normal Mach numbers (M_1). Turbulence kinetic energy (TKE) is amplified across the shock wave, but this amplification tends to saturate beyond $M_1 = 3.0$. TKE amplification and Reynolds stress anisotropy obtained in DNS are consistent with LIA predictions. Rapid evolution of TKE immediate downstream of the shock wave persists for all shock strengths and is attributed to the transfer between kinetic and potential modes of turbulence energy through acoustic fluctuations. Changes in energy spectra and various length scales across the shock wave are predicted by LIA, which is consistent with DNS results. Most turbulence length scales decrease across the shock. Dissipation length scale ($\overline{\rho}q^3/\epsilon$), however, increases slightly for shock waves with $M_1 < 1.65$. Fluctuations in thermodynamic variables behind the shock wave stay nearly isentropic for $M_1 < 1.2$, and deviate significantly from isentropy for the stronger shock waves due to large entropy fluctuation generated through the interaction.

1. Introduction

Understanding the mechanisms of turbulence interacting with a shock wave is of fundamental importance in predicting the interaction of turbulent boundary layers with the shock waves which occur in many engineering applications. Since 1950's, linear analyses (LIA) on the modification of elementary disturbance waves, such as vortical, acoustic, and entropic waves, by the shock wave have been performed with an emphasis on the acoustic wave generation behind the shock wave[1-7]. Recently, the applicability of homogeneous Rapid Distortion Theory (RDT) on shock/turbulence interaction is investigated by Jacquin et al.[8]

There has been a significant accumulation of experimental data on shock turbulence interaction during the last decade. Interaction of turbulent boundary layers with a shock wave over a corner was investigated by many research groups, among them are Dolling and Or[9], Andreopoulos and Muck[10], and Smits and Muck[11]. A general finding from these experiments is that Reynolds shear stress and turbulence intensities are amplified across the shock wave. The studies of oblique shock wave/turbulent boundary layer interaction included several additional phenomena which complicated the flow behavior[12]. To isolate the effects of a shock wave on turbulence, several experiments[12-15] on the interaction between the shock wave and grid-generated turbulence have been performed. An important finding is that turbulence is amplified and turbulence length scales increase across the shock wave. But the length scale increase contradicts the intuitive expectation that mean flow compression should decrease the relevant turbulence length scales. The issue of length scale change will be thoroughly discussed in the present paper (Sec. 3.2).

Numerical simulations of the shock turbulence interaction are just beginning to emerge. Using a shock capturing numerical technique, Rotman[16] calculated the change in a two dimensional turbulent flow caused by the passage of a travelling shock wave. He found that the shock causes an increase in the turbulent kinetic energy and that turbulence length scales are reduced upon passage of the shock. Lee et al.[17,18] conducted direct numerical simulations of two and three dimensional turbulence interacting with a shock wave. They found that vorticity amplification compared well with the linear analysis predictions, and turbulent kinetic energy undergoes rapid increase behind the shock wave. The spectrum was found to be enhanced more at large wave numbers, leading to an overall length scale decrease.

In the present paper, interaction of isotropic turbulence with a *strong* shock wave is studied to investigate the effects of shock strength on turbulence modification. We developed a numerical technique to simulate turbulence interacting with a strong shock wave without resolving its structure, and validated this technique against the shock-resolving simulations (Sec. 2). The simulation results are compared with the results from linear analysis, and are contrasted against the results from the weak shock case to highlight the shock strength effects (Sec. 3).

---

* Also with Department of Aeronautics and Astronautics

† Also with NASA Ames Research Center

1

2. Numerical Simulation and Linear Theory

2.1 Shock-Capturing Scheme

For the direct numerical simulation (DNS) of the interaction of isotropic turbulence with a weak shock wave, the shock wave structure was resolved as a solution of the Navier-Stokes equations. In addition, all the essential turbulence scales were resolved[19]. For a strong shock wave, however, resolving the shock structure is irrelevant because the Navier-Stokes equations are no longer valid inside the shock wave for a shock with a shock normal Mach number exceeding 2.0[20]. Therefore, for an efficient computation, a shock-capturing scheme is to be implemented for the simulation with a strong shock wave. The shock-capturing scheme is required to be high order accurate throughout the computational domain (to properly simulate the evolution of turbulence) as well as to be able to give smooth and accurate transition across the shock wave. The shock-capturing scheme chosen was an essentially non-oscillatory (ENO) scheme, which can be constructed up to any order of accuracy. The ENO scheme used in this paper was based on the Lax-Friedrichs scheme with an interpolation on fluxes, and for two and three dimensional cases the ENO scheme is applied independently for fluxes in each direction[21]. Some modifications described in the following were made to the basic scheme to improve the solution accuracy and to enhance the code performance.

The ENO scheme was implemented in the code developed for the simulation of shock turbulence interaction. Simulation of spatially decaying compressible turbulence without shocks was performed to validate the scheme and to determine the required order of the ENO scheme to reproduce the evolution of turbulence as determined from a corresponding DNS. During the validation procedure, an unexpected accuracy degeneracy was observed with the increase in the ENO scheme's order. As the order of the ENO scheme increases, the solution deviates further from the DNS result. Similar accuracy degeneracy was reported when the mesh was refined[22]. This degeneracy was due to the choice of linearly unstable stencils. Biasing toward a central difference stencil was implemented to avoid the accuracy degeneracy in a shock-free region[23]. With this fix, more accurate results could be obtained by raising the order of accuracy. Results comparable to the corresponding DNS (with a sixth-order accurate Pade scheme) was obtained with a sixth-order ENO scheme.

When the ENO scheme is implemented throughout the domain, the operation count and, accordingly, the CPU time increase significantly compared to the Pade scheme. The region where the ENO scheme plays a significant role is quite localized, usually less than a tenth of the computational domain in DNS of weak shock waves, and is expected to be even smaller for strong shock waves. The idea of applying the ENO scheme only where it plays an active role and switching elsewhere into the usual Pade central differencing was tested to save computer resources. The local region of ENO application can even be specified *a priori* to be a zone around the shock for a simulation performed in a coordinate system fixed on the mean shock wave. The concept of local application of the ENO scheme was validated against fully resolved DNS results both for the case of two dimensional shock turbulence interaction[17] with $M_1 = 1.2, M_t = 0.07$ and the case of three dimensional spatially decaying turbulence[24] with $M_t = 0.51$ and $Re_\lambda = 25$. Here, $M_1 = \overline{u}_1/\overline{c}, M_t = q/\overline{c}$, and $Re_\lambda = \overline{\rho} u_{rms} \lambda/\overline{\mu}$, where $u_{rms} = \sqrt{\overline{u_1''^2}}, q^2 = \overline{u_i'' u_i''}$, c is the sound speed, λ is a Taylor microscale, and μ is the dynamic viscosity. The overline denotes an ensemble average, and f' and f'' are the deviations from the ensemble average and the mass-weighted average[25] $\tilde{f} = \overline{\rho f}/\overline{\rho}$, that is, $f' = f - \overline{f}$ and $f'' = f - \tilde{f}$.

The next validation computation was to reproduce three dimensional shock turbulence interaction using the ENO scheme. Significant additional dissipation of turbulent kinetic energy (TKE) was found in the shock vicinity where the ENO scheme was applied independently in all directions, which was not observed in two dimensional shock turbulence simulations. This suggested that the ENO scheme be applied only in the shock normal direction. With the one-directional ENO scheme application, more accurate results were obtained with less CPU time used. For $M_1 = 1.2$, the ENO scheme required only a quarter of the CPU time in the corresponding shock-resolving simulation[26].

The final validation calculation was made for two dimensional turbulence interacting with a strong shock wave. Results from the ENO scheme on two dimensional shock turbulence interaction were compared with the corresponding shock resolving simulation, where $M_1 = 2.0$ and $M_t = 0.07$ at the inflow. The minimum grid spacing required by the ENO scheme was five times larger than that used in the shock-resolving simulation. Figure 1 compares the evolution of velocity fluctuation variances, where inflow turbulence is generated using the energy spectrum of $E(k) \simeq u_o^2 (k/k_o)^4 \exp[-2(k/k_o)^2]$ with k_o the peak wave number and u_o the rms velocity fluctuation. The amplification and evolution behind the shock wave were reproduced by the ENO scheme with six times larger computational mesh near the shock wave. In order to accurately predict the interaction of turbulence with stronger shock waves, where a shock-

resolving simulation is not practical, reliable results can only be obtained after a thorough grid-refinement test. Grid refinement is necessary to predict thermodynamic fluctuations correctly, since the convergence of the thermodynamic variables is slowest due to spurious numerical oscillations behind the shock wave in the shock-capturing scheme[27,28]. Details of the validation tests have been reported in ref. 26.
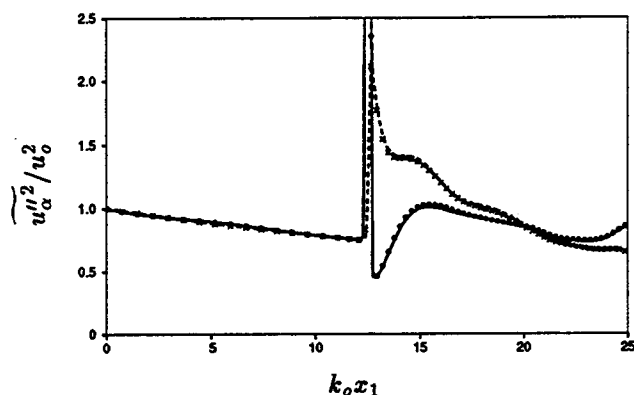

FIGURE 1. Evolution of the velocity fluctuation variances ($M_1 = 2.0, M_t = 0.07$): lines denote results from shock resolving simulation and symbols from shock capturing simulation. ———, • : R_{11}, ---- , × : R_{22}.

Numerical procedures used in this paper can be summarized as follows: The fluid is assumed to be an ideal gas with the specific heat ratio of $\gamma = 1.40$. The Prandtl number is assumed constant with $Pr = 0.75$. The density, three components of momentum, and the total internal energy are advanced in time using a third-order compact-storage Runge-Kutta scheme[29]. Spatial derivatives are approximated by the sixth order ENO scheme only for the inviscid fluxes near the shock wave, and by the sixth order Pade scheme[30] for other terms. The simulation is performed in a coordinate system *fixed on the mean shock position*, where flow is supersonic upstream and subsonic downstream. The direction of the mean flow was chosen to be normal to the shock wave, which was aligned with the x_1 axis. At the inflow, isotropic turbulence is added to the supersonic mean flow. A "realistic" turbulence is prescribed at the inflow using a data base from a temporally decaying turbulence[31]. Special care is taken, so that turbulence interacting with a shock wave is fully developed with proper velocity derivative skewnesses. A nonreflecting boundary condition[32] is applied at the outflow boundary. Periodic boundary condition is imposed in transverse directions due to homogeneity of turbulence in these directions. More details of the numerical schemes can be found in ref. 18.

2.2 Linear Interaction Analysis (LIA)

Some aspects of the interaction of shock turbulence interaction are predictable through linear analysis. For the linear analysis to apply, the upstream Mach number variation must be a small perturbation to the mean upstream Mach number. Furthermore, the time required for turbulence to pass through the shock wave should be small compared to the turbulence time scale, $\overline{\rho}q^2/\epsilon$ (ϵ is the dissipation rate of turbulence kinetic energy), so that there would be insufficient time for the redistribution of energy into different scales through nonlinear processes.

In this work, we employed the linear interaction analysis (LIA) of Ribner[1], where the main interest is the interaction of the upstream vorticity wave with a shock. In LIA, inviscid linear equations for the disturbances are solved downstream of the shock wave, and the boundary conditions at the downstream side of the shock front are expressed in terms of the upstream disturbances by the use of Rankine-Hugoniot relations. Through LIA, amplitudes, length scales, and orientations of downstream refracted or generated waves are represented in terms of those of the upstream vorticity wave.

Since fluctuations in weak compressible turbulence can be regarded as a sum of vorticity, entropy, and acoustic waves, the modification of turbulence through the shock can be predicted via LIA[2,3].

3. Results and Discussion

The parameters of the simulation are the mean Mach number (M_1), the fluctuation Mach number (M_t), and the turbulence Reynolds number based on the Taylor microscale (Re_λ) upstream of the shock wave. In the simulation, all the turbulence scales are fully resolved, while the effect of the shock wave on turbulence is captured (rather than fully resolved). Two simulations with $M_1 = 2.0$ and 3.0 are conducted for the interaction with strong shock waves, and the results from shock-resolving simulations[19] for the interaction with a weak shock wave ($M_1 = 1.05, 1.1, 1.2$) are quoted to investigate the effects of the shock normal Mach number. Table 1 lists the simulation parameters, where the values of M_t and Re_λ are taken at the location immediately upstream of the shock.

Table 1. Simulation parameters

Case	M_1	M_t	Re_λ	k_o
A	2.0	0.108	19.0	4.0
B	3.0	0.110	19.7	4.0

3

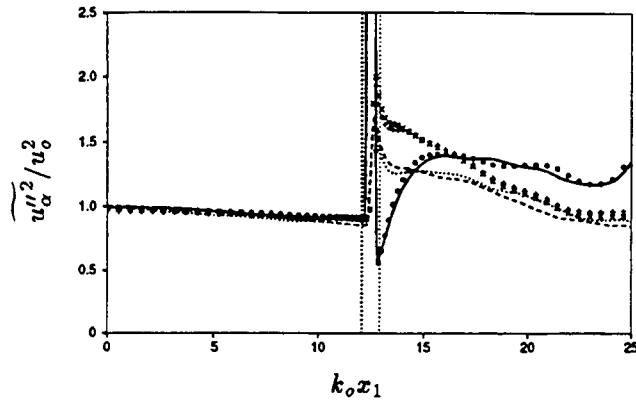FIGURE 2(A). Evolution of the normal components of the Reynolds stress: lines for $M_1 = 2.0$, and symbols for $M_1 = 3.0$. ——— , ● : R_{11}, ———— , × : R_{22}, ········· , + : R_{33}. Vertical lines denote the boundaries of shock intermittency.
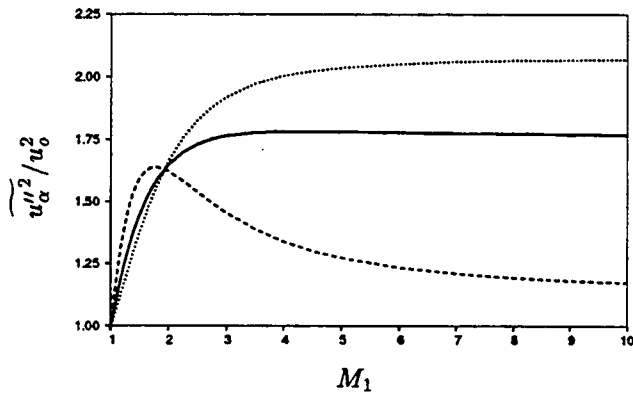

FIGURE 2(B). Amplification of velocity fluctuation variances across the shock wave predicted by LIA far away from the shock. ——— q^2/q_o^2, ———— $\widetilde{u_1''^2}$, ········· $\widetilde{u_2''^2}$ & $\widetilde{u_3''^2}$.
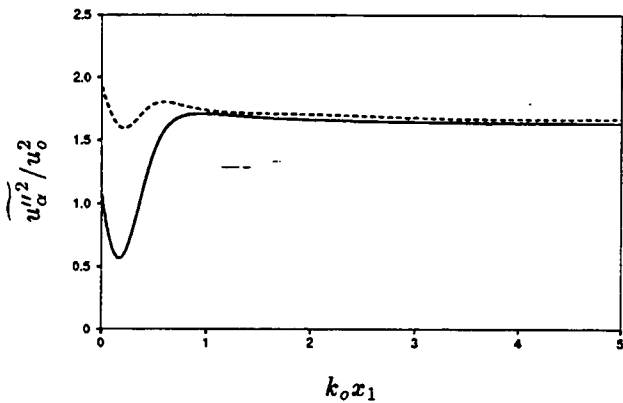
FIGURE 2(C). Evolution of velocity fluctuation variances behind the shock wave predicted by LIA ($M_1 = 2.0$). ——— $\widetilde{u_1''^2}$, ———— $\widetilde{u_2''^2}$ & $\widetilde{u_3''^2}$.

3.1 Turbulence Velocity Fluctuation

Interaction of turbulence with a shock wave generates acoustic waves downstream of the shock, part of which undergo rapid decay[1]. LIA predicts that turbulent kinetic energy is amplified across the shock wave and the decaying acoustic waves contribute significantly to the streamwise fluctuations just behind the shock wave. Figure 2(A) shows the evolution of the diagonal components of the Reynolds stress tensor, $R_{ij} = \widetilde{u_i''u_j''}$. The off-diagonal components stay close to zero over the entire flow field since turbulence is isotropic upstream and axisymmetric downstream of the shock. The streamwise component of turbulence intensity in the shock region contains the intermittency effects due to the oscillations of the shock (for more details on the intermittency effects on turbulence statistics, see ref. 18). The boundaries of the shock oscillations are defined as the locations where mean dilatation $d\bar{u}_1/dx_1 = 0$; $d\bar{u}_1/dx_1$ is negative inside the shock wave and slightly positive away from the shock due to viscous heating. All the velocity fluctuations are enhanced during the interaction. The velocity fluctuations are axisymmetric behind the shock, and their return to isotropy is negligible compared to the decay. Away from the shock wave, all the velocity fluctuations decay monotonically due to viscous dissipation.

Mach number dependence of the far-field velocity fluctuation amplification predicted by LIA is shown in Figure 2(B). All components of the velocity fluctuation are amplified across the shock wave, and the amplification of TKE tends to saturate beyond $M_1 = 3.0$. The shock normal component is amplified more for shock waves with $M_1 < 2.0$ while the opposite is true for $M_1 > 2.0$. In DNS, however, the streamwise velocity fluctuation away from the shock is larger than the transverse velocity fluctuations, which apparently contradicts the LIA prediction. Viscous TKE dissipation rate behind the shock for the transverse components are found to be significantly higher than the streamwise component. Therefore, comparing low Reynolds number DNS results directly with the inviscid linear analysis may not be appropriate. After the viscous decay is compensated for by extrapolating the curves to the shock location, the DNS results were found to be consistent with the LIA prediction.

The rapid downstream evolution of velocity fluctuations which was observed for weak shock turbulence interaction[19] persists in the present simulations of strong shock turbulence interaction. The evolution of the velocity fluctuations downstream of the shock wave predicted by LIA is shown in Figure 2(C), which reproduces the main feature of the rapid evolution from the

4

DNS. Hence, the rapid TKE evolution behind the shock wave can be explained mainly as a linear process. This rapid evolution in the streamwise velocity fluctuation is due to a correlation between the vortical and decaying acoustic fluctuations behind the shock wave. The acoustic velocity fluctuations and vortical velocity fluctuations are anti-correlated just behind the shock, and the correlation between the two fluctuations decreases rapidly as the amplitude of the acoustic wave decays exponentially away from the shock wave. In previous studies[17-19], the correlations between vortical and acoustic waves were not properly accounted for, and the prediction capability of the linear analysis was not fully appreciated.

Further insight into the rapid evolution of velocity fluctuations is revealed by the equation for linear acoustic energy balance[33]. The continuity and momentum equations for the linearized fluctuating components can be written as

$$\frac{\partial \rho'}{\partial t} + \tilde{u}_k \frac{\partial \rho'}{\partial x_k} + \bar{p}\frac{\partial u_k''}{\partial x_k} = 0,$$

$$\frac{\partial u_i''}{\partial t} + \tilde{u}_k \frac{\partial u_i''}{\partial x_k} + \frac{1}{\bar{p}}\frac{\partial p'}{\partial x_i} - \frac{\partial \sigma_{ik}''}{\partial x_k} = 0$$

by assuming that there exist no mean flow gradients, where $\bar{p}\sigma_{ij}''(= \tau_{ij}'')$ denotes the viscous stress. For an ideal gas, an infinitesimal density fluctuation can be related to the pressure and entropy (s) fluctuations by

$$\frac{\rho'}{\bar{p}} = \frac{1}{\gamma}\frac{p'}{\bar{p}} - \frac{s'}{c_p}, \tag{1}$$

where c_p is the specific heat at constant pressure. Multiplying the continuity equation by ρ', contracting the momentum equations by u_i'', and cancelling density-dilatation correlation by using above thermodynamic relation with neglecting entropy fluctuation effect $(-\overline{s'u_{i,i}''}/c_p\bar{c})$, the following equation (in the averaged form) follows

$$\frac{\partial}{\partial x_k}\left[\frac{\tilde{u}_k}{\bar{c}}\left(\frac{\overline{u_i''u_i''}}{2\bar{c}^2} + \frac{\overline{\rho'^2}}{2\bar{p}^2}\right) + \frac{1}{\gamma}\frac{\overline{p'u_k''}}{\bar{p}\,\bar{c}}\right] - \frac{\overline{u_i''}}{\bar{c}^3}\frac{\partial \sigma_{ik}''}{\partial x_k} = 0.$$

If this relation is satisfied the rapid post-shock evolution phenomenon can be explained in terms of linear acoustic energy balance.
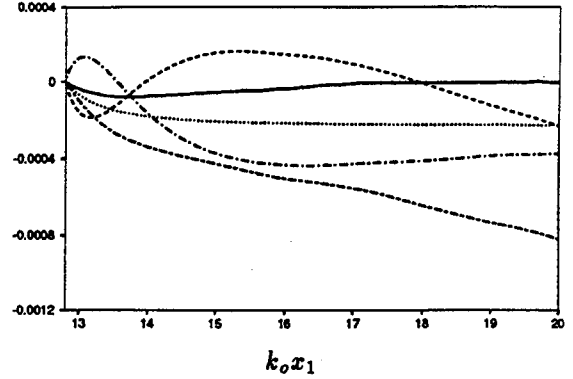

FIGURE 3(A). Evolution of the integrated quantities from the acoustic energy balance for $M_1 = 2.0$: ---- A, ········ B, —·— C, ——— $A+B+C$, ———— $A+B+C+D$.
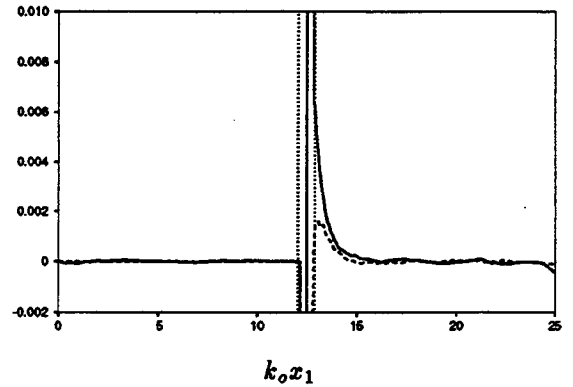

FIGURE 3(B). Evolutions of pressure-dilatation correlation and entropy-dilatation correlation for $M_1 = 2.0$: ——— $\overline{p'u_{k,k}''}/\gamma\bar{p}u_ok_o$, ———— $-\overline{s'u_{k,k}''}/c_pu_ok_o$. Vertical lines denote the boundaries of shock intermittency.

The acoustic balance equation is integrated in the streamwise direction from the downstream side of the shock (x_s) to give

$$\underbrace{\left\|\frac{\tilde{u}_1}{\bar{c}}\frac{\overline{u_i''u_i''}}{2\bar{c}^2}\right\|_{x_s}^{x_1}}_{A} + \underbrace{\left\|\frac{\tilde{u}_1}{\bar{c}}\frac{\overline{\rho'^2}}{2\bar{p}^2}\right\|_{x_s}^{x_1}}_{B} + \underbrace{\left\|\frac{1}{\gamma}\frac{\overline{p'u_1''}}{\bar{p}\,\bar{c}}\right\|_{x_s}^{x_1}}_{C}$$

$$\underbrace{- \int_{x_s}^{x_1}\frac{\overline{u_i''}}{\bar{c}^3}\frac{\partial \sigma_{ik}''}{\partial x_k}dx_1 = 0,}_{D}$$

where $\|f\|_a^b = f(b) - f(a)$. The integrated results are shown in Figure 3(A). In all the cases we investigated (with different shock strengths and upstream turbulence intensities) the acoustic energy balance is satisfied with little deviation. The rapidly evolving acoustic energy— sum of scaled density and velocity

fluctuations— is found to be mainly balanced by the pressure transport. Therefore, the rapid evolution of velocity fluctuations can be attributed to the acoustic energy balance: energy transfer from the acoustic potential energy in the form of density (or pressure) fluctuations to turbulence kinetic energy. This is consistent with the fact that the pressure-transport term is scaled best by flow variables associated with acoustic wave propagation[19]. Note that density fluctuation is replaced by the pressure fluctuation using the isentropic relation in deriving the acoustic energy balance equation, even though entropy fluctuation behind the shock wave contributes significantly to the density fluctuation (as is shown in Sec. 3.3). This is justified because the neglected entropy-dilatation correlation is found to be less than 5% of the pressure transport term, which also is less than 30% of the pressure-dilatation correlation in the region of interest as shown in Figure 3(B). Even though thermodynamic fluctuations are far from isentropic, the contribution of entropy fluctuations to the acoustic energy balance can be neglected. The entropy-dilatation correlation vanishes in the linear limit and the acoustic energy balance derived above holds exactly in the linear analysis, which ignores viscous dissipation.

In summary, the apparent higher amplification of the streamwise velocity fluctuation far from the shock wave compared to the transverse velocity fluctuations (which is not consistent with the LIA prediction) is due to the faster viscous decay for the transverse components. The DNS results compensated for the viscous decay are consistent with the LIA predictions. The rapid increase in the streamwise velocity fluctuation downstream of the shock is caused by the pressure transport. Acoustic energy balance just behind the shock wave indicates that most acoustic energy is stored in the form of density (or pressure) fluctuations and this energy is transferred into velocity fluctuations as turbulence relaxes from its strained state.

— — —

Variance of vorticity fluctuation is the main contributor to the TKE dissipation rate. Figure 4(A) shows the evolution of vorticity components. The transverse components are amplified across the shock, while the streamwise component is hardly affected. Mach number dependence of transverse vorticity variance amplification predicted by LIA is shown in Figure 4(B). LIA predicts no amplification of the streamwise component. The amplification ratio obtained from DNS is found to be consistent with the LIA prediction.
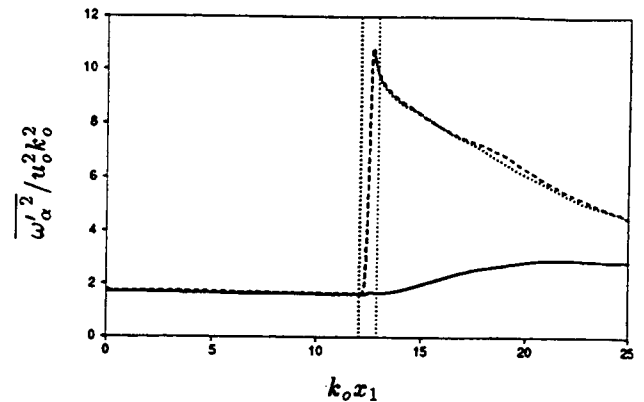

FIGURE 4(A). Evolution of the vorticity fluctuation variances with $M_1 = 2.0$: —— $\overline{\omega_1'^2}$, – – – – $\overline{\omega_2'^2}$, ········ $\overline{\omega_3'^2}$.
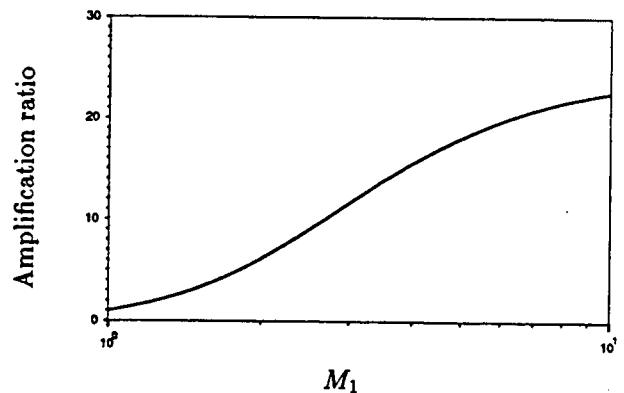

FIGURE 4(B). Amplification of transverse vorticity fluctuation variances predicted by LIA.

3.2 Turbulence Length Scales

Experimental studies[12,13,14] have reported that large scale turbulent motions are enhanced more than small scale motions as turbulence passes through a shock wave, leading to the overall increase of turbulence length scales, especially of microscales. However, LIA predicts that Taylor microscales decrease across the shock wave for all shock strengths, which was confirmed by DNS for weak shock waves[17,19]. For weak shock waves, changes in some turbulence length scales were too small to draw definite conclusions on the issue.

To investigate the scale-dependent amplification of turbulence, the modification of power spectra across the shock wave ($M_1 = 2.0$) is computed through LIA for the one dimensional spectrum in the shock-normal (longitudinal) and transverse direction which is shown in Figure 5(A) and (B), respectively. In the longitudinal spectra, significant scale-dependent amplification is observed: more amplification at small scales than at
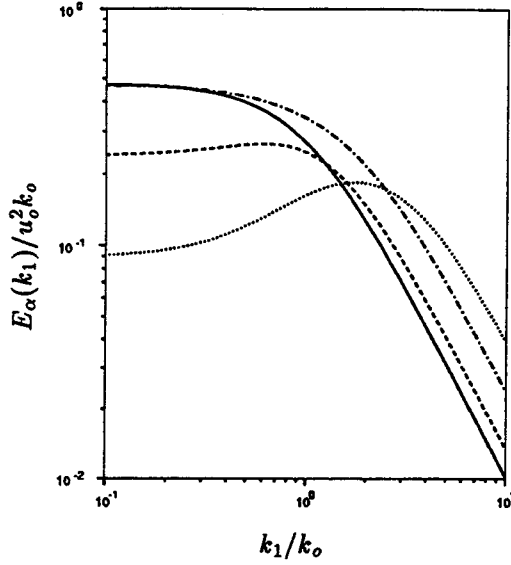
6

FIGURE 5(A). LIA prediction of the shock-normal direction (vs. k_1) one dimensional energy spectra change across the shock wave for $M_1 = 2.0$: E_1: ——— upstream, —·— downstream, E_2 & E_3: ——— upstream, ········ downstream.

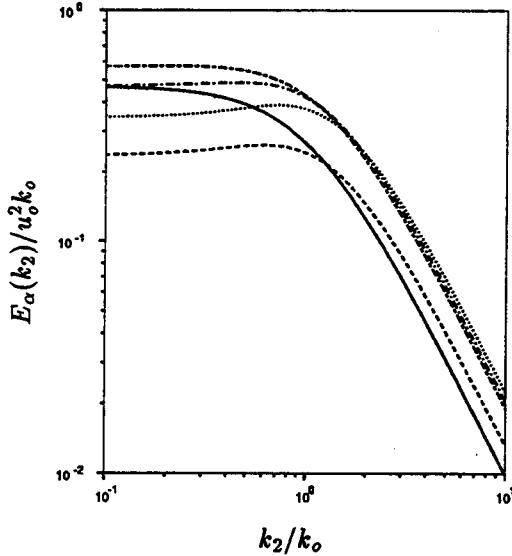

FIGURE 5(B). LIA prediction of the transverse direction (vs. k_2) one dimensional energy spectra change across the shock wave for $M_1 = 2.0$: E_2: ——— upstream, —·— downstream, E_1: ——— upstream, ········ downstream, E_3: ——— upstream, —·— downstream.

large scales. Large scale part of $E_2(k_1)$ is even suppressed through the interaction. In the transverse spectra, more amplification at small scales is found for $E_1(k_2)$ and $E_2(k_2)$, while more amplification at large scale is found for $E_3(k_2)$. Since the spectrum amplification pattern is different for different spectrum (e.g. $E_1(k_2)$ or

$E_3(k_2)$), the issue of length scale change should be addressed for the specific length scale only. In the following, changes in various turbulence length scales are discussed.
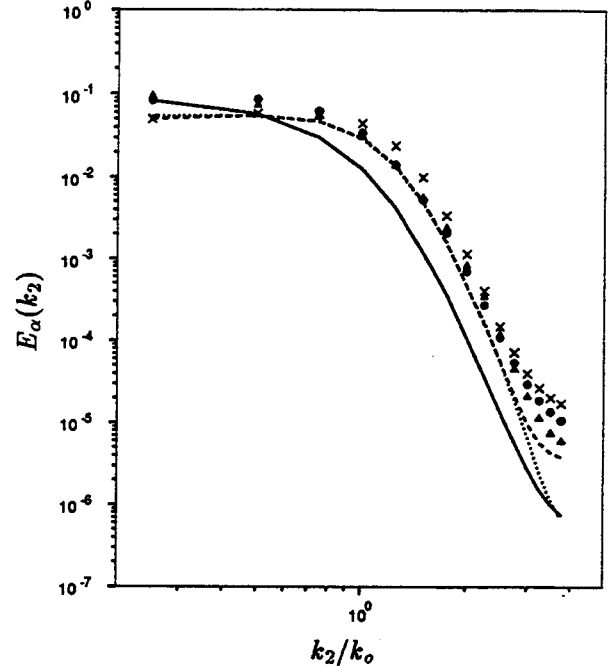

FIGURE 6. Changes in one dimensional spectra across the shock wave which is at $k_o x_s = 12.29$: lines for upstream spectra at $k_o x_1 = 10.59$, and symbols for downstream spectra at $k_o x_1 = 13.68$. ——— , • : $E_2(k_2)$, ——— , × : $E_1(k_2)$, ········ , △ : $E_3(k_2)$.

Transverse power spectra of velocity fluctuations in a numerically simulated field from case A are shown for upstream and downstream of the shock wave in Figure 6. Amplification is more pronounced at the large wave numbers, which is consistent with the prediction by the linear analysis in Figure 5(B).

Keller et al.[14] reported that both the density microscale and the integral length scale in the shock normal direction increase for shock waves with $M_1 < 1.24$. In the present simulation, the spectrum changes of density and temperature fluctuations across the shock are found to be similar to those of velocity fluctuations: Spectra are amplified more at small scales than at large scales. The difference between the present study and the experiment of Keller et al.[14] may be due to the assumptions made in the experimental data analysis, such as turbulence isotropy/homogeneity, and negligible pressure fluctuations, which may be too crude in light of the simulation results. Velocity fluctuation variances are axisymmetric as shown in Sec. 3.1, and thermodynamic property fluctuations are not isobaric and

7

decay rapidly behind the shock wave as shown in Sec. 3.3. The effects of these assumptions on the data analysis are not clearly documented in Keller *et al.*[14].
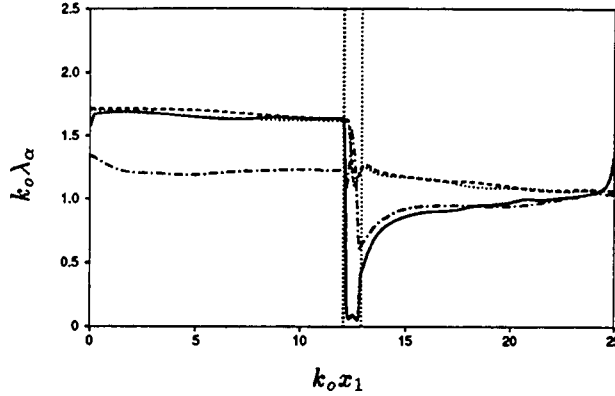

FIGURE 7(A). Evolution of microscales throughout the computational domain for $M_1 = 2.0$: —— λ_1, - - - - λ_2, ········ λ_3, —·— λ_ρ. Vertical lines denote the boundaries of shock intermittency.
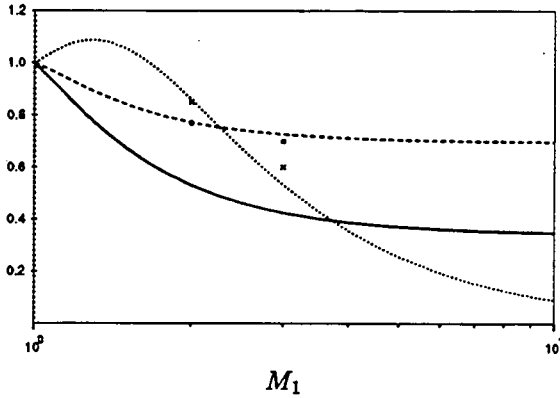
FIGURE 7(B). Change of Taylor microscales and dissipation length scale across the shock wave predicted by LIA. —— λ_1, - - - - λ_2 & λ_3, ········ l_ϵ. Symbols for DNS: • λ_2, × l_ϵ.

Figure 7(A) shows the evolutions of Taylor microscales (λ_α) and the transverse density microscale (λ_ρ), which are defined as —·· ·

$$\lambda_\alpha = \frac{\sqrt{\overline{u_\alpha'^2}}}{\sqrt{\overline{u_{\alpha,\alpha}'^2}}} \quad \text{and} \quad \lambda_\rho = \frac{\sqrt{\overline{\rho'^2}}}{\sqrt{\overline{\rho_{,2}'^2}}},$$

respectively. All the microscales decrease significantly across the shock wave: the streamwise Taylor microscale by about 50%, the transverse Taylor microscales by about 20%, and the density microscale by about 30%. Mach number dependence of Taylor microscale change

predicted by LIA is shown in Figure 7(B). The higher the Mach number, the more is the reduction of the Taylor microscales through the shock wave. The reduction is more pronounced in the shock-normal direction. The reduction observed in the simulation agrees well with the LIA prediction. The experimental result indicating Taylor microscale increase[13] was referred to time scale, not length scale (Debieve 1992, private communication). If the mean velocity decrease across the shock is properly accounted for, their experimental result would be consistent with the present simulation and analysis.

Integral scale (Λ_f) of turbulent fluctuation f' in the x_2-direction is defined from its two-point correlation, $C_f(r; x_1)$, defined as

$$C_f(r; x_1) = \frac{\overline{f'(x_1, x_2, x_3, t) f'(x_1, x_2 + r, x_3, t)}}{\overline{f'^2(x_1, x_2, x_3, t)}},$$

where the average is taken over time and homogeneous directions (x_2- and x_3-directions). The integral scale (Λ_f) is, then, defined as

$$\Lambda_f(x_1) = \int_0^\infty C_f(r; x_1) dr,$$

where the upper limit of the integration is replace by $L/2$ when dealing with numerically simulated field with L being the computational box size in the x_2-direction, where periodic boundary condition is enforced. Figure 8 shows the evolutions of four integral scales throughout the flow field. Three integral scales ($\Lambda_{u_1}, \Lambda_{u_2}$, and Λ_ρ) undergo reductions across the shock wave, most significantly in Λ_{u_2} by about 45%, while Λ_{u_3} increases across the shock by about 30%. Mach number dependence of the integral length scale change can be predicted by LIA. For the shock wave with $M_1 = 2.0$, the ratio of the downstream to the upstream integral length scale (with the von Karman upstream spectrum[34]) is 0.91, 0.60, 1.46 for $\Lambda_{u_1}, \Lambda_{u_2}$, and Λ_{u_3}, respectively. The simulation results agree well with the LIA predictions considering the difference in the upstream energy spectrum shape (see Fig. 5).

8

FIGURE 8. Evolution of integral scales throughout the computational domain for $M_1 = 2.0$: —— Λ_{u_2}, ———— Λ_{u_1}, ········ Λ_{u_3}, —·— Λ_ρ. Vertical lines denote the boundaries of shock intermittency.

FIGURE 9. Evolution of the dissipation length scale throughout the computational domain for $M_1 = 3.0$. Vertical lines denote the boundaries of shock intermittency.
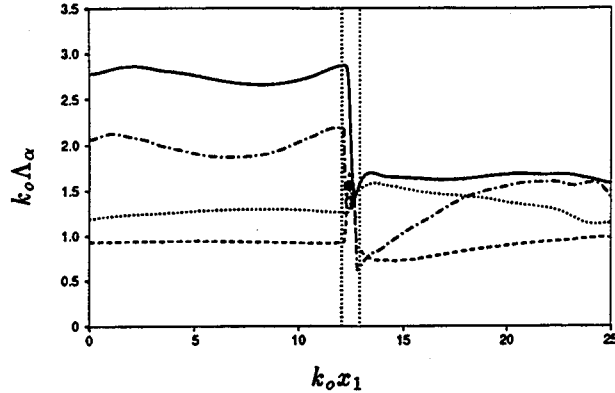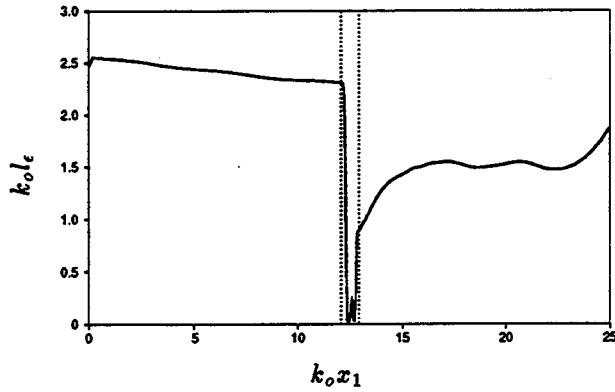
The most widely used length scale in turbulence modelling is the dissipation length scale (l_ϵ), defined as

$$l_\epsilon = \overline{p}q^3/\epsilon,$$

where ϵ is the dissipation rate of turbulence kinetic energy, which includes contributions from both solenoidal and dilatational motions. Figure 9 shows the evolution of the length scale l_ϵ. The dissipation length scale also decreases across the shock wave. Just behind the shock wave, l_ϵ undergoes rapid increase as was the case with the streamwise Taylor microscale (Figure 7(A)), due to the rapid decay of the acoustic waves (or, the dilatational motions). The Mach number dependence of the dissipation length scale change predicted by LIA is presented in Figure 7(B). The length scale is reduced for strong shock waves, while it shows a mild increase for

shock waves with $M_1 < 1.65$. For weak shock waves, TKE and its dissipation rate are comparably amplified to give slight increase in l_ϵ across the shock wave, while at higher Mach numbers TKE amplification saturate much faster than vorticity variance amplification to give the reduction in the length scale (see Fig. 2(B) and Fig. 4(B)). The length scale increase observed by Honkan et al.[12] at $M_1 = 1.24$ (the equivalent shock normal Mach number in their experiment is 1.24 not 1.62) might be explained as the phenomenon occurring for weak shock waves. However, the experimental results are not in quantitative agreement with the simulation and analysis: LIA predicts less than 10% increase, while the experimental data show more than 600% increase. This difference seems to suggest that the assumptions used in the experimental data analysis may be erroneous: these include neglecting pressure fluctuations and application of Taylor's hypothesis in high intensity turbulence.

3.3 Thermodynamic Quantities

Thermodynamic fields which are obtained from the freely decaying turbulence[31] and prescribed at the inflow are nearly isentropic. As the flow passes through the shock wave, all the fluctuations are amplified, followed by decay. Polytropic assumption is generally used for the relation between thermodynamic fluctuations

$$\frac{p'}{\overline{p}} = n\frac{\rho'}{\overline{\rho}} = \frac{n}{n-1}\frac{T''}{\widetilde{T}},$$

where n is the polytropic exponent. For polytropic fluctuations, specification of one property fluctuation and the polytropic exponent is sufficient to describe all the thermodynamic fluctuations. Based on the above relations, different polytropic exponents can be defined using normalized rms fluctuations $(n_{p\rho}, n_{\rho T})$ and the correlations between instantaneous fluctuations $(c_{\rho T})$ as

$$n_{p\rho} = \frac{\sqrt{\overline{p'^2}}/\overline{p}}{\sqrt{\overline{\rho'^2}}/\overline{\rho}}, \qquad n_{\rho T} = 1 + \frac{\sqrt{\overline{T'^2}}/\widetilde{T}}{\sqrt{\overline{\rho'^2}}/\overline{\rho}},$$

and

$$c_{\rho T} = 1 + \frac{\overline{p}}{\widetilde{T}}\frac{\overline{\rho'T''}}{\overline{\rho'^2}}.$$

For weak shock waves with $M_1 \leq 1.20$, relations between thermodynamic property fluctuations are close to isentropic $(n = \gamma)$ throughout the flow field[19].

The polytropic exponents, $n_{p\rho}, n_{\rho T}$, are plotted Figure 10. If the fluctuations are indeed polytropic, the

9

two exponents should be the same, which is defined as the polytropic exponent. The exponents are the same upstream of the shock wave with $n_{p\rho} = n_{\rho T} \simeq \gamma$. Downstream of the shock wave, however, they differ significantly with $n_{p\rho}$ decreasing and $n_{\rho T}$ increasing. Their return to polytropy is very slow.
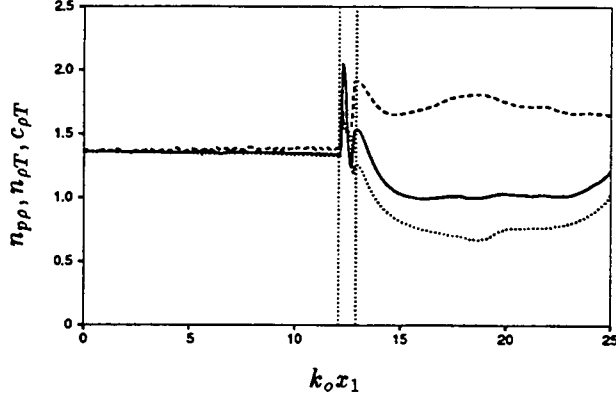

FIGURE 10.   Evolution of exponents for the fluctuations in thermodynamic variables for $M_1 = 2.0$: —— $n_{p\rho}$, ---- $n_{\rho T}$, ········ $c_{\rho T}$. Vertical lines denote the boundaries of shock intermittency.

The evolution of $c_{\rho T}$ is also shown in Figure 10. Upstream of the shock wave, it is nearly equal to $\gamma (= 1.40)$. It drops significantly across the shock wave, and its further evolution is rather slow. The change in the exponents across the shock wave is found to be consistent with the LIA prediction (shown in Figure 11). Upstream thermodynamic fluctuations are polytropic (close to isentropic), and downstream fluctuations are not isentropic due to significant entropy fluctuations produced by the shock turbulence interaction. To properly describe the thermodynamic fluctuations in strong shock turbulence interaction, specification of at least one thermodynamic fluctuation along with two exponents (i.e., $n_{p\rho}$ and $n_{\rho T}$) are required.

The shock strength effects on thermodynamic fluctuations for wider range of shock normal Mach numbers can easily be investigated through the linear analysis. In the following, polytropic exponents downstream of the shock in the interaction of solenoidal velocity fluctuations with a shock wave is studied. The effects of the shock strength on downstream polytropic exponents are shown in Figure 11. For isentropic or acoustic fluctuations, all the exponents are the same and equal to the specific heat ratio. For entropic or isobaric fluctuations, $n_{p\rho}$ and $c_{\rho T}$ become 0 and $n_{\rho T}$ becomes 2. For weak shock waves with $M_1 < 1.2$, thermodynamic fluctuations behind the shock can be regarded as isentropic. As the shock becomes stronger,

the entropy fluctuation behind the shock cannot be neglected, and its importance increases for the stronger shock waves. The results of the polytropic exponents from DNS are consistent with LIA predictions with the values from DNS systematically deviating from the LIA predictions toward the isentropic value of 1.4. This may be due to (incompressible) pressure fluctuations associated with dilatation-free velocity fluctuations[35], which accompany mainly isentropic thermodynamic fluctuations.
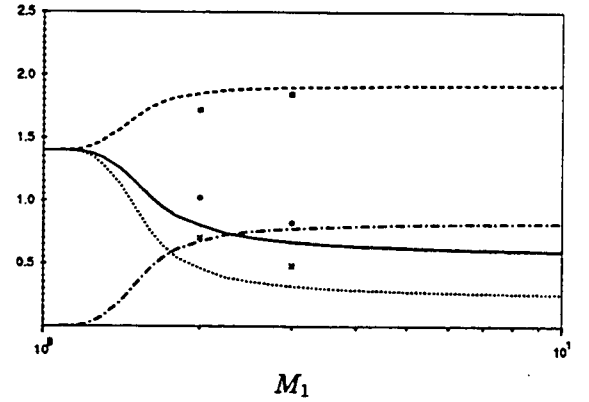

FIGURE 11.   Downstream polytropic exponents and entropy fluctuation contribution predicted by LIA. —— $n_{p\rho}$, ---- $n_{\rho T}$, ········ $c_{\rho T}$, —·— Entropy fluctuation contribution. Symbols for DNS: • $n_{p\rho}$, □ $n_{\rho T}$, × $c_{\rho T}$.

In order to quantify the significance of entropy fluctuations behind the shock wave, the contribution of entropic fluctuations to the density fluctuation by the linear analysis is shown in Figure 11. Since the acoustic fluctuations and entropic fluctuations are completely decorrelated in the linear limit, the relative significance of entropy fluctuations can be expressed as $\frac{\overline{s'^2}/c_p^2}{\overline{p'^2}/\bar{p}^2}$ using Equation (1). For weak shock waves with $M_1 < 1.2$, entropy fluctuations contribute less than 2% to the density fluctuations. However, entropy fluctuations become more significant than acoustic fluctuations beyond $M_1 = 1.65$.

In summary, thermodynamic fluctuations downstream of the shock wave is found to be isentropic for weak shock waves ($M_1 < 1.2$) and become non-polytropic for strong shock waves, where the importance of entropy fluctuations are comparable to the acoustic fluctuations. The thermodynamic fluctuations cannot be modeled using polytropic exponents in this regime. Therefore, acoustic and entropic fluctuations should be modeled separately. Zeman[36] stressed the need for such a separation for the mean thermodynamic quantities.

10

4. Conclusion

A shock-capturing scheme is developed for the simulation of the interaction of isotropic turbulence with a strong shock wave. A modified version of sixth-order essentially non-oscillatory (ENO) scheme was used.

Direct numerical simulation has been performed for turbulence interacting with a strong shock wave with $M_1 = 2.0$ and 3.0, where turbulence is fully resolved and the shock wave is captured. Turbulence kinetic energy is amplified across the shock wave, and the amount of turbulence amplification is consistent with linear analysis. The streamwise velocity fluctuation undergoes rapid evolution just behind the shock wave, which can be interpreted as the energy transfer from acoustic pressure fluctuations to velocity fluctuations via pressure transport in the shock-normal direction. Vorticity amplification is in accordance with the linear analysis.

Most energy spectra are found more amplified at large wave numbers than at small wave numbers. Most length scales decrease across the shock wave, which confirms the results of LIA and those of shock-resolving simulations with $M_1 \leq 1.20$. However, some length scales— the dissipation length scale, a transverse integral length scale — are found to increase in a certain range of shock strengths.

Thermodynamic fluctuations downstream of the shock wave are found to be non-polytropic for strong shock waves, which is consistent with the LIA prediction. Linear analysis predicts that thermodynamic fluctuations behind the shock contain significant entropy fluctuations leading to nonpolytropic behavior beyond $M_1 = 1.20$. The entropy fluctuations are more significant than the acoustic fluctuations beyond $M_1 = 1.65$.

Acknowledgement

References

[1] Ribner, H.S., "Convection of a Pattern of Vorticity through a Shock Wave," *NACA TN-2864*, 1953.

[2] Ribner, H.S., "Shock-turbulence Interaction and the Generation of Noise," *NACA TN-3255*, 1954.

[3] Ribner, H.S., "Spectra of Noise and Amplified Turbulence Emanating from Shock-Turbulence Interaction," *AIAA Journal*, Vol. 25, 1987, pp. 436-442.

[4] Moore, F.K., "Unsteady Oblique Interaction of a Shock Wave with a Plane Disturbances," *NACA TN-2879*, 1953.

[5] Kerrebrock, J.L., "The Interaction of Flow Discontinuities with Small Disturbances in a Compressible Fluid," *Ph.D. Thesis*, California Institute of Technology, 1956.

[6] Chang, C.-T., "Interaction of a Plane Shock Wave and Oblique Plane Disturbances with Special Reference to Entropy Waves," *J. Aero. Sci.*, Vol. 24, 1957, pp. 675-682.

[7] McKenzie, J.F., and Westphal, K.O., "Interaction of Linear Waves with Oblique Shock Waves," *Phys. Fluids*, Vol. 11, 1968, pp. 2350-2362.

[8] Jacquin, L., Cambon, C., and Blin, E., "Turbulence Amplification by a Shock Wave and Rapid Distortion Theory," *Phys. Fluids A*, Vol. 5, 1993, pp.2539-2550.

[9] Dolling, D.S., and Or, C.T., "Unsteadiness of the Shock Wave Structure in Attached and Separated Compression Ramp Flows," *Exp. Fluids*, Vol. 3, 1985, pp. 24-32.

[10] Andreopoulos, J., and Muck, K.-C., "Some New Aspects of the Shock-Wave Boundary Layer Interaction in Compression Ramp Corner," *J. Fluid Mech.*, Vol. 180, 1987, pp. 405-428.

[11] Smits, A.J., and Muck, K.-C., "Experimental Study of Three Shock Wave/ Turbulent Boundary Layer Interactions," *J. Fluid Mech.*, Vol. 182, 1987, pp. 294-314.

[12] Honkan, A., and Andreopoulos, J., "Rapid Compression of Grid-Generated Turbulence by a Moving Shock Wave," *Phys. Fluids A*, Vol. 4, 1992, pp. 2562-2572.

[13] Debieve, J.F., and Lacharme, J.P., "A Shock-Wave/ Free Turbulence Interaction," *Turbulent Shear Layer/ Shock Wave Interactions*, J. Délery (ed.), 1986, Springer, Berlin.

[14] Keller, J., and Merzkirch, W., "Interaction of a Normal Shock Wave with a Compressible Turbulent Flow," *Exp. Fluids*, Vol. 8, 1990, pp. 241-248.

[15] Jacquin, L., Blin, E., and Geffroy, P., "Experiments on Free Turbulence/ Shock Wave Interaction," *Eighth Symposium on Turbulent Shear Flows*, Munich, 1991.

[16] Rotman, D., "Shock Wave Effects on a Turbulent Flow," *Phys. Fluids A*, Vol. 3, 1991, pp. 1792-1806.

[17] Lee, S., Lele, S.K., and Moin, P., "Direct Numerical Simulation and Analysis of Shock Turbulence Interaction," *AIAA Paper No.* 91-0523, 1991, Reno, Nevada.

[18] Lee, S., Moin, P., and Lele, S.K., "Interaction of Isotropic Turbulence with a Shock Wave," *Report TF-52*, Department of Mechanical Engineering, Stanford University, 1992.

[19] Lee, S., Lele, S.K., and Moin, P., "Direct Numerical

Simulation of Isotropic Turbulence Interacting with a Weak Shock Wave," *J. Fluid Mech.*, Vol. 251, 1993, pp. 533-562.

[20] Sherman, F.S. "A Low-Density Wind-Tunnel Study of Shock-Wave Structure and Relaxation Phenomena in Gases," *NASA TN-3298*, 1955.

[21] Shu, C.-W., and Osher, S., "Efficient Implementation of Essentially Non-oscillatory Shock-Capturing Schemes, II," *J. comp. Phys.*, Vol. 83, 1989, pp.32-78.

[22] Rogerson, A., and Meiburg, E., "A Numerical Study of the Convergence Properties of ENO Scheme," *J. Sci. Comp.*, Vol. 5, 1990, pp. 151-167.

[23] Shu, C.-W., "Numerical Experimentation on the Accuracy of ENO and Modified ENO Schemes," *J. Sci. Comp.*, Vol. 5, 1990, pp. 127-149.

[24] Lee, S., Lele, S.K., and Moin, P., "Simulation of Spatially Evolving Compressible Turbulence and the Applicability of Taylor's Hypothesis," *Phys. Fluids A*, 1992, pp. 1521-1530.

[25] Favre, A., "Équations des gaz turbulents compressibles I," *Journal Mécanique*, Vol. 4, 1965, pp. 361-390.

[26] Lee, S., "Large Eddy Simulation of Shock Turbulence Interaction," *Annual Research Brief*, Center for Turbulence Research, Stanford University, 1992.

[27] Roberts, T.W., "The Behavior of Flux Difference Splitting Schemes near Slowly Moving Shock Waves," *J. Comp. Phys.*, Vol. 90, 1990, pp. 141-160.

[28] Meadows, K.R., Caughey, D.A., and Casper, J., "Computing Unsteady Shock Waves for Aeroacoustic Applications," *AIAA Paper No.* 93-4329, 1993, Long Beach, CA.

[29] Wray, A.A., "Very Low Storage Time-Advancement Schemes," *Internal Report*, NASA-Ames Research Center, 1986.

[30] Lele, S.K., "Compact Finite Difference Schemes with Spectral-Like Resolution," *J. Comp. Phys.*, Vol. 103, 1992, pp. 16-42.

[31] Lee, S., Lele, S.K., and Moin, P., "Eddy Shocklets in Decaying Compressible Turbulence," *Phys. Fluids A*, Vol. 3, 1991, pp.657-664.

[32] Giles, M.B., "Nonreflecting Boundary Conditions for Euler Equation Calculations," *AIAA Journal*, Vol. 28, 1990, pp. 2050-2058.

[33] Thompson, P.A., *Compressible-Fluid Dynamics*, Maple Press, 1985, p. 183.

[34] Hinze, J.O., *Turbulence*, McGraw-Hill, 1975, p. 247.

[35] Sarkar, S., Erlebacher, G., Hussaini, M.Y., and Kreiss, H.O., "The Analysis and Modelling of Dilatational Terms in Compressible Turbulence," *J. Fluid Mech.*, Vol. 227, 1991, pp. 473-493.

[36] Zeman, O., "A New Model for Super/Hypersonic Turbulent Boundary Layers," *AIAA Paper No.* 93-0897, 1993, Reno, Nevada.